Universidade Federal do Rio de Janeiro
Escola de Química
Programa de Pós-graduação em Engenharia de Processos Químicos e Bioquímicos

MODELING AND OPTIMIZATION OF DESALINATION SYSTEMS

TESE DE DOUTORADO

Abdón Parra López

Rio de Janeiro, março de 2019

ABDON PARRA LOPEZ

MODELING AND OPTIMIZATION OF DESALINATION SYSTEMS

Tese de Doutorado submetida ao Corpo Docente do Curso de Pós-Graduação em Engenharia de Processos Químicos e Bioquímicos da Escola de Química da Universidade Federal do Rio de Janeiro, como parte dos requisitos necessários para a obtenção do grau de Doutor em Ciências (D.Sc.).

Orientadores: Lidia Yokoyama
Miguel Jorge Bagajewicz

Rio de Janeiro
Março de 2019

CIP - Catalogação na Publicação

P258m

Parra Lopez, Abdon
Modeling and Optimization of Desalination Systems / Abdon Parra Lopez. -- Rio de Janeiro, 2019.
121 f.

Orientadora: Lidia Yokoyama.
Coorientador: Miguel Bagajewicz.
Tese (doutorado) - Universidade Federal do Rio de Janeiro, Escola de Química, Programa de Pós Graduação em Engenharia de Processos Químicos e Bioquímicos, 2019.

1. Dessalinização. 2. Osmose Inversa. 3. Optimização. 4. Meta-modelos. 5. MINLP. I. Yokoyama, Lidia, orient. II. Bagajewicz, Miguel, coorient. III. Título.

Elaborado pelo Sistema de Geração Automática da UFRJ com os dados fornecidos pelo(a) autor(a), sob a responsabilidade de Miguel Romeu Amorim Neto - CRB-7/6283.

MODELING AND OPTIMIZATION OF DESALINATION SYSTEMS

Abdon Parra Lopez

TESE DE DOUTORADO SUBMETIDA AO CORPO DOCENTE DO CURSO DE PÓS-GRADUAÇÃO EM ENGENHARIA DE PROCESSOS QUÍMICOS E BIOQUÍMICOS DA ESCOLA DE QUÍMICA DA UNIVERSIDADE FEDERAL DO RIO DE JANEIRO, COMO PARTE DOS REQUISITOS NECESSÁRIOS PARA A OBTENÇÃO DO GRAU DE DOUTOR EM CIÊNCIAS (D.SC.).

Examinada por:

_____

Prof. Lidia Yokoyama, D.Sc. - Orientadora, (UFRJ)

_____

Prof. Miguel Jorge Bagajewicz, Ph.D. - Orientador, (OU)

_____

Prof. André Luiz Hemerly Costa , D.Sc., (UERJ)

_____

Prof. Fernando Luiz Pellegrini Pessoa, D.Sc., (UFRJ)

_____

Prof. Heloisa Lajas Sanches , D.Sc., (UFRJ)

_____

Prof. Reinaldo Coelho Mirre, D.Sc., (UFBA)

Rio de Janeiro

Março de 2019

RESUMO

Tendo em conta a crescente demanda por água tanto urbana quanto industrial, e considerando a atual escassez de água doce, geralmente extraída de reservatórios superficiais e subterrâneos, é necessário considerar a água salgada, devidamente tratada, como um recurso viável para consumo humano e industrial.

As tecnologias de dessalinização disponíveis no mercado podem ser classificadas como em térmicas e de membranas. A osmose inversa (RO), o flash multi-estágio (MSF) e a destilação multi-efeito (MED) são as principais tecnologias comerciais de dessalinização, sendo a osmose inversa a de maior crescimento.

As plantas de osmose inversa têm sido tradicionalmente projetadas pelos fabricantes usando abordagens empíricas e heurísticas. No entanto, o desempenho de custo da dessalinização por osmose inversa, é sensível aos parâmetros de projeto e às condições de operação e, portanto, é necessário dar atenção à obtenção de projetos com ótimo custo-benefício.

O problema da síntese de uma rede de osmose inversa (RON) consiste em obter uma solução econômica baseada em valores ótimos das seguintes variáveis: número de estágios, número de vasos de pressão por estágio, número de módulos de membrana por vaso de pressão, número e tipo de equipamentos auxiliares, bem como as variáveis operacionais para todos os dispositivos da rede, este problema poderia ser formulado como uma programação não linear inteira mista (MINLP).

Neste trabalho, propõe-se uma metodologia para resolver um modelo matemático não-linear para o projeto ótimo de redes de osmose inversa, que melhore as deficiências do desempenho computacional e, às vezes, falhas de convergência de software comercias para resolver os modelos rigorosos MINLP. A estratégia consiste no uso de um algoritmo genético para obter valores iniciais para um modelo completo não linear MINLP. Além disso, como o algoritmo genético baseado nas equações do modelo rigoroso é muito lento, o uso de meta-modelos para reduzir a complexidade matemática e acelerar consideravelmente a corrida é proposto. O efeito da vazão de alimentação, a concentração de água do mar, o número de estágios de osmose inversa e o número máximo de módulos de membrana em cada vaso de pressão no custo total anualizado da planta é explorado.

Palavras-chave: Osmose Inversa, optimização, meta-modelos, MINLP.

ABSTRACT

The increasing demand for freshwater both urban and industrial, and considering the current scarcity of freshwater, usually extracted from superficial and underground reservoirs, it is necessary to consider salt water, properly treated, as a viable resource for human and industrial consumption.

The available desalination technologies in the market can be classified as thermal-based and membrane-based processes. Reverse osmosis (RO), multi-stage flash (MSF), and multi-effect distillation (MED) are the main commercial desalination technologies, with RO being the fastest growing (GHAFFOUR et al., 2015).

Desalination plants using RO have been traditionally designed by manufacturers using empirical approaches and heuristics (GHOBEITY; MITSOS, 2014). However, the cost performance of RO desalination is sensitive to the design parameters and operating conditions (CHOI; KIM, 2015) and therefore, attention needs to be placed in obtaining cost-optimal designs.

The problem of synthesizing a reverse osmosis network (RON) consists of obtaining a cost-effective solution based on optimum values of the following: number of stages, number of pressure vessels per stage, number of modules per pressure vessel, number and type of auxiliary equipment, as well as the operational variables for all the devices of the network, this problem could be formulated as a mixed integer nonlinear programming (MINLP).

In this work, a methodology to solve a nonlinear mathematical model for the optimal design of RO networks, which ameliorates the shortcomings of the computational performance and sometimes convergence failures of commercial software to solve the rigorous MINLP models is proposed. The strategy consists of the use of a genetic algorithm to obtain initial values for a full nonlinear MINLP model. In addition, because the genetic algorithm based on the rigorous model equations is insurmountably slow, the use of metamodels to reduce the mathematical complexity and considerably speed up the run is proposed. The effect of the feed flow, seawater concentration, number of reverse osmosis stages, and the maximum number of membrane modules in each pressure vessel on the total annualized cost of the plant is explored.

Keywords: Reverse osmosis network, optimization, metamodels, MINLP.

LIST OF FIGURES

Figure 1. Global optimum vs, local optimum.....23
Figure 2. Convex function.....24
Figure 3. Desalination market growth forecasts.....26
Figure 4. Multi-effect distillation.....27
Figure 5. Multiple Stage Flash.....27
Figure 6. Spiral wound membrane module.....29
Figure 7. Concentration polarization – salt concentration gradients adjacent to the membrane 31
Figure 8. Osmotic driving force profiles for PRO. Internal and external polarization.....33
Figure 9. Superstructure of two stages Reverse Osmosis configuration.....43
Figure 10. Structure of reverse osmosis (RO) stage and pressure vessel.....45
Figure 11. By-pass representation of a single pressure vessel.....47
Figure 12. Permeate and brine transport through the membrane.....48
Figure 13. Superstructure of RO+PRO (Configuration 1).....54
Figure 14. Superstructure of a RO+PRO (Configuration 2).....54
Figure 15. PRO unit arrangement.....54
Figure 16. Bound contraction – interval elimination strategy.....62
Figure 17. Genetic algorithm set up.....65
Figure 18. Stochastic – deterministic flowchart methodology.....66
Figure 19. Extended interval elimination – RO inlet Pressure.....71
Figure 20. Influence of feed pressure and concentration on the permeate concentration.....76
Figure 21. Influence of feed pressure and concentration on permeate flow rate, brine concentration and brine flow rate.....78
Figure 22. Linear metamodel correlation and rigorous solutions.....79
Figure 23. Non-Linear metamodel correlation and validation.....81
Figure 24. TAC for different inlet flows and seawater concentrations (two stages).....85
Figure 25. Effect of the number of stages.....87
Figure 26. TAC for different inlet flows and seawater concentrations max number of membrane modules (N^{max}_{e}) equal to 16.....88
Figure 27. Optimal TAC per unit permeate flow.....89
Figure 28. Permeate flow (2 stages, 500 ppm permeate).....89
Figure 29. Water flux rigorous and metamodel meshes.....93

Figure 30. Solute flux rigorous and metamodel meshes.. 94
Figure 31. TAC RO+PRO configuration 2 for different inlet flows and seawater concentrations. 97
Figure 32. Comparison between TAC for RO and RO+PRO (configuration 2) for different feed concentration and flow. 98

LIST OF TABLES

Table 1. Reverse osmosis module parameters. 60
Table 2. Pressure retarded osmosis module parameters. 60
Table 3. Economic parameters 60
Table 4. Results using RYSIA for General superstructure 69
Table 5. Results using RYSIA for one stage RON 73
Table 6. Bound contraction using extended interval elimination (5 intervals) 74
Table 7. Limits and points of solution mesh for RO metamodel. 75
Table 8. Linear metamodel constants 80
Table 9. Non-Linear metamodel constants and objective function. 81
Table 10. Optimization results. 82
Table 11. Optimal solutions for different scenarios 84
Table 12. Water production costs for existing plants. 90
Table 13. Water production costs calculated with the model. 91
Table 14. Limits and points of solution mesh for PRO metamodel. 92
Table 15. Linear metamodel constants for PRO model 94
Table 16. Optimization results for hybrid RO+PRO. 95
Table 17. Optimal solutions for different scenarios 96

ACRONYMS

ACM – *Aspen Custom Modeler*

AOC – *Annual Operational Cost*

BARON – *Computational system for solving nonconvex optimization problems to global optimality*

CONOPT – *Generalized reduced-gradient (GRG) algorithm for solving large-scale nonlinear programs involving sparse nonlinear constraints*

CPLEX – *Simplex method as implemented in the C programming language*

DAOPs – *Differential Algebraic Optimization Problems*

DICOPT – *Discrete and Continuous Optimizer*

FO – *Forward Osmosis*

GAMS – *General Algebraic Modeling System*

gPROMS – *general Process Modeling System*

IP – *Integer Programming*

IPOPT – *Interior Point Optimizer*

LINDO – *Software for Integer Programming, Linear Programming, Nonlinear Programming, Stochastic Programming, Global Optimization*

LINGO – *Optimization Modeling Software for Linear, Nonlinear, and Integer Programming*

MED – *Multi-effect Distillation*

MEE – *Multiple Effect Evaporation*

MILP – *Mixed Integer Linear Programming*

MINLP – *Mixed Integer Nonlinear Programming*

MINOS – *Modular In-core Nonlinear Optimization System*

MIP – *Mixed Integer Programming*

MSF – *Multi-stage Flash*

MSF-BR – *Multi-effect Distillation with Brine Recirculation*

MVMD – *Multi-stage vacuum membrane distillation*

NLP – *Non-Linear Programming*

PRO – *Pressure Retarded Osmosis*

RO – *Reverse Osmosis*

RON – *Reverse Osmosis Network*

ROSA – *Reverse Osmosis System Analyzer*

SBB – *Spatial Branch and Bound*

SPSPRO – *Split Partial Second Pass Reverse Osmosis*

TAC – *Total Annualized Cost*

TCC – *Total Capital Cost*

TVC – *Thermal Vapor Compression*

NOMENCLATURE

AOC	Annual operational cost [$]
C	salt concentration [ppm]
$C^{B,wall}$	membrane wall concentration [ppm]
C_P^{Max}	maximum permeate concentration [ppm]
$C^{D,in}$	high salinity current inlet concentration [ppm]
$C^{F,in}$	low salinity current inlet concentration [ppm]
$C^{D,out}$	high salinity current out concentration [ppm]
$C^{F,out}$	low salinity current inlet concentration [ppm]
$C^{D,b}$	high salinity current bulk concentration [ppm]
$C^{F,b}$	low salinity current bulk concentration [ppm]
CC_{equip}	total equipment cost [$]
ccf	capital charge factor
CC_{HPP}	high pressure pump cost [$]
CC_{mem}	membrane module cost [$]
CC_{mempro}	PRO membrane module cost [$]
c_{lab}	labor cost factor [$]
C_{en}	electricity cost [$/(kWh)]
c_{mem}	membrane module unitary cost [$]
c_{mempro}	PRO membrane module unitary cost [$]
CC_{pv}	total pressure vessel cost [$]
CC_{pvpro}	PRO total pressure vessel cost [$]
c_{pv}	unitary pressure vessel cost [$]
c_{pvpro}	PRO unitary pressure vessel cost [$]
CC_{swip}	Seawater intake and pretreatment system cost [$]
CC_T	turbine cost [$]
CC_{Tpro}	PRO turbine cost [$]
F	flow rate [kg/s]
F_D	high salinity flow rate [kg/s]
F_D^T	high salinity turbine flow rate [kg/s]
$F^{D,in}$	high salinity inlet flow rate to a single PRO module [kg/s]
$F^{D,out}$	high salinity out flow rate from a single PRO module [kg/s]
$F^{F,in}$	low salinity inlet flow rate to a single PRO module [kg/s]
$F^{F,out}$	low salinity out flow rate from a single PRO module [kg/s]
F_F	low salinity flow rate [kg/s]

F_S^{RO}	seawater flow rate to RO [kg/s]
F_S^{PRO}	seawater flow rate to PRO [kg/s]
F^{av}	average flow rate [kg/s]
F_R	recycle flow rate [kg/s]
J^S	solute flux [kg/(s.m^2)]
J^W	water flux [kg/(s.m^2)]
J_S^{PRO}	solute reverse flux for PRO [kg/(s.m^2)]
J_W^{PRO}	water flux for PRO [kg/(s.m^2)]
ir	annual interest rate
ks	mass transfer coefficient [m/s]
Ne	number of membrane modules per pressure vessel
N_{pv}	number of pressure vessels of the stage m
N_{pvpro}	number of pressure vessels for the PRO unit
N_{RO}	number of reverse osmosis stages
N_{PRO}	number of membrane modules for the PRO unit
OC_{chem}	cost of chemicals [$]
OC_{ins}	Insurance costs [$]
OC_{lab}	labors cost [$]
OC_{pow}	Electric energy costs [$]
OCm	cost for replacement and maintenance [$]
OC_{memr}	Membrane replacement cost [$]
OC_{mempro}	PRO membrane replacement cost [$]
P	pressure [bar]
PP_{SWIP}	Energy consumed for intake and pre-treatment system [kWh]
PP_{RO}	Electric energy consumed by the reverse osmosis plant [kWh]
Q	flow rate [m^3/h]
Q^R	recycle flow rate [m^3/h]
Q_{SW-IN}	feed flow rate to the system [m^3/h]
Q^{Tpro}	PRO turbine flow rate [m^3/h]
Re	Reynold's number
Sc	Schmidt number,
TAC	total annualized cost [$]
TCC	total capital cost [$]
U^s	superficial velocity [m/s]
V^w	permeation velocity [m/s]
y	binary variable
t_a	annual operation time [hours]

t_1	lifetime of the plant [years]
ΔP^B	brine side pressure difference [bar]
ΔP^{nd}	net driving pressure difference [bar]
ΔP^{Tpro}	PRO turbine pressure difference [bar]
ΔP^{HPPR}	Recycle pump pressure difference [bar]
ΔP	pressure difference [bar]

Parameters

$\hat{A}$	Pure water permeability [kg/(s.m^2.bar)]
$\hat{a}_\pi$	Van't Hoff ´s constant [bar/(K.ppm)]
$\hat{B}$	Salt permeability [kg/(s.m^2)]
$\hat{d}$	membrane module feed space thickness [m]
$\hat{D}$	salt diffusivity [m^2/s]
$\hat{d}_h$	hydraulic diameter [m]
$\hat{K}$	solute resistivity for diffusion
$\hat{h}_{sp}$	membrane module channel height [m]
$\hat{l}_L$	effective length of the module [m]
$\hat{n}_L$	number of leaves
$\hat{P}^{Pe}$	permeate outlet pressure [bar]
$\hat{S}_{fc}$	feed cross-section open area [m^2]
$\hat{S}_{mem}$	RO active membrane area [m^2]
$\hat{S}_{mem}^{PRO}$	PRO active membrane area [m^2]
$\hat{S}_{sp}$	specific surface area of the spacer for the membrane module [m^2]
$\hat{T}$	inlet temperature [K]
$\hat{t}$	support layer thickness [m]
$\hat{\tau}$	support layer tortuosity [m]
$\hat{w}_L$	width of the module [m]
$\Delta\hat{P}_{SWIP}$	seawater intake pressure difference [bar]

Superscripts

av	average
B	brine
Be	brine current of module e from the stage m
$B-F_{BO}$	interconnection between brine and brine final discharge
HPP	high pressure pump
$HPPR$	recycle high pressure pump
IN	inlet
$inem$	inlet of firsts modules of the stage m

O	outlet
P	permeate
Pe	permeate current of module e from the stage m
PRO	reverse osmosis
RO	reverse osmosis
T	turbine
$T-F_{BO}$	interconnection between turbine and brine final discharge
W	membrane wall

Subscripts

BO	brine final discharge
e	membrane module e
d	discretized interval d
m	RO stage m
p	pump p
pv	pressure vessel
PO	permeate final current
S	feed current
$SWIP$	seawater intake and pretreatment
t	turbine t

Symbols

$\hat{\rho}$	density [kg/m^3]
$\hat{\varepsilon}$	membrane module void fraction
Γ	maximum value for the corresponding variable
$\hat{\mu}$	dynamic viscosity [kg/m.s]
η	efficiency
π	osmotic pressure [bar]

SUMMARY

1 INTRODUCTION 17
1.1 Document description: 19
1.2 Literature contributions: 20
2 LITERATURE REVIEW 21
2.1 Mathematical models: 21
2.2 Optimization problems and definitions: 21
2.3 Mixed Integer Optimization: 22
2.4 Process synthesis: 23
2.5 Global Optimization: 23
2.6 Desalination: 25
2.7 Desalination Technologies: 25
2.8 Challenges and advances in desalination: 34
2.9 Reverse osmosis networks design and some hybrid systems: 35
3 OBJECTIVES 41
3.1 General Objective: 41
3.2 Specific objectives: 41
4 METHODOLOGY 42
4.1 Reverse osmosis network – superstructure representation: 42
4.2 Reverse osmosis network – MINLP model: 43
4.2.1 Mass Balances: 43
4.2.2 Reverse osmosis stages model: 44
4.2.3 Membrane modules model: 47
4.2.4 Costs and objective function: 52
4.3 Hybrid reverse osmosis - pressure retarded osmosis superstructure 53
4.3.1 RO+PRO mathematical model 55
4.4 MINLP problem statement 59
4.5 Bound contraction methodology 61
4.6 Stochastic – deterministic methodology 62
4.6.1 Reverse osmosis metamodel construction: 63
4.6.2 Pressure retarded osmosis metamodel construction: 64
5 BOUND CONTRACTION METHODOLOGY RESULTS FOR REVERSE OSMOSIS NETWORKS 67
6 STOCHASTIC-DETERMINISTIC METHODOLOGY RESULTS FOR REVERSE OSMOSIS NETWORKS 75
6.1 Reverse osmosis metamodel adjustment 75

6.2 Reverse osmosis network results 82
6.3 Water production costs comparison with existing facilities: 90
7 STOCHASTIC-DETERMINISTIC METHODOLOGY RESULTS FOR RO+PRO HYBRID SUPERSTRUCTURES. 92
7.1 Pressure retarded osmosis metamodel adjustment 92
7.2 Reverse osmosis – pressure retarded osmosis (RO+PRO) results: 95
8 CONCLUSIONS AND RECOMMENDATIONS 99
8.1 Conclusions 99
8.2 Recommendations to future works 101
9 REFERENCES 102
APPENDIX 110

1 INTRODUCTION

Industrialization and urbanization has caused a per capita increase by fresh water making the desalination a competitive technology for the generation of pure water from the sea water, as well as other low-quality water containing salts and other dissolved solids (KUCERA, 2014).

The available desalination technologies in the market can be classified as thermal-based and membrane-based processes. Reverse osmosis (RO), multi-stage flash (MSF), and multi-effect distillation (MED) are the main commercial desalination technologies, with RO being the fastest growing (GHAFFOUR et al., 2015). This last technology (RO) is, in most cases, the technology of choice for seawater desalination in places where inexpensive waste heat is not available.

Desalination plants using RO have been traditionally designed by manufacturers using empirical approaches and heuristics (GHOBEITY; MITSOS, 2014). However, the cost performance of RO desalination is sensitive to the design parameters and operating conditions (CHOI; KIM, 2015) and therefore, attention needs to be placed in obtaining cost-optimal designs.

The problem of synthesizing a reverse osmosis network (RON) consists of obtaining a cost-effective solution based on optimum values of the following: number of stages, number of pressure vessels per stage, number of modules per pressure vessel, number and type of auxiliary equipment, as well as the operational variables for all the devices of the network.

After the early works of Evangelista (1985), El-Halwagi (1997) and Voros et al. (1996; 1997) many papers have followed (MASKAN et al., 2000; MARCOVECCHIO; AGUIRRE; SCENNA, 2005; GERALDES; PEREIRA; NORBERTA DE PINHO, 2005; LU, Y. Y. et al., 2007; VINCE et al., 2008; KIM, Y. S. Y. M. et al., 2009; OH; HWANG; LEE, 2009;), mainly using the solution-diffusion model proposed by Al-Bastaki et al. (2000), a model that includes the effect of concentration polarization, which eliminates the problem of significant overestimation of the total recovery (WANG. et al., 2014) and the economic model from Malek et al. (1996).

Many authors proposed solving the problem of the design of a RON using Mixed Integer Nonlinear Programming (MINLP) or Nonlinear Programming (NLP) (GHOBEITY; MITSOS, 2014). For example, Du et al. (2012) used a two-stage superstructure representation and solved the resulting MINLP using the solvers CPLEX/MINOS using several starting points

to obtain the best solution. However, it was not clarified how to generate these starting points. Sassi and Mujtaba (2012) proposed a MINLP model and solved the problem using an outer approximation algorithm within gPROMS to evaluate the effects of temperature and salt concentration in the feed current. The work was based on generating "various structures and design alternatives that are all candidates for a feasible and optimal solution", without specifying how their initial values are obtained. Alnouri and Linke (2012) explored different specific RON structures and they optimized each using the ''what'sBest'' Mixed-Integer Global Solver for Microsoft Excel by LINDO Systems Inc. The solver is global and does not require initial points. The authors used "reduced super-structures resembling fundamentally distinct design classes". Lu et al. (2013) obtained an optimal RON using a two stages RON structure and used an MINLP technique with several starting points obtained from an ad-hoc preliminary simulation. Finally, Skyborowsky et al. (2012) proposed an optimization strategy with a special initialization scheme where a feasible initial solution is obtained in two steps: first, all variables are initialized with reasonable values (some obtained by heuristics) and then a solution is obtained using SBB and SNOPT solvers. These local minima are reportedly obtained within a few minutes of computation. It was also reported an attempt to solve a RON using the global solver Baron indicating that the solver finished after 240 hours with a relative gap of 15.66%.

All the aforementioned works have a few things in common: it is observed the complexity of the problem modeling and the difficulty of the solution procedure that stem from the nonlinearities associated with the concentration polarization model. In some cases, it is not shown in detail what pre-processing was done and how the initial data and/or the computing time were obtained. Regarding computing time, it varies: one to few minutes (SKIBOROWSKI et al., 2012), 3 to 16 minutes (MARCOVECCHIO; AGUIRRE; SCENNA, 2005) or 5 to 28 hours (DU et al., 2012). The experience indicates that without the initial values, there is no convergence in several solvers. In addition, although computational time is not critical in design procedures, it is believed it ought to be reasonable. In some cases, the computational time is unacceptable (DU et al., 2012), as it is in the order of days. In this work, an intend to ameliorate these shortcomings providing these initial data systematically and reducing the computing time to the order of minutes is done.

To aid in this work, surrogate models often called Metamodels are also used, which have been proposed to address the issue of model complexity and the associated difficulties of convergence when poor or no initial points are given. Such metamodels are sets of equations of

simple structure (low-order polynomial regression, and Kriging or Gaussian process (KLEIJNEN, 2017)) that facilitate an increased computational performance (mostly time (MAHMOUDI; TRIVAUDEY; BOUHADDI, 2016)). It can be built with the information of the rigorous method and their functions approximate well the image of the more complicated models (PRACTICE, 2015). Metamodels were implemented in the optimization for heat exchanger network (PSALTIS; SINOQUET; PAGOT, 2016; WEN et al., 2016), also, the optimization of water infrastructure planning (BEH et al., 2017; BROAD; DANDY; MAIER, 2015), in stochastic structural optimization (BUCHER, 2017) and building energy performance (JAFFAL; INARD, 2017).

In this work, the RON optimization problem is formulated as an MINLP problem that minimizes the total annualized cost (TAC). First, the model is solved using a genetic algorithm, which provides good initial values for the rigorous MINLP model. As it shall be observed, a genetic algorithm, using the full non-linear and rigorous equations is computationally very expensive, while the MINLP is rather fast when good initial values are provided. This work will show that replacing the use of rigorous equations of the model by the use of a metamodel in genetic algorithm speeds up the solution time orders of magnitude and provides a similar solution.

The previously described solution methodology was also used to optimize a reverse osmosis (RO) – pressure retarded osmosis (PRO) hybrid superstructure.

1.1 Document description:

This work is organized in eight (8) chapters. In chapter 2 is presented a literature review, where the most relevant desalination technologies are presented, the main transport phenomena for reverse osmosis and pressure retarded osmosis are discussed, and finally, previous related optimization works are cited.

In chapter 3 are presented the general and specific objectives of this thesis.

Chapter 4 denominated methodology presents the detailed mathematical model for the RON optimization, and the two optimization methodologies used: bound contraction and the new stochastic-deterministic technique proposed.

Chapter 5 presents the bound contraction methodology for the RON optimization results, with the intention to emphasize the difficulties of the mathematical problem.

Chapter 6 presents the new stochastic-deterministic methodology for the RON optimization, successfully implemented to explore the influence of the feed flow, seawater

concentration, number of reverse osmosis stages, and the maximum number of membrane modules in each pressure vessel on the total annualized cost of the plant.

Chapter 7 shows the optimization results of the proposed solution methodology for a hybrid RO+PRO superstructure.

And finally, chapter 8 presents general conclusions and some recommendations for future continuity of this work.

1.2 Literature contributions:

After implementing both proposed methodologies, bound contraction and the stochastic-deterministic methodology for the optimal design of a reverse osmosis network, an international paper was published and a second one using the proposed methodology for a hybrid RO+PRO superstructure will be submitted.

Published paper:

1. PARRA, A.; NORIEGA, M.; YOKOYAMA, L.; BAGAJEWICZ, M. J. "Reverse Osmosis Network Rigorous Design Optimization", **Industrial & Engineering Chemistry Research,** v. 58, p. 3060–3071, 2019. ISSN: 0888-5885, DOI: 10.1021/acs.iecr.8b02639.

Paper to be submitted:

1. "Reverse Osmosis Network integrated with Pressure Retarded Osmosis: Rigorous Design Optimization", **Industrial & Engineering Chemistry Research.**

2 LITERATURE REVIEW

2.1 Mathematical models:

The mathematical model of a system is a set of mathematical relations, which represent an abstraction of a real system that is being studied. Mathematical models can be developed using (1) fundamental approaches (theories accepted by science used to obtain equations), (2) empirical methods (input and output data are used in conjunction with the principles of statistical analysis to generate empirical models also called "black box models" (3) methods based on analogy (the analogy is used to determine the essential characteristics of the system of interest from a well understood similar system) (FLOUDAS, C. a, 1995).

A mathematical model of a system usually has three fundamental elements:

(1) Variables: the variables can take different values and their values define different states of the system, they can be continuous, integer, or a mix of both.

(2) Parameters: are fixed values, that are data provided externally. Different case studies have different parameters values.

(3) Mathematical relations and constraints: these can be classified as equalities, inequalities and logical conditions.

Equalities are usually related to mass balances, energy balances, equilibrium relationships, physical property calculations, and engineering design relationships that describe the physical phenomena of the system.

Inequalities usually consist of operational regimes, quality specifications, the feasibility of mass and heat transfer, equipment performance, and limits of availability and demand. Logical conditions provide the link between continuous and integer variables.

2.2 Optimization problems and definitions:

An optimization problem is a mathematical model, which contains, in addition to the previously described elements, one or multiple performance criteria. The performance criterion is called the objective function, which can be cost minimization, profit maximization, process efficiency, etc. If the problem has multiple selection criteria, the problem is classified as a multi-objective optimization (FLOUDAS, C. a, 1995).

Generally, an optimization problem can be associated with three essential categories:

(1) One or multiple objective functions to be optimized.

(2) Equality constraints (equations).

(3) Inequality constraints.

Categories (2) and (3) constitute the model of the process or equipment and category (1) is commonly called the economic model.

A feasible solution to an optimization problem is defined as a set of variables that meet the categories (2) and (3) with a desired degree of accuracy. An optimal solution is a set of variables satisfying the components of categories (2) and (3), as well as providing an optimal value for the function of category (1). In most cases, the optimal solution is one, in others, there are multiple solutions (EDGAR; HIMMELBLAU; LASDON, 2001).

2.3 Mixed Integer Optimization:

There are many problems regarding the design, operation, location, and established programming for the operation of process units, involve continuous and integer variables. Decision variables for which levels are a dichotomy (whether to install equipment, for example), are termed "0-1" or binary variables. In some cases, that integer variables are treated as continuous variables, without affecting significantly the value of the objective function (EDGAR; HIMMELBLAU; LASDON, 2001). In other words, are solve with the continuous variable and after the solution is obtained the objective function is recalculated.

The structure of a Mixed Integer Programming (MIP) problem, is presented as follows:

$$\begin{aligned} &\min_{x,y} && f(x,y) \\ &\text{subject to:} && h(x,y)=0 \\ & && g(x,y)\le 0 \\ & && x\in X\subseteq \Re^n \\ & && y\in Y \ \text{ integer} \end{aligned}$$

Where x, is a vector of n continue variables, y is an integer variables vector, $h(x,y) = 0$, represents m equality constraints, $g(x,y) \leq 0$, p inequality constraints and $f(x,y)$ the objective function.

A problem involving only integer variables is classified as an integer programming (IP) problem. The case of an optimization problem where the objective function and all constraints are linear, containing continuous and integer variables is classified as mixed integer linear

programming (MILP) and finally, problems involving discrete variables in which some of the functions are nonlinear are classified as mixed integer nonlinear programming (MINLP).

2.4 Process synthesis:

The main objective of process synthesis is to obtain systematically process diagrams for the transformation of available raw materials into desired products, that satisfy the following performance criteria: maximum profit and minimum cost, energy efficiency and good operability (FLOUDAS, C. a, 1995).

To determine optimal process diagrams according to the previous performance criteria imposed, the following questions need to be answered (FLOUDAS, C. a, 1995):

- Which process units should be included in the process diagram.
- How the involved process units should be interconnected.
- What are the optimum operating conditions and size of the selected process units.

2.5 Global Optimization:

A local optimum, of an optimization problem, is an optimal solution of a set of nearby set of solutions, while a global optimum is an optimal solution among all possible solutions. In Figure 1 point (X_2, Y_2), is a local optimum, and point (X_1, Y_1) is a local and a global optimum.

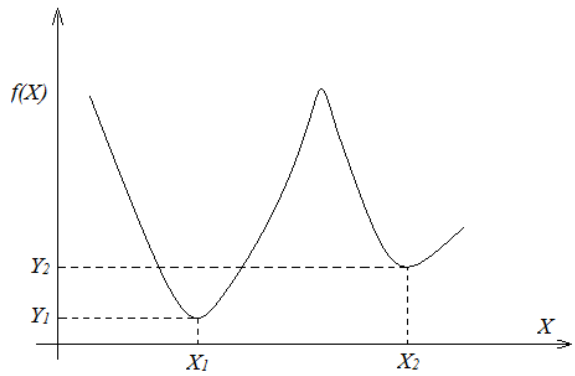

Figure 1. Global optimum vs, local optimum

Global optimization deals with computation and characterization of global solutions for continuous non-convex, mixed integer, algebraic differential, two-level, and non-factorizable problems. Given an objective function f that must be minimized and a set of equality and inequality constraints S, the main function of global deterministic optimization is to determine

(with theoretical guarantees) a global minimum for the objective function *f* subject to the set of constraints *S* (FLOUDAS, C. A.; GOUNARIS, 2009).

A function is convex (Figure 2), if the midpoint B of each chord A_1A_2 lies above the corresponding point A_0 of the graph of the function or coincides with this point. When solving minimization problems of continuous variables with convex viable regions and convex objective functions, any local minimum is a global minimum (EDGAR; HIMMELBLAU; LASDON, 2001).

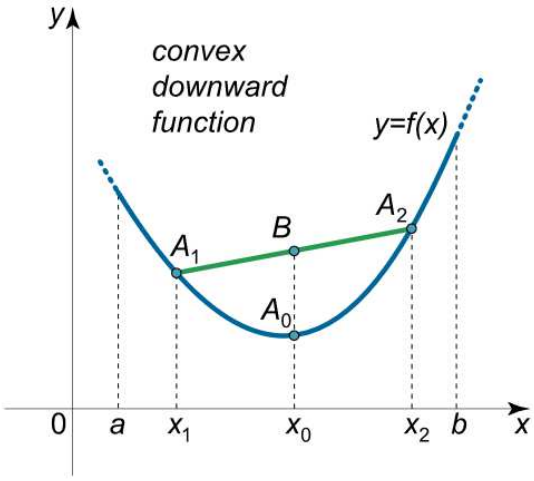

Figure 2. Convex function

The models that include non-linear equality constraints, such as those of mass balances (bilinear terms - concentration flow product), non-linear physical property relations, nonlinear blending equations, non-linear process models, and so, non-convexity that does not guaranty that any local minimum is a global minimum. Any problem containing discretely valued variables is a nonconvex problem (EDGAR; HIMMELBLAU; LASDON, 2001).

For global optimization, there are two categories of methods, deterministic methods and heuristic methods. Deterministic methods, when executed until they reach their termination criteria, allows to find a solution close to a global optimum and theoretically demonstrate that this optimal value corresponds to a global solution. Heuristic methods can find globally optimal solutions, but it is not theoretically possible to prove that the solution is a global solution (EDGAR; HIMMELBLAU; LASDON, 2001).

2.6 Desalination:

Desalination process is a relatively consolidated technology for removing dissolved ions in brackish water, seawater, or industrial effluents. This technique has allowed seawater to be used for industrial purposes as well as for human consumption or even for water reuse (KUCERA, 2014).

Desalination is seen as a relatively sustainable and viable technology to attain the need of water increasing demand. However, the high energy demand of the processes currently used combined to environmental concerns, water scarcity, high energy costs and the potential use of renewable energy sources for desalination it has revived research and development in water desalination.

Desalination has a great potential for development on a global scale. This is attributed to the fact that of the 71 largest cities in the world that do not have local access to new freshwater sources, 42 are located along the coasts, in addition, 2,400 million of the entire world population, representing 39% of the total, live at a distance of less than 100 km from the sea (GHAFFOUR; MISSIMER; AMY, 2013).

This shows the use of desalination technology in large proportions, to attain urban and industrial freshwater demand.

2.7 Desalination Technologies:

Commercially available desalination technologies can be classified into thermals and membranes, reverse osmosis (RO), multi-effect distillation (MED) and multi-stage flash (MSF) are the dominant technologies in the market, of which, reverse osmosis being the fastest growing application (SHATAT; RIFFAT, 2014).

The global desalination capacity in 2015 was 100 million m3/day. On a global scale, 68% of desalinated water is produced by membrane technologies, 30% by thermal technologies and the remaining 2% is produced with other technologies. Desalination water supplies are divided into 59% seawater, 22% ground brackish water, and the remainder, surface water, and effluents with some degree of salinity (GHAFFOUR et al., 2015).

The forecast for market growth for the following years is shown in Figure 3 and it is expected that by the year 2024 the desalination capacity will be close to 180 million m^3/day and by the year 2030 will be 280 million m^3/day.

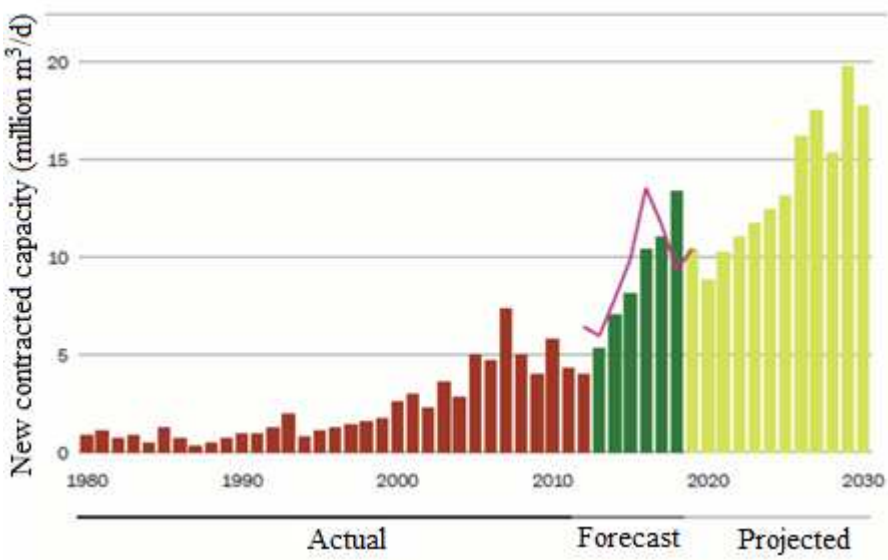

Figure 3. Desalination market growth forecasts (Desaldata.com)

Following are some generalities of the technologies that dominate the global market:

2.7.1 Multi-effect Distillation (MED):

Another water desalination technology is by means of the distillation separation process. MED occurs in a series of vessels or evaporators called effects, it uses the evaporation/condensation principle with a progressive reduction of the operational pressure of each of the effects. With this, the feed water can reach different boiling points without providing additional energy from the first effect. The feed stream is brought to its boiling point after being preheated. Salt water is sprayed onto the surface of pipes to promote its evaporation, these pipes have been heated with steam from an external source, usually, a dual-purpose generating plant (Figure 4).

The energy savings of the MED plant are related to the number of effects. The total number of effects is limited by the total available temperature range and the minimum allowed temperature difference between one effect and the next (KHAWAJI; KUTUBKHANAH; WIE, 2008).

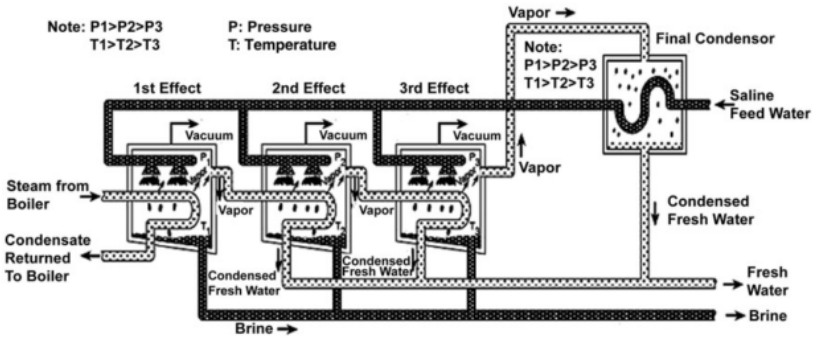

Figure 4. Multi-effect distillation (SHATAT; RIFFAT, 2014)

2.7.2 Multiple Stage Flash (MSF):

In this case, the multistage flash distillation process is based on the flash evaporation principle.

In the MSF process, the saline water is evaporated by reducing the pressure rather than raising the temperature. The economy of the MSF technology is achieved by regenerative heating where the saline water that is suffering the flash at each stage or camera flash is giving some of its heat to the brine stream being fed at this stage.

The heat of condensation released by water vapor condensing on each step increases gradually the temperature of the incoming stream. An MSF plant consists of heat input, heat recovery system, waste heat sections (KHAWAJI; KUTUBKHANAH; WIE, 2008). Figure 5 presents an MSF representation.

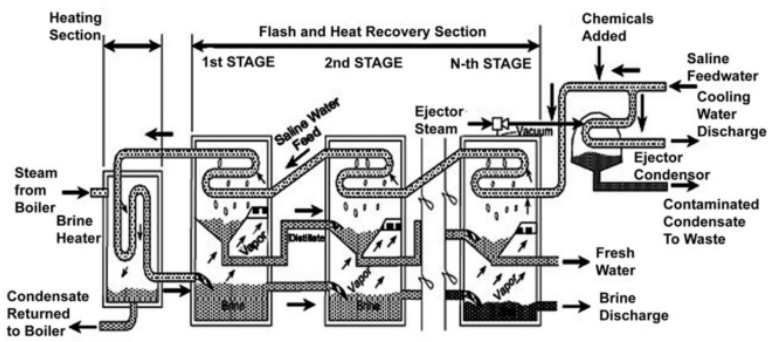

Figure 5. Multiple Stage Flash (SHATAT; RIFFAT, 2014)

Project and design of desalination plants are usually based on a series of environmental studies and engineering decisions such as: water source assessment (chemical composition, salinity, distance from the source to the plant), concentrate management options, pretreatment options, desalination technology selection (MSF, MED, RO, or others), plant capacity,

estimation of energy requirements, post-treatment requirements (if necessary), among others (VOUTCHKOV, 2012).

2.7.3 Reverse Osmosis (RO):

Water desalination by RO occurs when the feed solution is subjected to pressure larger than the value its osmotic pressure, causing the water ions diffusion through a semipermeable membrane, obtaining two streams: permeate (water desalted) and concentrated (a concentrated aqueous solution containing salts). The amount of desalinated water obtained will depend on the quantity and quality of the feed water, the quantity, and quality of the desired product, as well as the technology and types of membranes involved and the operating pressure.

A reverse osmosis desalination system usually has five components: a water supply system, a pre-treatment system, high-pressure pumping, arrangement of membrane modules and post-treatment. These components are referenced as reverse osmosis network (RON).

Prior to the reverse osmosis process, there are the pretreatment steps. Pre-treatment aims to remove suspended and colloidal solids to prevent fouling and biofilm growth on the surface of the membranes, which decrease the permeate flux. The high-pressure pump needs to provide sufficient pressure required to ensure the permeation of water through the membrane. Operating pressures depend on the concentration of salts in the water but typically range from 15-25 bar to brackish water and from 54-80 bar to seawater (SHATAT; RIFFAT, 2014).

Membrane modules arrangement consists of a number of pressure vessels in parallel, each of which containing a number of membrane modules in series, where the number of modules usually are 1 to 8 modules (Figure 10).

There are two types of market-leading desalination modules, hollow fiber modules, and spiral modules. Figure 6 shows a RO spiral wound module, which the membrane is used between two spacers. One of these serves as a collector channel for the permeate, while the other provides space for the feed solution to flow, as well as attempts to increase turbulence, decrease the concentration polarization and tendency to fouling. Usually, this type of membranes is composed of polyester support, a porous polysulfone intermediate layer and an outer thin layer of polyamide.

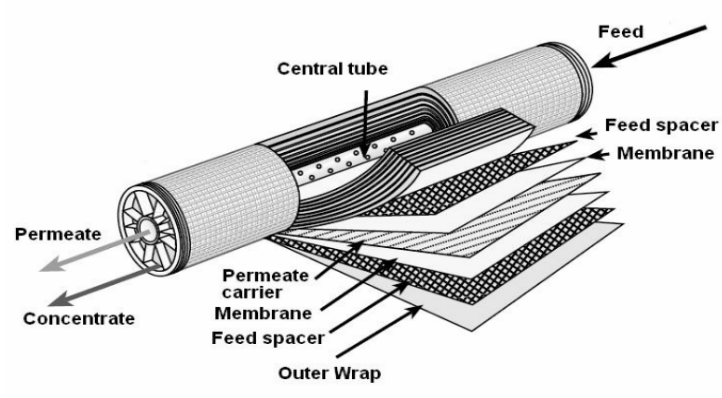

Figure 6. Spiral wound membrane module
(DOW WATER & PROCESS SOLUTIONS, 2011)

Since this work focuses on the use and modeling of this technology, more detail on the salt and water transport in reverse osmosis membranes is following:

The main transport properties of the processes that use pressure gradient as driving force are: permeate flux, rejection of a certain component present in the feed solution and recovery (HABERT; BORGES; NOBREGA, 2006).

The permeate flux (J) represents the volumetric water flowing through the membrane per unit of time and unit of permeation area. The permeate flux is a function of the membrane thickness, chemical composition of the feed, porosity, operating time and pressure across the membrane (SINCERO & SINCERO, 2003). For water desalination, there are two main fluxes, water, and salt (solute).

The model to describe the permeation mechanism used in this work is the solution-diffusion model. According to this mechanism, the water flux Jw, is linked to the pressure and concentration gradient across the membrane by the following equation:

$$J_W = A(\Delta p - \Delta \pi) \tag{1}$$

Where ΔP is the pressure difference across the membrane, $\Delta \pi$ is the osmotic pressure differential across the membrane and (A) is a constant (pure water permeability).

From this equation could see that when low pressure is applied ($\Delta P < \Delta \pi$) water flows from the dilute to the concentrated salt-solution side of the membrane by normal osmosis; when $\Delta P = \Delta \pi$ there is no flow, and when $\Delta P > \Delta \pi$, water flows from the concentrate site to the diluted side (desalination occurs).

The salt flux Js, is described by the equation:

$$J_S = B(C_F - C_P) \tag{2}$$

where (B) is the salt permeability constant and C_F and C_P, respectively, are the salt concentrations on the feed and permeate sides of the membrane.

From equations 1 and 2 could be observed that the water flux depends on the pressure, but the salt flux is independent of the operating pressure since it is diffusive.

Recovery is a measure of the membrane selectivity and usually it's calculated as a percentual relation between the produced permeate and the feed stream.

Temperature also affects both water and salt fluxes, since it affects the osmotic pressures calculations and the values of the parameters (A) and (B) usually given by the membrane fabricant and obtained in the laboratory.

So, the main operating parameters on membrane water and salt rejection are feed pressure, salt concentration of feed solution and temperature. In this work, the effect of the temperature is not considered (all problems solved at 25°C - standard conditions for the parameters (A) and (B) given by the membrane fabricant), the feed salt concentration becomes in an input parameter for a given problem living the pressure as the optimization variable.

In case of the RON arrangement where multiple membrane modules are used, the total number of modules and its configuration is also an optimization variable since it is related to the total membrane used and so to the total amount of fresh water produced.

In this work, for the transport phenomena model of the RO modules, the effect of the polarization of the concentration is also considered, a phenomenon that occurs when a solution permeates through a membrane selective to the solute, occurring an increase of solute concentration in the membrane/solution interface, causing an increase in the osmotic pressure of the solution near the membrane (C_F of the equation 2), and decrease in driving force for the separation and thus reducing the permeate flow (HABERT; BORGES; NOBREGA, 2006).

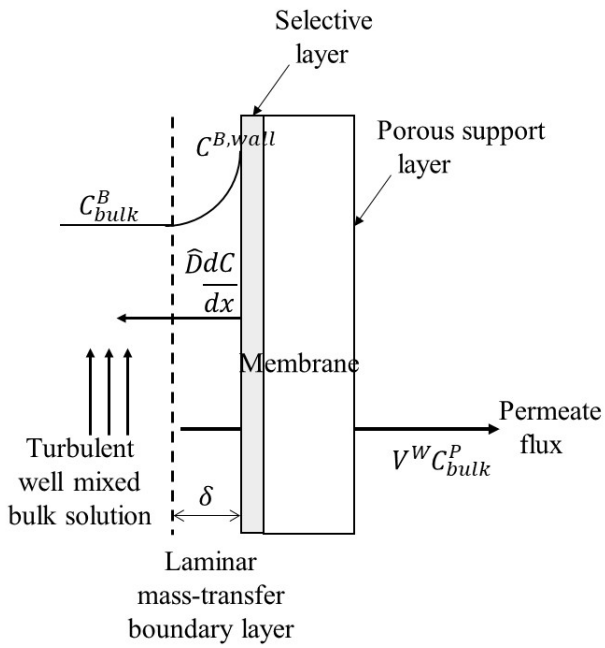

Figure 7. Concentration polarization – salt concentration gradients adjacent to the membrane (adapted from BAKER, 2004)

In Figure 7 are presented the salt concentration gradients adjacent to the membrane, for steady state, and so, the net salt flux at any point within the boundary layer must be equal to the permeate salt flux. This flux is the result of the convective salt flux towards the membrane minus the contra-diffusive salt flux from the membrane wall to the bulk solution. This means that the salt flux depends on the salt gradient concentration between the membrane wall salt concentration and the permeate salt concentration.

This effect modifies equation 2, to include the contra-diffusive flux and to consider the decrease of the driving force. It is presented in detail in the mathematical model in section 4.2.3.

2.7.4 Pressure Retarded Osmosis (RO):

Although pressure retarded osmosis is not especially a desalination technology, because it is more focused on taking the osmotic potentially of two different salinity streams to produce energy, it could be used in conjunction with reverse osmosis to propose a hybrid desalination process where the PRO serves to the RON as an energy recovery system (ERS), and also to deal with the brine disposal.

PRO is a membrane-based technology which uses a semipermeable membrane that separates two streams of different salinity (a low salinity solution and a high salinity pre-pressurized solution), allowing the low salinity solution to pass to the high salinity solution

side. The additional volume increases the pressure on this side, which can be depressurized by a hydro-turbine to produce power (HELFER; LEMCKERT; ANISSIMOV, 2014). Since PRO uses two streams with different osmotic potential to produce electrical power it can be aid to a RO network by using the brine reject of the RO as the high salinity stream, in case of the low salinity stream different authors has proposed the use of river water (NAGHILOO et al., 2015), wastewater retentate (WAN; CHUNG, 2015), treated sewage (SAITO et al., 2012) and so. With the aim of fully integrate RO and PRO technologies in this work pre-treated seawater as the low salinity stream was used.

As for RO and other membrane-based technology, the phenomena are described by determination of both salt and water fluxes, being the main operating variables the operating feed pressure, the feed solution (low salinity stream) flow and salt concentration, the draw solution (high salinity stream) flow and salt concentration, and temperature. In this work, as for RO optimization, the effect of temperature is not considered.

Membrane parameters used for modeling are also pure water permeability (*A)* and solute permeability (*B)*, and an additional parameter usually referred as solute resistivity for diffusion within the porous support layer (*K)* that group all the structural membrane parameters as thickness, tortuosity, and porosity of the support layer.

As for RO, another phenomenon which reduces the effective osmotic pressure difference across the membrane is the concentration polarization. As a result of water crossing the membrane, the solute is concentrated on the feed side of the membrane surface and diluted on the permeate side of the membrane surface (PRANTE et al., 2014).

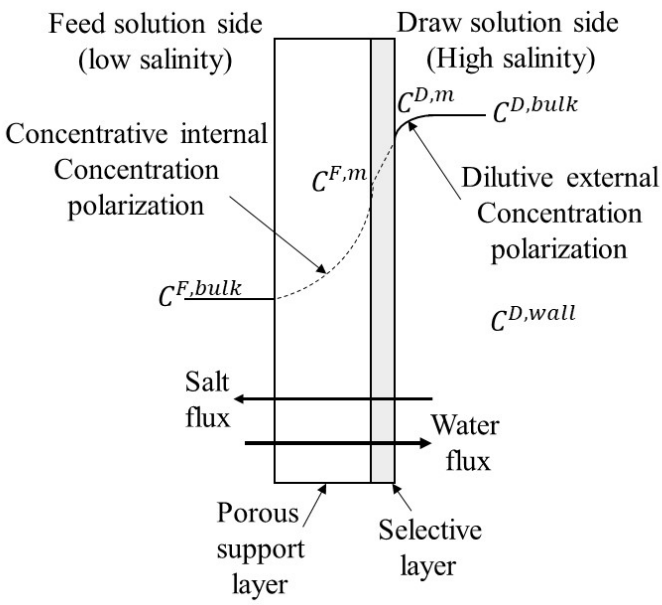

Figure 8. Osmotic driving force profiles for PRO. Internal and external polarization. (Adapted from (HELFER; LEMCKERT; ANISSIMOV, 2014)

Usually for PRO asymmetric membranes are used (a thin dense selective layer over a porous support layer), where the draw solution (high salinity) faces the selective layer and the feed solution (low salinity) faces the porous layer. As presented in Figure 8, two concentration polarization occurs, one externally on the selective layer side, that has a dilutive nature resulting from the solute been diluted on the draw solution side. Second concentration polarization occurs internally, and it has a concentrative nature resulting from the solute been concentrated inside the support layer of the membrane (ALTAEE; SHARIF, 2014). Both effects of internal and external concentration polarization are considered in the model presented and used in further sessions.

In PRO the power generated by unit membrane area is equal to the product of water flux and the pressure difference across the membrane:

$$W = \Delta p J_W = A(\Delta p - \Delta \pi)\Delta p \tag{3}$$

By differentiating Eq. (3) with respect to Δp, it can be shown that W reaches a maximum when $\Delta p = \frac{\Delta \pi}{2}$, being this condition the optimal pressure difference that maximizes the power generated (ACHILLI; CATH; CHILDRESS, 2009). This condition was used in this work to determinate the optimal operating feed pressure. The complete model is presented in section 4.3.1.

2.8 Challenges and advances in desalination:

The main challenges and recent advances in desalination are directly or indirectly related to the high energy cost of desalination. To meet desalination energy needs, researchers focused on cogeneration, the use of renewable energy sources, and optimization of design and operation. For desalination, power consumption is a key concern since energy costs constitute a major portion of the operating costs. (GHOBEITY; MITSOS, 2014).

Desalination plants have traditionally been designed by manufacturers using empirical and heuristic approaches (KUCERA, 2014). Membrane Manufacturers, for example, provide engineering simulation tools, like Osmose Reverse System Analyzer (ROSA) by Dow Chemicals, Rodesing and Rodata by Hydranautics, Ropro and Costpro by Koch Fluid systems, Winflows by osmonics and Wincarol and 2pflows by Toray, all for the evaluation of various types of membrane under several potential RO networks (RON). However, these tools have limited capabilities, and allow only typical designs and limited operating conditions, for example, constant operation.

The focus of advances has historically been the reduction of the specific capital cost of desalination through technological advances, for example, improvements in membranes and the development of low-cost heat exchangers for thermal desalination. However, advances in computer simulation and mathematical programming have opened new avenues for improving desalination technologies. Specifically, the development of new projects for desalination systems through experimentation is not practical because of the high costs of the technologies involved. The simulation of the design and, more specifically, the synthesis processes through systematic optimization are, however, relatively cheap, considering the advances in computational tools and numerical techniques.

In addition, optimization allows to explore various design configurations, for example, process conditions and connectivity of equipment that may initially appear as unpromising, but have not been evaluated or tested either experimentally or by simulation (GHOBEITY; MITSOS, 2014).

Computational advances and optimization-based models for solving complex problems, has provided opportunities to assess the performance of new systems, considering large numbers of design variables and minimum parameters for optimization problems. Specifically, nonlinear programming (NLP) has provided the opportunity to evaluate and develop new and innovative projects as well as operational strategies (DAHDAH; MITSOS, 2014).

2.9 Reverse osmosis networks design and some hybrid systems:

Following is a review of the state of the art and the main work developed, involving representation of desalination systems through superstructures, as well as the works involving hybrid systems of thermal technologies, membranes or mixture of both.

Evangelista (1985) presented a graphical method for the design of reverse osmosis plants, analogous to the stage calculations for unit operations, a turbulent regime, the polarization of concentration neglected, and constant mass transfer coefficient were considered.

El-Halwagi et al. (1992) were the first to employ the superstructure representation for a reverse osmosis network and developed a systematic procedure to solve the problem by minimizing the discharge stream.

Voros et al. (1996) employed the methodology presented by Halwagi (1992), modified for seawater desalination applications, the problem was formulated as an NLP, different structures were analyzed, and some optimum configurations were identified.

El - Halwagi et al. (1997) presented an iterative procedure to solve the problem of design and operation of a reverse osmosis network under different feeding conditions and maintenance routines. The problem was formulated as a MINLP, using the superstructure representation and using the Total Annualized Cost (TAC) as an objective function, the MINLP was solved using the LINGO software.

Maskan et al. (2000) formulated a multivariable nonlinear optimization problem for different configurations of the reverse osmosis network and different operating conditions. The objective function was the annual profit, and different two stages RO configurations were optimized.

Marcovecchio et al. (2005) presented a global optimization algorithm to find the optimum design and operating conditions of reverse osmosis networks for seawater desalination using hollow fiber modules and considering the polarization of the concentration. The proposed algorithm is deterministic and reaches finite convergence to the global optimum. The procedure is iterative and uses a bound contraction technique to accelerate convergence. The problem was solved using the CONOPT solver of the General Algebraic Modeling System (GAMS). They continued this work with a resolution of an MSF/RO hybrid system, proposed as an NLP problem and solved again with CONOPT/GAMS. However, due to the high non-convexity of the problem the global optimum could not be guaranteed (MARCOVECCHIO et al., 2005).

Vince et al. (2008) resolved a proposed RON as a MINLP problem, with multiple objective functions (economic, technological and environmental performance indicators) using an evolutionary algorithm as a solution method. In some cases, the authors found multiple solutions.

An extensive review of engineering approaches to the design of reverse osmosis plants for seawater desalination has been presented by KIM et al. (2009). The authors identified the factors that influence the total cost of the RO plant, considering feed, pre-treatment, process configuration, and post-treatment, specifically to the process configuration highlighted the following: type of modules used, the number and capacity of stages, the number of pressure vessels for each stage, mixture of different qualities of permeate and possibility of concentrate recycling.

Optimization tools have also been applied for thermal desalination systems. Kamali e Mohebinia (2008) used parametric optimization methods to increase the energy efficiency of MED-TVC (multi-effect distillation with vapor compression), Shakib et al. (2012) e Ansari et al.(2010) used genetic algorithms to improve the performance of a system MED-TVC coupled with a generation turbine and a nuclear power plant respectively.

Abdulrahim e Alasfour (2010) performed a multi-objective optimization study for a Multi-Stage Flash with concentrate recirculation (MSF-BR) and for a hybrid MSF/RO system, using a genetic algorithm as a solution strategy. The results showed that the optimization with multiple objectives tends to improve the performance of both systems.

Du et al. (2012) used a superstructure representation and formulated the optimization of a RON as a MINLP problem. It was solved using the GAMS software and the outer approximation algorithm, which consists of a series of iterations between NLP type subproblems and a MILP type master problem. The GAMS/CPLEX and GAMS/MINOS solvers were used to solve the MILP and NLP problems respectively. The global optimum condition could not be guaranteed according to the methods used, since changes in the initial values provided, produce different objective function results.

Park et al. (2012) used a Monte Carlo method to optimize forward osmosis and reverse osmosis (FO/RO) hybrid systems, to identify the parameters that affect the energy efficiency of the system. The authors found that the concentration polarization effect was the main influencing factor and decreasing it was essential to maximize energy efficiency.

Sassi e Mujtaba (2012) formulated a MINLP optimization problem for a RON to investigate the effects of temperature and concentration variations for the feed stream on the

optimum final structure. The objective of the optimization was to obtain the minimum total cost of the plant, and the solution method was the outer approximation method using the gPROMS software. The results revealed that the temperature and feed concentration have a significant impact on the resulting structure and operating conditions.

Skiborowski et al. (2012) used a superstructure representation for a multi-effect distillation/reverse osmose hybrid system (MED-RO). The problem is formulated as a MINLP, a generalized superstructure for the hybrid desalination plant is constructed and conceptual design considerations are used to reduce its complexity. The solvers GAMS/SBB and GAMS /SNOPT were used. They found that the hybrid system was not the best option than the individual MED or RO. The authors also solved a two-stage RON with commercial tool BARON to compute the global optimal. After a predefined user maximum time of 250 hours, it could not attain convergence, identifying the high structural complexity and non-linearity of the problem.

Alnouri e Linke (2012) used Microsoft Excel (LINDO) to get the optimal configuration of a RON considering generalized types of superstructures, in search of global optimal. The authors applied the approximation proposed to examples developed by other authors, the results were numerically close, but the computation times decreased considerably, however, the used structures end up being restricted.

Lu et al. (2013) used a simplified superstructure of RON, and formulated the problem as a MINLP, using as an objective function the Total Annual Cost (TAC).
The MINLP was solved using the GAMS software, and a previous simulation based on heuristics considerations were made to obtain initial conditions of the variables for the MINLP resolution. The type of membrane model used was an optimized variable.

Sassi e Mujtaba (2013) developed a MINLP model to evaluate boron rejection in an RO process, with the objective of analyzing and optimizing the design and operation of a RON, maintaining the desired levels of Boron in the desalinated water. The effects of seasonal variation of temperature and pH for seawater feed stream on boron removal were considered. The solution method was the outer approximation algorithm within software gPROMS. Results suggest that pH and temperature are determining factors for achieving the desired boron rejection.

Druetta et al. (2013) used structural optimization for thermal Multiple Effect Evaporation (MEE). The authors used flow patterns as optimization variables and using CONOPT / GAMS as a solution tool were able to reduce the specific area of heat exchange.

Saif et al. (2014) proposed a different operation of RON pressure vessels, considering the partial removal of permeate at different stages of membrane modules along the pressure vessel. Split partial second pass reverse osmoses (SPSPRO) is the concept and was formulated as a MINLP. The solver DICOPT/GAMS was used. Since the answer is a local optimum, it depends on the initial values provided. Although several starting points were used to solve the case studies the global solution could not be guaranteed.

Zak e Mitsos (2014) have used large-scale numerical simulation to evaluate several concepts of nontraditional hybrid thermal systems that mix the merits of MSF, MED, and MED-TVC, finding for certain operating conditions, thermal hybrids that present higher energy performance and required less area for heat exchange, compared to individual thermal systems, in addition to these results, the authors emphasize the need for more detailed models and more rigorous optimizations for future works that seek to propose new technological configurations.

Dahdah e Mitsos (2014) have used structural optimization to optimize the design of hybrid thermal systems, specifically to combine desalination systems with vapor compression systems, thus being able to propose new desalination technologies involving MSF, MED with TVC. The hybrid configurations reported higher performance (relation between the amount of distilled water obtained and energy supplied) and a smaller area of heat exchange compared to conventional configurations.

Jiang et al. (2014) proposed a process model for a RON based on solution-diffusion theory and mass transfer. The model is expressed in differential and algebraic equations with some equality and inequality constraints. The model was transformed by orthogonal collocation in an NLP model that was solved using the solver IPOPT/GAMS, the authors obtained profiles of the pressure and feed concentration, in these profiles an optimum value was identified in the energy consumption/desalinated water production curve, showing the potential of the optimization in the design of RON systems.

Wang et al. (2014) optimized the operation of a large reverse osmosis desalination plant (100.000 m^3/day), using an evolutionary differential algorithm. The scheduling operation problem was formulated as a MINLP, with the purpose to decrease the total cost of operation when the conditions for which the plant was designed changes over the years. For this case, when comparing the typical manual operation of the plant with the new operating routines suggested by the optimization method, the operating cost decreased by 5%.

Alamansoori e Saif (2014) formulated a MINLP problem for the optimization of a hybrid superstructure of Reverse Osmosis and Pressure Retarded Osmosis (RO/PRO) for the

simultaneous production of desalted water and electric energy. The MINLP problem was solved with the solver SBB/GAMS, being initialized with random starting points, the optimal values found are local optimum. The results show that the RO operation can be a viable source of the salinity gradient required by PRO for the generation of electric energy,

Malik et al. (2015) have used Aspen Custom Modeler (ACM) software for the modeling and simulation of an MSF/RO hybrid superstructure, to study and optimize various process configurations. The process conditions such as temperatures and pressures and the design variables such as MSF number of stages and the number of RON membrane modules were the optimization variables to minimize the objective function (energy cost per kilogram fed). The results suggest that the hybrid system is recommended for areas where high product quality is required.

Jiang et al. (2015) formulated a nonlinear optimization problem as a differential algebraic optimization problems (DAOPs), to reduce the operating costs of a full-scale RO plant for variations in operating conditions. The DAOPs problem was discretized to be transformed into an NLP problem that was resolved with the IPOPT/GAMS solver. The variables considered were feed temperature, seawater salinity, electricity cost, and desalinated water demand. The results showed that up to 26% cost savings can be achieved, compared to the conventional process.

Lee et al. (2015) proposed a Multi-stage vacuum membrane distillation (MVMD) and PRO hybrid system for the continuous production of desalinated water and electricity. The system is proposed and the equations that define the system are established by means of a numerical study, however, no optimization method was applied, resulting in a possibility of future study subject to optimization.

Du et al. (2015) present an optimization study of an SPSPRO structure, with the purpose of obtaining better qualities and permeate flows in the pressure vessel. The problem is proposed as a MINLP and solved with the DICOPT/GAMS solver. It was observed that the strategy does not guarantee the global optimum and the results depend strongly on the initial values provided. However, the authors report that the SPSPRO configuration could provide a lower cost, lower power consumption, and a smaller system size than the conventional process.

Wan e Chung (2016) have modeled a PRO / RO hybrid system with the option of closed-cycle operation, trying to reduce seawater pretreatment costs. The authors report that the specific energy consumption of a RO plant can be reduced by including PRO in the energy recovery system. In addition, they identified the need to determine the optimum operating

pressure of the PRO that maximizes the energy utilization and minimizes the power consumption of the PRO / RO hybrid system.

As previously mentioned this work aims to provide initial data systematically to reduce the computing time of a RON MINLP, since most of the aforementioned works, in some cases not give detail of how the preprocessing was done and how the initial data are obtained. The proposed methodology in this work is based in the use of surrogated models that replace the rigorous equations in a genetic algorithm that is used to provide the initial data used to solve the rigorous MINLP.

3 OBJECTIVES

3.1 General Objective:

The general objective of this work is to develop a mathematical model and optimization for the rigorous design of reverse osmosis networks and develop technological criteria, with no introduction of initial values by the user. This procedure is based on the hypothesis considering the possibility to achieve the optimal rigorous solution for the design of reverse osmosis networks with no initial values previously known.

3.2 Specific objectives:

- Construct a mathematical model for the design of reverse osmosis networks and formulate an optimization problem using the total annualized cost as the objective function and including the most relevant operational variables.
- Using a new deterministic optimization methodology to solve the optimization problem and obtain global solutions.
- Propose a new combined stochastic – deterministic optimization methodology to solve the optimization problem.
- Using the stochastic – deterministic methodology to explore the effect of the feed flow, seawater concentration, number of reverse osmosis stages, and the maximum number of membrane modules in each pressure vessel on the total annualized cost of the plant.
- Propose a reverse osmosis – pressure retarded osmosis hybrid superstructure where the PRO acts as an energy recovery unit and optimize it using the stochastic – deterministic methodology proposed.

4 METHODOLOGY

The problem of synthesizing a reverse osmosis network (RON) consist in propose a cost-effective network, including the optimum values for the number of reverse osmosis stages to be used, the number of pressure vessels per stage, the number of modules per pressure vessel, the number and type of auxiliary equipment, as well as the operational variables for all the devices of the network, so the RON structure is formulated as a MINLP with the total annualized cost TAC is used as an objective function.

To solve the problem of get optimal rigorous solutions for the design of RON, two methodologies are used, the first is based on a new deterministic bound contraction strategy not previously used for this kind of problems, and the second is a mixed stochastic – deterministic strategy that also use surrogated models to reduce the mathematical complexity and aims to reduce the computational effort.

Following are presented: the complete mathematical model, the metamodel construction, and both strategies solutions proposed.

4.1 Reverse osmosis network – superstructure representation:

Figure 9 presents a superstructure of two stages reverse osmosis network involving a set of parallel pressure vessels per reverse osmosis stage, high-pressure pumps and turbines. These are the units that are going to be considered in the superstructure representation. The feed flow enters a high-pressure pump and is sent to the first RO stage where it is separated into two streams: permeate and brine. The brine leaving the first RO stage feeds the second RO stage, but a fraction could be recycled. Recycling increases the velocity through the membrane module and thus reduces the concentration polarization. The final brine from the second stage goes to a turbine to recover the residual energy. The permeates from stages 1 and 2 are mixed to get the final permeate.

All the possible connections between the existing units are obtained by taking into account the following considerations:

- The feed stream (Fs) enters at atmospheric pressure, so it can't be connected directly to the RO stages.
- Blending the brine final stream (FB) is not necessary because there is no restriction of concentration discharge of the concentrated stream.
- The pressurization of product streams (FP and FB) is unnecessary.

- The permeate streams do not be blended with any brine streams.
- A pressurized stream does not be immediately depressurized.
- The heat transfer is not considered, so the feed temperature is just considered for the osmotic pressure calculations.

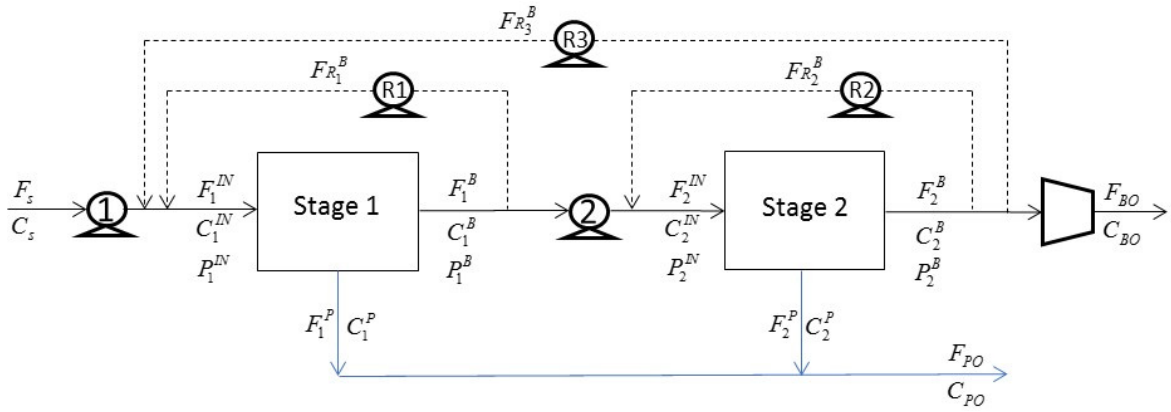

Figure 9. Superstructure of two stages Reverse Osmosis configuration

4.2 Reverse osmosis network – MINLP model:

The superstructure presented in Figure 9 is a simplified structure that represents the typical commercial set of a reverse osmosis plant, a general structure with all the possible connections between units could be seen on appendix 1, the model for the actual representation is composed by the mass balances, the reverse osmosis stage model, the transport phenomena model for each membrane module and the cost functions.

4.2.1 Mass Balances:

Following are presented the mass balances for a two reverse osmosis stage presented in Figure 9.

Global Balances:

$$F_S = \hat{F}_{PO} + F_{BO} \tag{4}$$

$$F_S C_S = \hat{F}_{PO} C_{PO} + F_{BO} C_{BO} \tag{5}$$

Recycle Balances:

$$F_1^{IN} = F_S + FR_1^B \tag{6}$$

$$F_1^{IN} C_1^{IN} = F_S C_S + FR_1^B C_1^B \tag{7}$$

$$F_2^{IN} = F_1^B - FR_1^B + FR_2^B \tag{8}$$

$$F_2^{IN} C_2^{IN} = F_1^B C_1^B - FR_1^B C_1^B + FR_2^B C_2^B \tag{9}$$

Balances for the outlet permeate stream:

$$\hat{F}_{PO} = \sum_{m=1}^{N_{RO}} F_m^P \tag{10}$$

$$\hat{F}_{PO} C_{PO} = \sum_{m=1}^{N_{RO}} F_m^P C_m^P \tag{11}$$

$$C_{PO} \leq C_P^{Max} \tag{12}$$

Balances for the outlet brine stream:

$$F_{BO} = \sum_{m=1}^{N_{RO}} F_m^{B-F_{BO}} + \sum_{t=1}^{N_T} F_t^{T-F_{BO}} \tag{13}$$

$$F_{BO} C_{BO} = \sum_{m=1}^{N_{RO}} F_m^{B-F_{BO}} C_m^B + \sum_{t=1}^{N_T} F_t^{T-F_{BO}} C_t^T \tag{14}$$

4.2.2 Reverse osmosis stages model:

A reverse osmosis stage is formed by a set of parallel pressure vessels, which separates equal fractions of the feed stream into permeate and brine streams. Each vessel is formed by a single or multiple membrane modules in series (Figure 10).

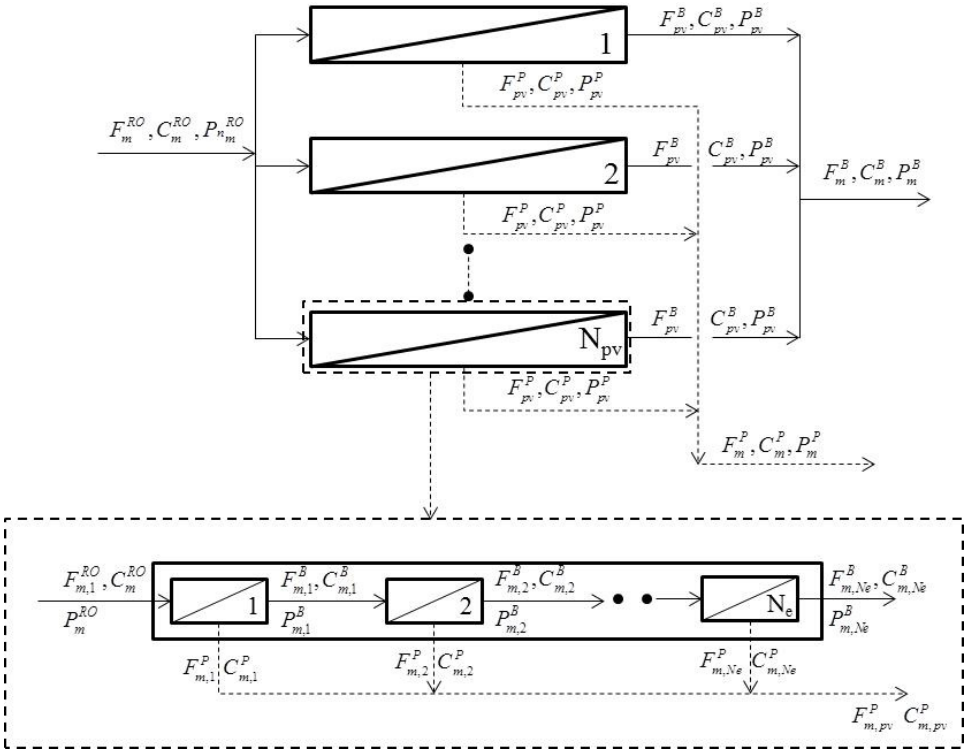

Figure 10. Structure of reverse osmosis (RO) stage and pressure vessel.

In this work spiral wound modules are used because of their high packing density and relatively low energy consumption. A diffusion model for spiral wound (SW) modules is presented below.

The feed of the RO stage is distributed equally to the N_{pv} pressure vessels of each stage:

$$F_m^{in} N_{pv_m} = F_m^{RO} \tag{15}$$

It was decided to make this a continuous variable to reduce the computation complexity, and the approximate result will be obtained by rounding the variable. Other authors also use the same concept, except Du et al. (2012), who used binaries to model the number of pressure vessels. In a later results analysis it will be presented the marginal effect of this assumption.

Since the inlet flow in a membrane module has physical constraints given by the manufacturer, the number of pressure vessels must respect the following restrictions (maximum and minimum permitted inlet flows)

$$F_m^{\min in} N_{pv_m} \leq F_m^{RO} \leq F_m^{\max in} N_{pv_m} \tag{16}$$

For the remaining $e = 2,...,Ne$ modules within each pressure vessel, the incoming properties are equal to those of the concentrated stream (brine) of the previous module, so the properties of the brine final stream are obtained from the last series module.

First module:

$$F_{m,1}^{Be} = F_m^{in} - F_{m,1}^{Pe} \tag{17}$$

$$F_{m,1}^{Be} C_{m,1}^{Be} = F_m^{in} C_m^{RO} - F_{m,1}^{Pe} C_{m,1}^{Pe} \tag{18}$$

Rest of the modules:

$$F_{m,e}^{Be} = F_{m,e-1}^{Be} - F_{m,e}^{Pe} - F_{m,e-1}^{O} \qquad \forall\ e \neq 1, \forall\ e \neq Ne \tag{19}$$

$$F_{m,e}^{Be} C_{m,e}^{Be} = F_{m,e-1}^{Be} C_{m,e-1}^{Be} - F_{m,e}^{Pe} C_{m,e}^{Pe} - F_{m,e-1}^{O} C_{m,e-1}^{Be} \quad \forall\ e \neq 1, \forall\ e \neq Ne \tag{20}$$

For the last membrane module, is written

$$F_{m,Ne}^{O} = F_{m,Ne-1}^{Be} - F_{m,Ne}^{Pe} - F_{m,Ne-1}^{O} \tag{21}$$

$$F_{m,Ne}^{O} C_{m,Ne}^{Be} = F_{m,Ne-1}^{Be} C_{m,Ne-1}^{Be} - F_{m,Ne}^{Pe} C_{m,Ne}^{Pe} - F_{m,Ne-1}^{O} C_{m,Ne-1}^{Be} \tag{22}$$

The final brine stream of the corresponding RO stage is obtained from:

$$F_m^{B} = N_{pv_m} \sum_{e=1}^{Ne} F_{m,e}^{O} \tag{23}$$

$$F_m^{B} C_m^{B} = N_{pv_m} \sum_{e=1}^{Ne} F_{m,e}^{O} C_{m,e}^{Be} \tag{24}$$

The flow of the permeate stream is obtained as follows:

$$F_m^{P} = N_{pv_m} \sum_{e=1}^{Ne} F_{m,e}^{Pe} \tag{25}$$

$$F_m^{P} C_m^{P} = N_{pv_m} \sum_{e=1}^{Ne} F_{m,e}^{Pe} C_{m,e}^{Pe} \tag{26}$$

Usually, the modules inside the pressure vessel are all connected in series. However, to make the model more general, the splits are added to remove some flowrate $F_{m,e}^{O}$ from each module. While, in general, this is acceptable, these flows that do not exist in industrial units, are introduced to determine the number of modules in each vessel. (Figure 11)

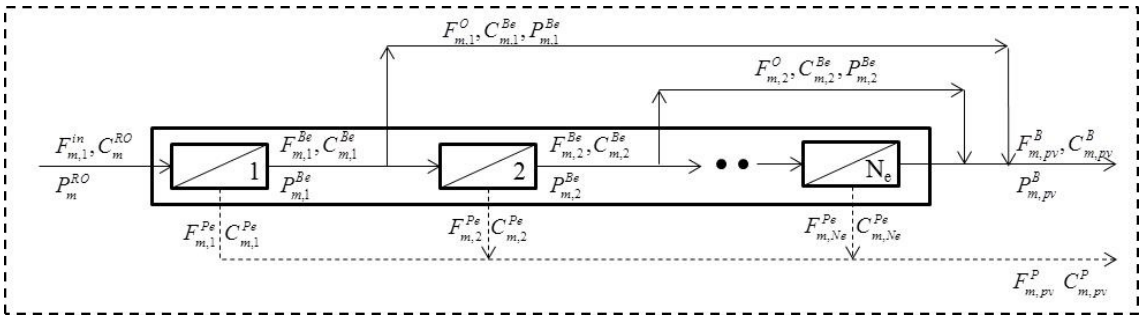

Figure 11. By-pass representation of a single pressure vessel.

For these, binary variables $y^{O}_{m,e}$ are further introduced which are one if a flow $F^{O}_{m,e}$ >0, and zero otherwise. Thus, the following equations are introduced:

$$F^{O}_{m,e} - \Gamma y^{O}_{m,e} \leq 0 \tag{27}$$

By adding the following equation, only one of the flows to be different from zero is forced:

$$\sum_{e=1}^{Ne} y^{O}_{m,e} = 1 \tag{28}$$

In addition, to make sure that $F^{Be}_{m,e} = F^{O}_{m,e}$ when $y^{O}_{m,e}$=1, is written:

$$(F^{Be}_{m,e} - F^{O}_{m,e}) - \Gamma(1 - y^{O}_{m,e}) \leq 0 \tag{29}$$

To obtain the number of modules *Ne* in a pressure vessel the next expression is used:

$$Ne = 1 * y^{O}_{m,1} + 2 * y^{O}_{m,2} + 3 * y^{O}_{m,3} + 4 * y^{O}_{m,4} + 5 * y^{O}_{m,5} + 6 * y^{O}_{m,6} + 7 * y^{O}_{m,7} + 8 * y^{O}_{m,8} \tag{30}$$

4.2.3 Membrane modules model:

To obtain the permeate flow and concentration of each membrane module a widely used and accepted solution-diffusion model is used (ALBASTAKI; ABBAS, 1999) which describes the transport phenomena of salt and water through the membrane (Figure 12). It depends on the pure water and salt permeabilities, which are parameters provided by the membrane modules manufactures (HABERT; BORGES; NOBREGA, 2006).

Another phenomenon that must be considered in the model is the polarization of the concentration since it decreases the permeate flux (BAKER, 2004). To describe this phenomenon is widely used the liquid film theory, being necessary to determine the mass transfer coefficient calculated as the relationship between the numbers of Sherwood, Reynolds, and Schmidt (SCHOCK; MIQUEL, 1987).

To determine the pressure drop of each module a correlation provided by the manufacturer is used (DOW WATER & PROCESS SOLUTIONS, 2011).

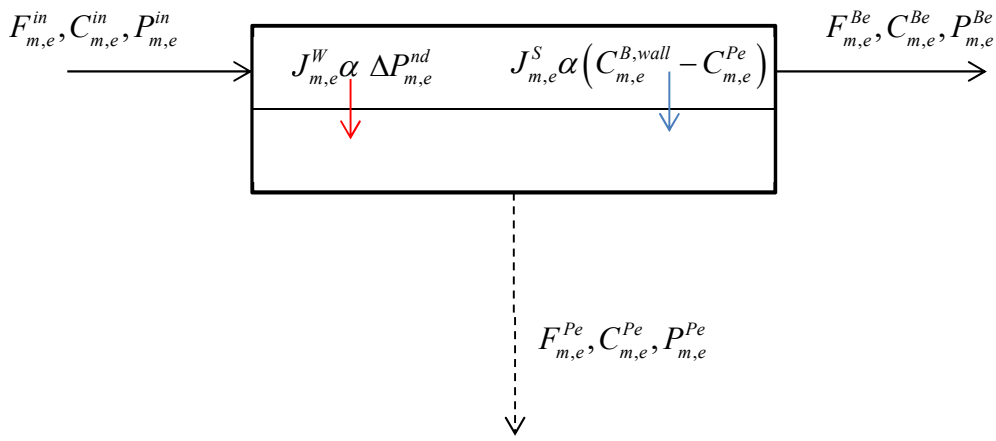

Figure 12. Permeate and brine transport through the membrane

Diffusion membrane module:

The flux for water $J^{W}_{m,e}$ for one membrane module is given by the following equations:

$$J^{W}_{m,e} = \hat{A}_{RO}\Delta P^{nd}_{m,e} \tag{31}$$

where $\hat{A}_{RO}$ is the pure water permeability, with the net driving pressure difference given by:

$$\Delta P^{nd}_{m,1} = Pn^{RO}_{m} - \frac{\Delta P^{B}_{m,1}}{2} - \hat{P}^{Pe}_{m,1} - (\pi^{B}_{m,1} - \pi^{P}_{m,1}) \tag{32}$$

$$\Delta P^{nd}_{m,e} = P^{Be}_{m,e-1} - \frac{\Delta P^{B}_{m,e}}{2} - \hat{P}^{Pe}_{m,e} - (\pi^{B}_{m,e} - \pi^{P}_{m,e}) \qquad \forall\ e \neq 1 \tag{33}$$

$$\pi^{B}_{m,e} = \hat{a}_{\pi}\hat{T}C^{Be}_{m,e} \tag{34}$$

$$\pi^{P}_{m,e} = \hat{a}_{\pi}\hat{T}C^{Pe}_{m,e} \tag{35}$$

where , $\hat{a}_{\pi} = 2.63\cdot 10^{-6}\left(\frac{bar}{K.ppm}\right)$. The brine pressure can be calculated as follows:

$$P^{Be}_{m,1} = Pn^{RO}_{m} - \Delta P^{B}_{m,1} \tag{36}$$

$$P^{Be}_{m,e} = P^{Be}_{m,e-1} - \Delta P^{B}_{m,e} \qquad \forall\ e \neq 1 \tag{37}$$

$$P^{B}_{m} = \sum_{e=1}^{Ne} y^{O}_{m,e}P^{Be}_{m,e} \tag{38}$$

Where $\Delta P^{B}_{m,e}$ is estimated from a SW RO membrane correlation given by the module producer:

$$\Delta P_{m,e}^{B} = 9532.4\left(\frac{F_{m,e}^{av}}{\hat{\rho}_{av}}\right)^{1.7} \tag{39}$$

$$F_{m,1}^{av} = \frac{F_{m}^{in} + F_{m,1}^{Be}}{2} \tag{40}$$

$$F_{m,e}^{av} = \frac{F_{m,e-1}^{Be} - F_{m,e-1}^{O} + F_{m,e}^{Be}}{2} \qquad \forall \;\; e \neq 1, e \neq Ne \tag{41}$$

$$F_{m,Ne}^{av} = \frac{F_{m,Ne-1}^{Be} - F_{m,Ne-1}^{O} + F_{m,Ne}^{O}}{2} \tag{42}$$

In turn, the flux solute $J_{m,e}^{S}$ is given by:

$$J_{m,e}^{S} = \hat{B}_{RO}\left(C_{m,e}^{B,wall} - C_{m,e}^{Pe}\right) \tag{43}$$

where $\hat{B}_{RO}$ is the salt permeability. The membrane wall concentration is:

$$C_{m,e}^{B,wall} = C_{m,e}^{Pe} + (C_{m,e}^{Be} - C_{m,e}^{Pe})e^{\frac{V_{m,e}^{w}}{ks_{m,e}}} \tag{44}$$

Where $ks_{m,e}\left(\frac{m}{s}\right)$ is the mass transfer coefficient, and $V_{m,e}^{w}\left(\frac{m}{s}\right)$ the permeation velocity, which are estimated using the following expressions:

$$ks_{m,e} = 0.04\,\mathrm{Re}_{m,e}^{0.75}\,\hat{S}c^{0.33}\,\frac{\hat{D}}{\hat{d}} \tag{45}$$

$$V_{m,e}^{w} = \frac{J_{m,e}^{W} + J_{m,e}^{S}}{\hat{\rho}_{P}} \tag{46}$$

$\mathrm{Re}_{m,e}$, Sc , $\hat{D}$ and $\hat{d}$ are the Reynolds, Schmidt, salt diffusivity, and feed space thickness, respectively. They are given by:

$$\mathrm{Re}_{m,e} = \frac{\hat{d}_{h} U_{m,e}^{s} \hat{\rho}}{\hat{\mu}} \tag{47}$$

$$\hat{S}c = \frac{\hat{\mu}}{\hat{\rho}\hat{D}} \tag{48}$$

The hydraulic diameter $\hat{d}_{h}$ of a spiral wound module used to calculate the Reynolds number depends on the channel height $\hat{h}_{sp}$, the specific surface area of the spacer $\hat{S}_{sp}$ and the void fraction $\hat{\varepsilon}$ (Figure 6):

$$\hat{d}_h = \frac{4\hat{\varepsilon}}{\frac{2}{\hat{h}_{sp}} + (1-\hat{\varepsilon})\hat{S}_{sp}} \tag{49}$$

The superficial velocity $U^s_{m,e}$ depends on the average flow rate $F^{av}_{m,e}$, the density, and the feed cross-section open area $\hat{S}_{fc}$.

$$U^s_{m,e} = \frac{F^{av}_{m,e}}{\hat{\rho}\hat{S}_{fc}} \tag{50}$$

$$\hat{S}_{fc} = \hat{w}_L \hat{n}_L \hat{h}_{sp} \tag{51}$$

The feed cross-section open area is the product of the membrane leaf width $\hat{w}_L$, the number of leaves $\hat{n}_L$ and the spacer height $\hat{h}_{sp}$.

Finally, the permeate concentration and flow rate are:

$$C^{Pe}_{m,e} = \frac{J^S_{m,e}}{V^W_{m,e}} * 1000 \tag{52}$$

$$F^{Pe}_{m,e} = V^W_{m,e} \hat{S}_{mem} \hat{\rho}_P \tag{53}$$

$$\hat{S}_{mem} = \hat{n}_L \hat{l}_L \hat{w}_L \tag{54}$$

Where $\hat{n}_L$ is the number of leaves, $\hat{l}_L$ is the effective length and $\hat{w}_L$ the width of the module.

To avoid numerical problems, caused by zero values for non-existing membrane modules in a pressure vessel the flux, a binary variable $y^{nd}_{m,e}$ is introduced in the water flux $J^W_{m,e}$ expression as follows:

$$J^W_{m,e} = \hat{A}_{RO} \Delta P^{nd}_{m,e} y^{nd}_{m,e} \tag{55}$$

The next constraint, guarantees that the binary variable $y^{nd}_{m,e}$ takes a value of zero if a flow $F^{av}_{m,e} = 0$, and one otherwise.

$$\sum_{e'=1}^{e-1} y^O_{m,e'} = (1 - y^{nd}_{m,e}) \tag{56}$$

Indeed, when the flux has been diverted in the previous vessel, the summation will become one and $y_{m,e}^{nd}$ will become zero. Before the flow is diverted, the summation is zero and $y_{m,e}^{nd}$ will be forced to one.

Now the following change of variable is introduced:

$$w_{m,e}^{nd} = \Delta P_{m,e}^{nd} y_{m,e}^{nd} \tag{57}$$

So, the water flux expression $J_{m,e}^{W}$ turns into:

$$J_{m,e}^{W} = \hat{A}_{RO} w_{m,e}^{nd} \tag{58}$$

With the corresponding set of equations, to deal with the product of a binary and a continuous variable, as follows:

$$w_{m,e}^{nd} - \Gamma^{nd} y_{m,e}^{nd} \leq 0 \tag{59}$$

$$w_{m,e}^{nd} \geq 0 \tag{60}$$

$$(\Delta P_{m,e}^{nd} - w_{m,e}^{nd}) - (1 - y_{m,e}^{nd}) \leq 0 \tag{61}$$

$$\Delta P_{m,e}^{nd} - w_{m,e}^{nd} \geq 0 \tag{62}$$

Now for the membrane wall concentration, because of the mass transfer coefficient $ks_{m,e}\left(\frac{m}{s}\right)$, could take zero values when there is no flux through the membrane module, the expression is re-written with the following change of variable:

$$C_{m,e}^{B,wall} = C_{m,e}^{Pe} + (C_{m,e}^{Be} - C_{m,e}^{Pe}) e^{\alpha_{m,e}} \tag{63}$$

Where:

$$\alpha_{m,e} ks_{m,e} = V_{m,e}^{w} \tag{64}$$

4.2.4 Costs and objective function:

The following economic model is based in the one proposed by Malek et al. (1996).

Objective function

Minimize the Total Annualized Cost (TAC), given by:

$$TAC = AOC + ccf \cdot TCC \tag{65}$$

where $ccf = \frac{(ir+1)^{t_1} i}{(ir+1)^{t_1} - 1}$. In turn,

$$TCC = 1.25\ (1.15 CC_{equip}) \tag{66}$$

The equipment cost is given by:

$$CC_{equip} = CC_{swip} + CC_{HPP} + CC_T + CC_{mem} + CC_{pv} \tag{67}$$

The salted water intake and pretreatment system cost:

$$CC_{swip} = 996(24(Q_{SW-IN}))^{0.8} \tag{68}$$

where Q_{SW-IN} is the feed flow rate to the system in m^3/h.

Cost of pump and turbines:

$$CC_{HPP} = 52\sum_p (\Delta P_p^{HPP} Q_p^{HPP}) \tag{69}$$

$$CC_{HPPR} = 52\sum_m (\Delta P_m^{HPPR} Q_{R_m}) \tag{70}$$

$$CC_T = 52\sum_t (\Delta P_t^T Q_t^T) \tag{71}$$

where $\Delta P_p^{HPP}, Q_p^{HPP}$, ΔP_m^{HPPR}, Q_{R_m} and ΔP_t^T, Q_t^T are the pressure drop in bar and flow rate in m^3/h for the high-pressure pump, recycle pump and turbine respectively. It should be noted that this cost of capital is linear with power, a known shortcoming of previous models because it cannot capture the nonlinear behaviors of costs (GUTHRIE, 1969). It will be discussed the impact of this assumption in the results section.

Membrane module cost:

$$CC_{mem} = \sum_{m=1}^{N_{RO}} N_{pv_m} Ne_m c_{mem} \tag{72}$$

Pressure vessels cost:

$$CC_{pv} = \sum_{m=1}^{N_{RO}} N_{pv_m} c_{pv} \tag{73}$$

Annual operational costs:

$$AOC = OC_{lab} + OC_{chem} + OCm + OC_{memr} + OC_{ins} + OC_{pow} \tag{74}$$

Labor cost

$$OC_{lab} = c_{lab} Q_P t_a \tag{75}$$

where the permeate production rate Q_P and the annual operational time t_a are used.

Cost of chemicals:

$$OC_{chem} = 0.018 Q_{SW-IN} t_a \tag{76}$$

Cost of replacement and maintenance:

$$OCm = 0.01 TCC \tag{77}$$

Membrane replacement cost:

$$OC_{memr} = 0.2 CC_{mem} \tag{78}$$

Insurance costs:

$$OC_{ins} = 0.005 TCC \tag{79}$$

Electric energy costs:

$$OC_{pow} = C_{en}(PP_{SWIP} + PP_{RO}) t_a \tag{80}$$

Energy consumed for intake and pre-treatment system:

$$PP_{SWIP} = \frac{1}{36} \frac{Q_{SW-IN} \Delta \hat{P}_{SWIP}}{\hat{\eta}_{SWIP}} \tag{81}$$

Electric energy consumed by the reverse osmosis plant:

$$PP_{RO} = \frac{1}{36} \left(\sum_p \frac{\Delta P_p^{HPP} Q_p^{HPP}}{\hat{\eta}_{HPP}} + \sum_m \frac{\Delta P_m^{HPPR} Q_{R_m}}{\hat{\eta}_{HPPR}} - \sum_t \Delta P_t^T Q_t^T \hat{\eta}_T \right) \tag{82}$$

4.3 Hybrid reverse osmosis - pressure retarded osmosis superstructure

Figure 13 presents a reverse osmosis network with two stages, pumps, and turbine where the pressure retarded osmosis unit uses the brine stream of the second RO stage after passing through the turbine, as draw solution (the one with high osmotic potential) and some pre-treated seawater stream as a feed solution (low salinity potential). From now, this arrangement is mentioned in this work as RO+PRO configuration 1.

Figure 14 presents an RO network where the PRO also uses the brine from the second stage after pressure conditioning by turbine as draw solution, but this time the pre-treated

seawater stream is divided in two, the one serving to the PRO unit as feed solution, and a second part that is by-passed through the PRO unit to be recombined with the low salinity side output solution, and afterward enters the RO first stage. This arrangement will be referred from now as RO+PRO configuration 2.

In both configurations, the PRO unit consists of a parallel membrane module arrangement where both entering flows (draw and feed solutions) are distributed equally to the N_{PRO} vessels as presented in Figure 15.

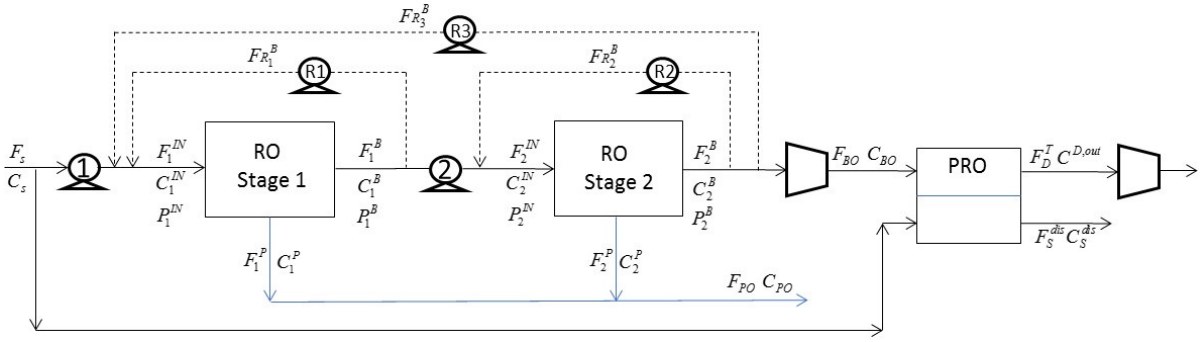

Figure 13. Superstructure of RO+PRO (Configuration 1).

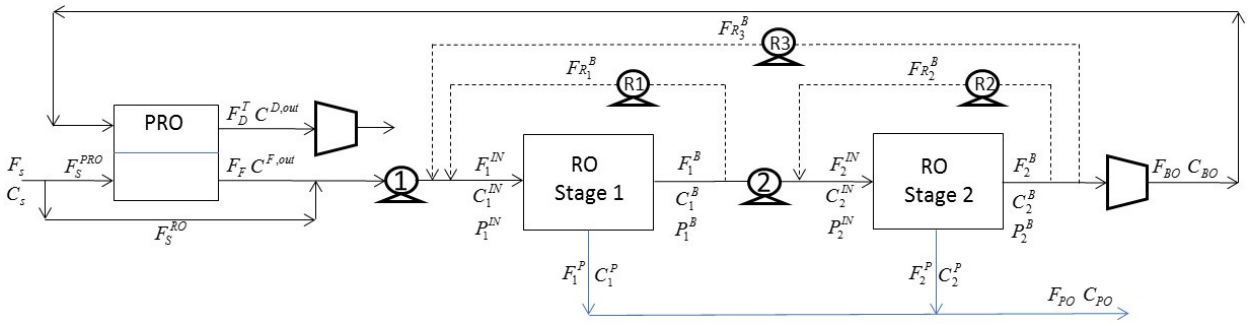

Figure 14. Superstructure of a RO+PRO (Configuration 2).

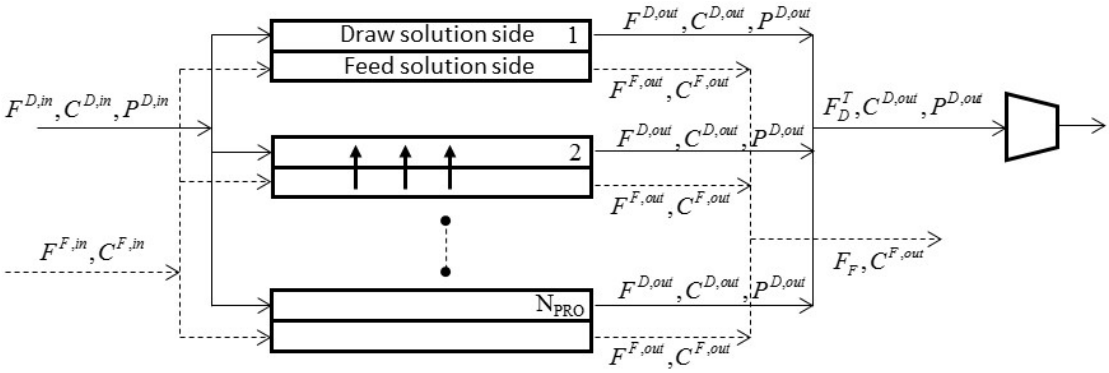

Figure 15. PRO unit arrangement.

4.3.1 RO+PRO mathematical model

Now the equations of the rigorous MINLP RO+PRO model are presented.

Global Balances:

$$F_S = \hat{F}_{PO} + F_D^T \tag{83}$$

$$F_S C_S = \hat{F}_{PO} C_{PO} + F_D^T C^{D,out} \tag{84}$$

Balances for the outlet permeate stream:

$$\hat{F}_{PO} = \sum_{m=1}^{N_{RO}} F_m^P \tag{85}$$

$$\hat{F}_{PO} C_{PO} = \sum_{m=1}^{N_{RO}} F_m^P C_m^P \tag{86}$$

$$C_{PO} \leq C_P^{Max} \tag{87}$$

Pressure retarded osmosis unit model: The feed (high and low salinity flows) of the PRO unit are distributed in N_{PRO} parallel membrane modules:

$$F_D = F^{D,in} N_{PRO} \tag{88}$$

$$F_S^{PRO} = F^{F,in} N_{PRO} \tag{89}$$

The high salinity flow leaving each membrane module is driven to a turbine to generate electrical power:

$$F_D^T = F^{D,out} N_{PRO} \tag{90}$$

The low salinity output flow is driven to the final discharge in case of RO+PRO configuration 1:

$$F_S^{dis} = F^{F,out} N_{PRO} \tag{91}$$

For the RO+PRO configuration 2, the low salinity output flow is mixed with the remaining by-passed seawater flow:

$$F_F = F^{F,out} N_{PRO} \tag{92}$$

$$F_S = F_S^{PRO} + F_S^{RO} \tag{93}$$

$$F_1^{IN} = F_F + F_S^{RO} \tag{94}$$

$$F_1^{IN} C_1^{IN} = F_F C^{F,out} + F_S^{RO} C_S \tag{95}$$

The inlet flows of a PRO membrane module are restricted to a specific range by the commercial provider:

$$F^{D,in\min} N_{PRO} \leq F^{D} \leq F^{D,in\max} N_{PRO} \tag{96}$$

$$F^{F,in\min} N_{PRO} \leq F_S^{PRO} \leq F^{F,in\max} N_{PRO} \tag{97}$$

The output conditions for the high salinity (draw solution) side:

$$F^{D,out} = F^{D,in} + J_W^{PRO} \hat{S}_{mem}^{PRO} \tag{98}$$

$$C^{D,out} = \frac{F^{D,in} C^{D,in} - J_S^{PRO} \hat{S}_{mem}^{PRO}}{F^{D,out}} \tag{99}$$

Output conditions for the low salinity (feed solution) side:

$$F^{F,out} = F^{F,in} - J_W^{PRO} \hat{S}_{mem}^{PRO} \tag{100}$$

$$C^{F,out} = \frac{F^{F,in} C^{F,in} + J_S^{PRO} \hat{S}_{mem}^{PRO}}{F^{F,out}} \tag{101}$$

Where $\hat{S}_{mem}^{PRO}$, is the PRO membrane area, and the PRO water flux J_W^{PRO}, considering internal and external polarization and the solute reverse flux could be obtained from:

$$J_W^{PRO} = \hat{A}_{PRO} \left(\frac{1}{2} \frac{\pi^D \exp\left(-\frac{J_W^{PRO}}{k^{PRO}\rho}\right) - \pi^F \exp\left(\frac{J_W^{PRO}\hat{K}}{\rho}\right)}{1 + \frac{\hat{B}_{PRO}}{J_W^{PRO}} \left[\exp\left(\frac{J_W^{PRO}\hat{K}}{\rho}\right) - \exp\left(-\frac{J_W^{PRO}}{k^{PRO}\rho}\right) \right]} + \Delta P^D \right) \tag{102}$$

where $\hat{A}_{PRO}$ is the pure water permeability, $\hat{B}_{PRO}$ is the salt permeability and $k^{PRO}\left(\frac{m}{s}\right)$ is the mass transfer coefficient that could be estimated as:

$$k^{PRO} = 0.2\,\mathrm{Re}^{0.57}\,\hat{S}c^{0.40}\,\frac{\hat{D}}{\hat{d}_h} \tag{103}$$

where $\mathrm{Re}_{m,e}$, Sc, $\hat{D}$ and $\hat{d}_h$ are the Reynolds, Schmidt, salt diffusivity, and hydraulic diameter, respectively. They are given by:

$$\mathrm{Re} = \frac{\hat{d}_h U^s \hat{\rho}}{\hat{\mu}} \tag{104}$$

$$\hat{S}c = \frac{\hat{\mu}}{\hat{\rho}\hat{D}} \tag{105}$$

The superficial velocity $U^s_{m,e}$ depends on the average flow rate $F^{av}_{m,e}$, the density, and the feed cross-section open area $\hat{S}_{fc}$.

$$U^s = \frac{F^{av}}{\hat{\rho}\hat{S}_{fc}} \tag{106}$$

$$F^{av} = \frac{F^{D,in} + F^{D,out}}{2} \tag{107}$$

The parameter $\hat{K}$ is the solute resistivity for diffusion within the porous support layer and is defined by:

$$\hat{K} = \frac{\hat{t}\hat{\tau}}{\hat{D}\hat{\varepsilon}} = \frac{\hat{S}}{\hat{D}} \tag{108}$$

Where $\hat{t}$, $\hat{\tau}$, and $\hat{\varepsilon}$, are the thickness, tortuosity, and porosity of the support layer, respectively and $\hat{S}$ is known as the structural parameter.

According to Schock (SCHOCK; MIQUEL, 1987), for low Reynolds numbers (100<Re<1000) the local solution pressure losses in spiral wound modules can be calculated as (where ΔP^D is in pascals):

$$\Delta P^D = \frac{6.23\,\mathrm{Re}^{-0.3}(U^s)^2 L\rho}{2\hat{d}_h} \tag{109}$$

With the osmotic pressure of the draw and feed solution:

$$\pi^D = \hat{a}_\pi \hat{T} C^{D,b} \tag{110}$$

$$\pi^F = \hat{a}_\pi \hat{T} C^{F,b} \tag{111}$$

Calculated at bulk concentration conditions:

$$C^{D,b} = \frac{C^{D,out} + C^{D,in}}{2} \tag{112}$$

$$C^{F,b} = \frac{C^{F,out} + C^{F,in}}{2} \tag{113}$$

The reverse salt flux is given by:

$$J_S^{PRO} = \hat{B}_{PRO}\left(\frac{C^{D,b}\exp\left(-\frac{J_W^{PRO}}{\rho k^{PRO}}\right) - C^{F,b}\exp\left(\frac{J_W^{PRO}\hat{K}}{\rho}\right)}{1 + \frac{\hat{B}_{PRO}}{J_W^{PRO}}\left[\exp\left(\frac{J_W^{PRO}\hat{K}}{\rho}\right) - \exp\left(-\frac{J_W^{PRO}}{\rho k^{PRO}}\right)\right]}\right) \tag{114}$$

The reverse osmosis stages model is the same as presented in sections 4.2.2 and 4.2.3.

The objective function and the cost equations for the RO+PRO superstructure are essentially the same as presented in section 4.2.4 with the following modifications (all related with the additional costs associated with the PRO unit):

The equipment cost is given by:

$$CC_{equip} = CC_{swip} + CC_{HPP} + CC_{HPPR} + CC_{T} + CC_{mem} + CC_{pv} + CC_{Tpro} + CC_{mempro} + CC_{pvpro} \tag{115}$$

Additional required turbine:

$$CC_{Tpro} = 52(\Delta P^{Tpro} Q^{Tpro}) \tag{116}$$

Membrane module cost for PRO:

$$CC_{mempro} = \sum^{N_{PRO}} N_{pvpro} c_{mempro} \tag{117}$$

Pressure vessels cost for PRO:

$$CC_{pvpro} = N_{pvpro} c_{pvpro} \tag{118}$$

Annual operational costs:

$$AOC = OC_{lab} + OC_{chem} + OCm + OC_{memr} + OC_{ins} + OC_{pow} + OC_{mempro} \tag{119}$$

Membrane replacement cost for PRO:

$$OC_{mempro} = 0.2CC_{mempro} \tag{120}$$

Electric energy consumed by the RO+PRO plant:

$$PP_{RO} = \frac{1}{36}\left(\sum_{p} \frac{\Delta P_{p}^{HPP} Q_{p}^{HPP}}{\hat{\eta}_{HPP}} + \sum_{m} \frac{\Delta P_{m}^{HPPR} Q_{R_m}}{\hat{\eta}_{HPPR}} - \sum_{t} \Delta P_{t}^{T} Q_{t}^{T} \hat{\eta}_{T} - \Delta P^{Tpro} Q^{Tpro} \hat{\eta}_{T} \right) \tag{121}$$

4.4 MINLP problem statement

The mass balances of mixing and division nodes for the distribution box, the reverse osmosis stages model, the transport model for each module, the cost functions, the objective function, as well as all possible physical constraints (flow and concentration of permeate, maximum pressures and brine concentration allowed) form the proposed MINLP model for the optimization of a reverse osmosis network.

Thus, the optimization problem is state as the following considerations:

Given:

Feed water concentration, membrane module parameters to be used, permeate flow required, maximum salt concentration allowed for discharge stream, and energy costs.

Optimize:

Number of membrane modules in each pressure vessel, recycles, and operational variables (seawater flowrate, feed pressure for each RO stage, and inlet flow to the first membrane module).

To minimize:

Total annualized cost for the RO network, subject to process constraints: equality constraints such as model equations, and inequality constraints such as the limits of the optimization variables.

In case of the hybrid RO+PRO superstructure, the optimization problem statement is basically the same, it just includes the additional PRO membrane model equations and its respective operational parameters.

The data for the for spiral wound (SW) modules with FilmTec™ SW30HR-380 is presented in

Table 1, the membrane parameters for PRO are presented in Table 2, and the economic parameters are presented in Table 3.

Table 1. Reverse osmosis module parameters.

Parameter	Value
Effective area - S_{mem} (m^2)	35.33
Water permeability - A ($kg/m^2 \cdot s \cdot bar$)	2.4×10^{-4}
Salt permeability - B ($kg/m^2 \cdot s$)	2×10^{-5}
Diffusivity coefficient - D (m^2/s)	1.35×10^{-9}
Hydraulic diameter - dh (m)	9.35×10^{-4}
Feed cross-section open area - S_{fc} (m^2)	0.0147
Maximum inlet flow rate – F^{maxin} (kg/s)	5
Minimum inlet flow rate – F^{minin} (kg/s)	1

Table 2. Pressure retarded osmosis module parameters.

Parameter	Value
Effective area - S_{mem} (m^2)	37.6
Water permeability - A ($kg/m^2 \cdot s \cdot bar$)	1.2×10^{-3}
Salt permeability - B ($kg/m^2 \cdot s$)	4.57×10^{-4}
Feed space thickness - d (m)	2.5×10^{-3}
Diffusivity coefficient - D (m^2/s)	1.493×10^{-9}
Structural parameter - S (m)	340×10^{-6}
Hydraulic diameter - dh (m)	9.46×10^{-4}
Length of element - L (m)	2.25

Table 3. Economic parameters

Parameter	Value
Capital charge factor – ccf	0.088
Membrane unitary cost - C_{mem} (USD)	750
Pressure vessel unitary cost - C_{pvm} (USD)	1,000
Labor cost factor – C_{lab} (USD)	0.05
Annual operational time - t_a (h/y)	8,000
Pressure difference for intake - ΔP_{swip} (bar)	5
Energy price - C_{en} ($/kwh)	0.05
Intake pump efficiency - η_{swip}	0.75
High pressure pump efficiency - η_{swip}	0.75
Turbine efficiency - η_{swip}	0.75

4.5 Bound contraction methodology

The new bound contraction methodology for MINLP problems proposed by Faria; Bagajewicz, (2012), is going to be implemented for the RON rigorous design, it consists in using a MILP model as lower bound, which corresponds to a relaxed solution (linearized solution) of the original MINLP problem, constructed from the discretization or partitioning of some chosen variables.

Selected variables to be discretized are those that appear involved in a greater number of nonlinearities.

Once the variables are discretized in a fixed number of intervals, the bound contraction procedure is done using an interval elimination strategy.

The partition methodology generates linear models that guarantee to be local optima (lower bounds) of the problem.

To apply the bound contraction procedure, it is necessary to establish an upper bound to compare with the lower bound obtained from the MILP. The upper bound can be obtained using the original MINLP model initialized with the results of the linearized MILP model, which in many cases generates feasible solutions for the original MINLP problem, thus obtaining an upper bound for comparison.

Optimization strategy is presented as follows (FARIA; BAGAJEWICZ, 2012):

1. Construct a linearized model that corresponds to a lower bound for the problem. This model is obtained by partitioning some of the variables involved in bi-linearities (i.e., the product between concentrations and flows) and other possible non-linearities of the model.
2. Fixing the number of intervals for the partitioned variables.
3. Run the linear MILP model without forbidden any interval, identifying the interval where is located the answer for each of the discretized variables.
4. Use the results of the MILP model as initial values for the original MINLP model to get an upper bound.
5. If the difference between the objective values of the upper and lower bounds is lower than a tolerance ε, a global optimum was found, else continue to 6.
6. Run the linear MILP, this time excluding the interval containing the answer for the first partitioned variable.

7. If an infeasible solution, or feasible with an objective value greater than the actual upper bound are obtained, all the intervals that were not excluded are eliminated, and the surviving feasible interval is partitioned again.
8. Repeat steps 6 and 7 for the rest of the partitioned variables, one at the time.
9. Return to step number 3, a new iteration starts with the new contracted bounds.

Iterations are made until attaining convergence or until the bounds cannot be contracted anymore, in that case, there are two possibilities:

- Increase the number of intervals to a level at which the size of the intervals is small enough to generate a lower bound with an acceptable tolerance to the upper bound.
- Divide the problem into two or more subproblems using a strategy similar to the branch and bound procedures.

Figure 16 presents the bound contraction methodology summarized.

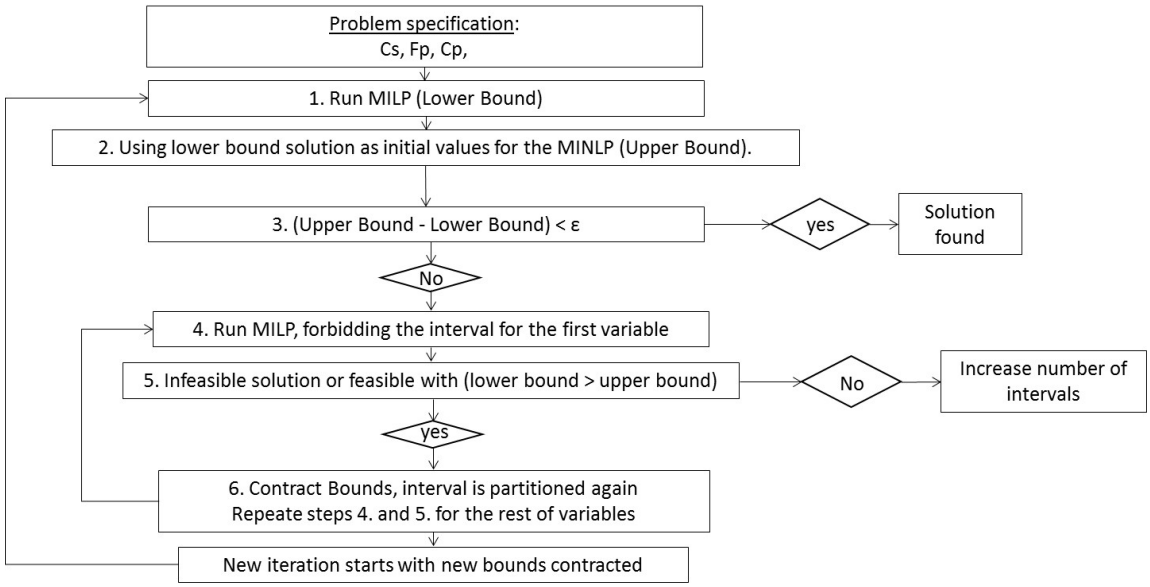

Figure 16. Bound contraction – interval elimination strategy.

4.6 Stochastic – deterministic methodology

A genetic algorithm is used to provide good initial values for the rigorous MINLP model, to compute optimal solutions. Two different solutions are tested, first the genetic algorithm using the rigorous equations is solved followed by the rigorous MINLP, and second, the use of rigorous equations of the model in the genetic algorithm is replaced by a metamodel and the solution is again used as initial values for the rigorous MINLP.

4.6.1 Reverse osmosis metamodel construction:

Simple quadratic polynomials are used as metamodels: The equations of the membrane diffusion model were solved numerically for different inlet conditions (values selected according to the bounds of the problem) to obtain a mesh of input-output data pairs. Two different regions were identified for the permeate concentration: A *Linear Region* and a *Non-Linear Region*, the expressions are presented next.

Linear Region: The concentration was adjusted to first order polynomial as follows:

$$C^{Pe} = K_1 + K_2 P^{IN} + K_3 C^{IN} + K_4 F^{IN} \tag{122}$$

Non-Linear Region: Permeate concentration was adjusted according to the mathematical expression presented below:

$$\begin{aligned} C^{Pe} &= K_1 + K_2 \left(P^{IN}\right)^2 + K_3 \left(C^{IN}\right)^2 + K_4 \left(F^{IN}\right)^2 + K_5 P^{IN} + K_6 C^{IN} \\ &+ K_7 F_{m,e}^{in} + K_8 \left(P^{IN}\right)^2 \left(C^{IN}\right)^2 + K_9 \left(P^{IN}\right)^2 \left(F^{IN}\right)^2 + K_{10} \left(C^{IN}\right)^2 \left(F^{IN}\right)^2 \\ &+ K_{11} \left(P^{IN}\right)^2 \left(C^{IN}\right)^2 \left(F^{IN}\right)^2 + K_{12} P^{IN} C^{IN} + K_{13} P^{IN} F^{IN} + K_{14} C^{IN} F^{IN} \\ &+ K_{15} P^{IN} C^{IN} F^{IN} \end{aligned} \tag{123}$$

The permeate flow was adjusted to a first-order polynomial for all the operation region:

$$\begin{aligned} F^{Pe} &= K_1 + K_2 P^{IN} + K_3 C^{IN} + K_4 F^{IN} + K_5 P^{IN} C^{IN} \\ &+ K_6 P^{IN} F^{IN} + K_7 C^{IN} F^{IN} + K_8 P^{IN} C^{IN} F^{IN} \end{aligned} \tag{124}$$

To obtain the coefficients of the metamodel a Diploid Genetic Algorithm (DGA) programmed in MATLAB® (THE MATHWORKS INC., 2016) was used. The Simulations were developed in a laptop with processor Intel(R) Core (TM) i7 – 3610QM CPU @ 2.3GHz (8 CPUs) with 8192MB of RAM. Each variable (C^{Pe}, F^{Pe}), was evaluated using the equations (122-124) for different inlet conditions (P^{IN}, C^{IN} and F^{IN}) using estimated coefficients, to generate the metamodel solutions mesh. The same inlet conditions were used with equations (31-54) to generate the rigorous solutions mesh. The fitness function that was minimized to obtain the coefficients is the following:

$$Fobj = \sum_{i}^{N} \left(V^{Rig} - V^{Met}\right)^2 \tag{125}$$

where V is the variable to be adjusted (C^{Pe}, F^{Pe}), N is the total number of points and the superscripts Rig. and Met. represent the value obtained from the rigorous method and the metamodel prediction, respectively.

4.6.2 Pressure retarded osmosis metamodel construction:

The approach to obtain the PRO metamodel is the same presented in the previous section, the adjusted variables were, the water and solute fluxes (J_W^{PRO}, J_S^{PRO}).

The expressions are presented as following:

$$J_W^{PRO} = K_1 + K_2 F^{D,in} + K_3 F^{F,in} + K_4 C^{F,in} \quad (126)$$

$$J_S^{PRO} = K_1 + K_2 F^{D,in} + K_3 F^{F,in} + K_4 C^{F,in} \quad (127)$$

This time the equations (92-114) are used to obtain the rigorous mesh, and equations (126-127) with estimated coefficients are used to generate the metamodel solution mesh, once again equation (125) was used to fitting the coefficients minimizing the square difference between rigorous and metamodel mesh.

4.6.3 Genetic Algorithm:

The diploid genetic algorithm code used for both strategies (using rigorous equations and the metamodels equations as well) was the same used to obtain the metamodel coefficients and it follows the description given by Fonteix et al., (1995). The method tends to imitate principles of organic evolution processes as rules for an optimization procedure, this is based in generic concepts such as population, recombination, and mutation as evolution rules to guide the optimum search.

The parameters used were 1000 individuals, 10 generations, 100 survivors and 100 mutants, for both strategies.

The GA has 4 random variables per stage: Flow entering each pressure vessel, pressure entering all pressure vessels, the number of modules in each stage and the recycling ratio. Once these are fixed for each individual of the population (1000), the respective model is solved by calculating first the sequence of membrane models using the transport phenomena equations or the metamodel expressions according to the case, then the recycle is calculated and the stage is recalculated based on the new inlet conditions of flow and concentration until convergence. The rest is the classical set up of a diploid GA algorithm. The rigorous model and the linear and

non-linear metamodels depending on the regions where they are the most accurate were considered. Indeed, the linear model was used when the ratio between inlet concentration and inlet pressure is lower than 950 and the nonlinear model when this ratio is equal or greater than 950, this boundary ratio was obtained from the model adjustment for different inlet flows.

The classical set up of the genetic algorithm used is presented in Figure 17.

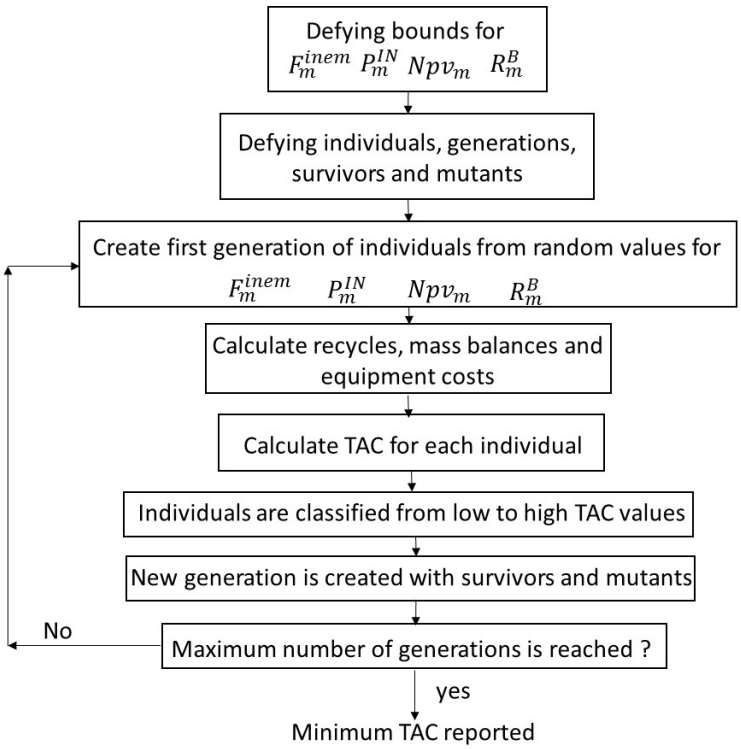

Figure 17. Genetic algorithm set up

4.6.4 Stochastic – deterministic methodology (flowchart):

A new solution methodology is proposed: a rigorous MINLP composed of the mass balances (Eqs. 4-14), the reverse stages model (Eqs. 15-30), the membrane transport phenomena (diffusion) model (Eqs. 31-54) and the economic model (Eqs. 65-82) solved with DICOPT (GROSSMANN et al., 2016) programmed in GAMS™ (ROSENTHAL, 2015) using the results obtained from the genetic algorithm as initial values. In particular, the MINLP is solved considering the number of pressure vessels (*Npv*) as a continuous variable and then is re-run fixing the *Npv* to the nearest integer value.

Figure 18 presents the summary of the proposed methodology, two stages are identified, the first stage consists in the pre-processing of the rigorous data to obtain the metamodel

coefficients, this is done only one time since the metamodel is adjusted to all the operational region. The second stage consists of the use of a genetic algorithm with the metamodel obtained in the first stage (pre-processing) to compute initial values used to solve the rigorous MINLP.

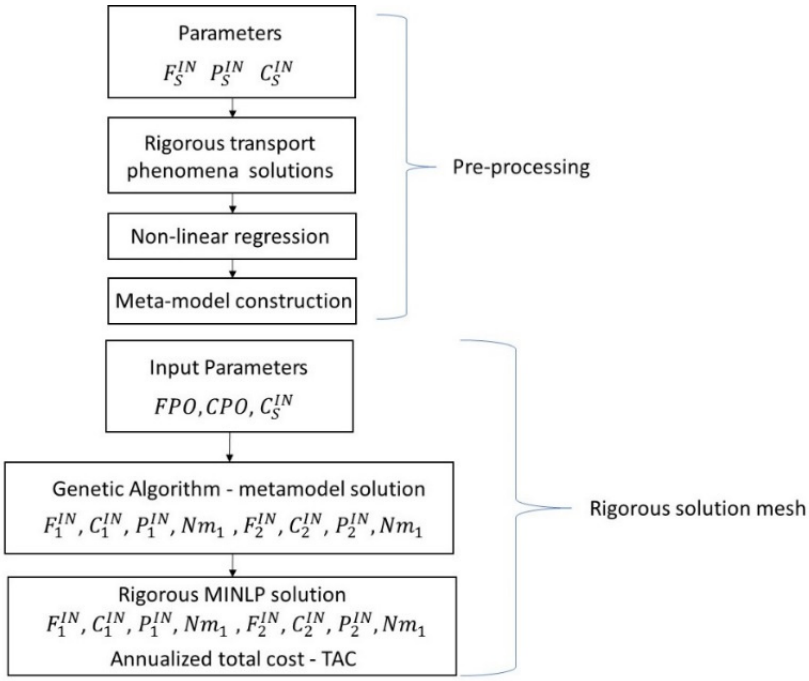

Figure 18. Stochastic – deterministic flowchart methodology

5 BOUND CONTRACTION METHODOLOGY RESULTS FOR REVERSE OSMOSIS NETWORKS

In an attempt to implement Rysia, the bound contraction strategy proposed by (FARIA; BAGAJEWICZ, 2012), there is a need to develop a relaxed version (linear lower bound) of the rigorous MINLP. To construct a MILP lower bound, the bilinear terms (product of flow and concentration) from the mass component balances are linearize partitioning one of the variables, and for the product of a continuous and binary variable, the direct partitioning procedure 1 (DPP1) is used, see appendix 2 for more details.

For the membrane diffusion model the presence of exponential terms made to select a different approach, which is the use of images of monotone functions in each domain variable's partition, as it was performed in several papers (CARVALHO; SECCHI; BAGAJEWICZ, 2016; KIM, S Y; BAGAJEWICZ, 2017; KIM, Sung Young et al., 2017; KIM, Sung Young; BAGAJEWICZ, 2016) that follow the one introducing Rysia (FARIA; BAGAJEWICZ, 2012).

To obtain the aforementioned images, after an algebraic manipulation of equations 31 – 54, the following expressions are obtained:

$$W1_{m,e} = W2_{m,e} - \hat{P}_{m,e}^{Pe} W3 - \hat{a}_{\pi} \hat{T} W4_{m,e} + \hat{a}_{\pi} \hat{T} W5_{m,e} * \hat{S}_{mem} 1000 \hat{\rho}_P + \hat{a}_{\pi} \hat{T} W6_{m,e} * 1000 \hat{\rho}_P \quad (128)$$

$$W7_{m,e} = \hat{b}\left(W8_{m,e} - W9_{m,e} \hat{S}_{mem} 1000 \hat{\rho}_P - W10_{m,e} (1000 \hat{\rho}_P) \right) \quad (129)$$

Where $W1_{m,e}$ to $W10_{m,e}$ are functions of different variables that need to be discretized, so it is necessary to determinate the monotonicity of these functions to see if they are increasing or decreasing functions. For these is necessary to differentiate each function respect to each variable and determinate according to the bounds of the variable if the value of the derivative is positive or negative.

Following is presented the obtained expressions for $W1_{m,e}$, just for illustrative purposes, the remaining variables and is corresponding expressions are available in appendix 3.

$$\sum_{d_{\Delta P}} \sum_{d_F} \sum_{d_{\hat{J}}} \begin{bmatrix} \Delta\hat{P}^{nd}_{m,e,d_{\Delta P}} \hat{F}^{in}_{m,e,d_F} (\hat{a}\Delta\hat{P}^{nd}_{m,e,d_{\Delta P}} + \hat{J}^{S}_{m,e,d_{\hat{J}}}) \\ -\Delta\hat{P}^{nd}_{m,e,d_{\Delta P}} (\hat{a}\Delta\hat{P}^{nd}_{m,e,d_{\Delta P}} + \hat{J}^{S}_{m,e,d_{\hat{J}}})^2 \hat{S}_{mem} \end{bmatrix} W^{\Delta\hat{P},\hat{F}in,\hat{J}s}_{m,e,d_{\Delta P},d_F,d_{\hat{J}}} \leq W1_{m,e}$$

$$W1_{m,e} \leq \sum_{d_{\Delta P}} \sum_{d_F} \sum_{d_{\hat{J}}} \begin{bmatrix} \Delta\hat{P}^{nd}_{m,e,(d_{\Delta P}+1)} \hat{F}^{in}_{m,e,(d_F+1)} (\hat{a}\Delta\hat{P}^{nd}_{m,e,(d_{\Delta P}+1)} + \hat{J}^{S}_{m,e,(d_{\hat{J}}+1)}) \\ -\Delta\hat{P}^{nd}_{m,e,(d_{\Delta P}+1)} (\hat{a}\Delta\hat{P}^{nd}_{m,e,(d_{\Delta P}+1)} + \hat{J}^{S}_{m,e,(d_{\hat{J}}+1)})^2 \hat{S}_{mem} \end{bmatrix} W^{\Delta\hat{P},\hat{F}in,\hat{J}s}_{m,e,d_{\Delta P},d_F,d_{\hat{J}}} \quad (130)$$

Where the product of binary variables is substituted by the following continuous variable and its corresponding set of equations:

$$W^{\Delta\hat{P},\hat{F}in,\hat{J}s}_{m,e,d_{\Delta P},d_F,d_{\hat{J}}} \leq y^{\Delta\hat{P}}_{m,e,d_{\Delta P}} \quad (131)$$

$$W^{\Delta\hat{P},\hat{F}in,\hat{J}s}_{m,e,d_{\Delta P},d_F,d_{\hat{J}}} \leq y^{\hat{F}in}_{m,e,d_F} \quad (132)$$

$$W^{\Delta\hat{P},\hat{F}in,\hat{J}s}_{m,e,d_{\Delta P},d_F,d_{\hat{J}}} \leq y^{\hat{J}s}_{m,e,d_{\hat{J}}} \quad (133)$$

$$W^{\Delta\hat{P},\hat{F}in,\hat{J}s}_{m,e,d_{\Delta P},d_F,d_{\hat{J}}} \geq y^{\Delta\hat{P}}_{m,e,d_{\Delta P}} + y^{\hat{F}in}_{m,e,d_F} + y^{\hat{J}s}_{m,e,d_{\hat{J}}} - 2 \quad (134)$$

To use the expressions presented in appendix 3, the partitioned variables appearing in equations needs are discretized according to:

$$\sum_{d_{\Delta P}} \Delta\hat{P}^{nd}_{m,e,d_{\Delta P}} y^{\Delta\hat{P}}_{m,e,d_{\Delta P}} \leq \Delta P^{nd}_{m,e} \leq \sum_{d_{\Delta P}} \Delta\hat{P}^{nd}_{m,e,(d_{\Delta P}+1)} y^{\Delta\hat{P}}_{m,e,d_{\Delta P}} \quad (135)$$

$$\sum_{d_{\hat{J}}} \hat{J}^{S}_{m,e,d_{\hat{J}}} y^{\hat{J}s}_{m,e,d_{\hat{J}}} \leq J^{S}_{m,e} \leq \sum_{d_{\hat{J}}} \hat{J}^{S}_{m,e,(d_{\hat{J}}+1)} y^{\hat{J}s}_{m,e,d_{\hat{J}}} \quad (136)$$

$$\sum_{d_F} \hat{F}^{in}_{m,e,d_F} y^{\hat{F}in}_{m,e,d_F} \leq F^{in}_{m,e} \leq \sum_{d_F} \hat{F}^{in}_{m,e,(d_F+1)} y^{\hat{F}in}_{m,e,d_F} \quad (137)$$

$$\sum_{d_C} \hat{C}^{in}_{m,e,d_C} y^{\hat{C}in}_{m,e,d_C} \leq C^{in}_{m,e} \leq \sum_{d_C} \hat{C}^{in}_{m,e,(d_C+1)} y^{\hat{C}in}_{m,e,d_C} \quad (138)$$

$$\sum_{d_P} \hat{P}^{in}_{m,e,d_P} y^{\hat{P}in}_{m,e,d_P} \leq P^{in}_{m,e} \leq \sum_{d_P} \hat{P}^{in}_{m,e,(d_P+1)} y^{\hat{P}in}_{m,e,d_P} \quad (139)$$

When running Rysia, the upper bound is the rigorous MINLP and is run using the results from the lower bound as initial values, although some results for the general superstructure can be obtained with the lower bound model, the system was evaluated rigorously by fixing as many variables as possible with the values of the LB to obtain a feasible solution.

Before trying bound contraction, an attempted to increase the number of partitions in the lower bound to see if the gap at the root node can be reduced, was done. Results for a two stages RON, with seawater concentration of 35,000 ppm and a target permeate production of 100 kg/s (maximum permeate concentration 500 ppm, and maximum brine concentration 87,000 ppm) are presented in Table 4. Results show that a region where there is no improvement

in the objective value when the number of intervals for the partitioned variables was increased, is reached.

When running with 2,4,8 and 10 intervals to partition the decision variables, a sequence of slowly increasing lower bound values ($1,293,594, $1,318,176, $1,528,365, and $1,540,456) at an elevated computational cost of 0.1,1.3,6.0, and 10 hours, respectively, are obtained. In all cases, the upper bound rendered and optimum with an objective of $1,814,528. The gap with the MINLP at the best feasible solution attained was 15.1%. Clearly, an increase in the number of intervals leads to unacceptable computing times.

Table 4. Results using RYSIA for General superstructure (Two stages, Fp=100kg/s)

	2 intervals	4 intervals	8 intervals	10 intervals
Lower Bound	1,293,594	1,318,176	1,528,365	1,540,456
Upper Bound	1,814,528	1,814,528	1,814,528	1,814,528
Time	00:05:30	01:19:18	05:58:34	10:05:28

When bound contraction was attempted using two intervals, none of the bounds for the partitioned variables could be contracted, instead of using a bound contraction procedure using a greater number of partitions for all the variables, different numbers of partitions for pressure, solute flux, flows, and concentration were used.

Figure 19 presents the iterations for the inlet pressure partitioned variable, this is for a seawater concentration of 35,000 ppm, a permeate flow of 100 kg/s, and the number of intervals for the partitioned variables used were: 4 intervals for pressure, 4 intervals for solute flux, 9 intervals for net driven pressure, and 2 intervals for the flows. The results are summarized as the following:

- The first run takes about 10 minutes, then the intervals for each partitioned variable where the answer is located, are identified. (Lower bound: 1,676,770, Upper bound: 1,781,493).
- It started with the inlet pressure for stage 1 - Pn_1^{RO}, first iteration: the answer is in the first interval, so, interval 1, interval 1 + 2, interval 1+2+3, are forbidden, respectively. After the third run (intervals 1, 2 and 3 forbidden) the bounds can be contracted. (Total number of runs: 3).
- Inlet pressure for stage 2 - Pn_2^{RO}, first iteration: the answer is in the third interval, so, interval 3 and interval 3 + 4, are forbidden, respectively. After the

second run (intervals 3 and 4, forbidden) the bounds can be contracted. (Total number of runs: 2).

- Variables: first stage concentration (C_1^{RO}) and turbine pressure difference (ΔP_t^T), also allows to contract their bounds in the first iteration. (Total number of runs: 3).
- Second iteration: Pn_1^{RO} - the answer is located in interval 1, forbidding intervals 1, 2, and 3 bounds can be contracted. (Total number of runs: 3)
- Second iteration: Pn_2^{RO} - the answer is located in interval 2, forbidding intervals 1 + 2, 2, 1+2+3, 2+3, 2+3+4 bounds cannot be contracted (Total number of runs: 5).
- This time variables C_1^{RO}, ΔP_t^T cannot be contracted.
- Third iteration: for each variable Pn_1^{RO}, Pn_2^{RO}, 5 runs are made, but no bound contraction is possible. The procedure finishes. Lower and upper bounds by the end of the extended interval elimination strategy: 1,713,724 (LB) vs 1,781,493 (UB), gap = 3.78%.

After a total number of 21 runs of the MILP lower bound, the extended interval elimination took about 3.5 hours to reach a gap of 3.78% between the lower and the corresponding MINLP. Getting a better result than those presented in Table 4.

1° Iteration					
Pro(1)	60	65	70	75	80
	x			infes	
Pro(2)	60	65	70	75	80
	infes	infes	x		
2° Iteration					
Pro(1)	60	63.75	67.5	71.25	75
	x			infes	
Pro(2)	70	72.5	75	77.5	80
		x			
3° Iteration					
Pro(1)	60	62.8	65.6	68.4	71.25
		x			
Pro(2)	70	72.5	75	77.5	80
		x			

Figure 19. Extended interval elimination – RO inlet Pressure

The rigorous MINLP was also run without initial values in Dicopt (GROSSMANN et al., 2016) and Antigone (MISENER; FLOUDAS, 2014) obtaining an infeasible solution. When trying Baron (SAHINIDIS, 1996), after a predefined time limit of 250 hours the solver finished without attaining convergence, with the relative gap at 18.72%. Baron (SAHINIDIS, 1996) fixing the binary variables for the number of membrane modules was also ran, without obtaining a feasible solution.

All the above results show that the nonlinearity of the RON-MINLP model presents important convergence difficulties, and is computationally expensive, especially if good initial values are unknown for local solvers. While it results difficult to explain the reasons why Baron and Antigone fail, in the case of Rysia, it could be said that it should be able to solve the problem with enough number of partitions, if it was not for the computational effort involved, as previously mentioned.

Given the solution difficulties associated with the nonlinearities of the solution-diffusion model, an additional approach was tested, this time the equations 31 – 54 were replaced by the metamodel equations 124 for the linear permeate flow, Eq.122 for a linear approximation of permeate concentration and Eq.123 for a permeate concentration quadratic approximation. So, if equations 124 and 122 are used the resulted model will be referred as linear metamodel, and if equations 124 and 123 are used this will be a non-linear metamodel.

Then these variables ($F_{m,e}^{Pe}, C_{m,e}^{Pe}$) are partitioned using the following expressions:

$$\sum_{d_P}\sum_{d_C}\sum_{d_F}\begin{bmatrix} K_1+K_2\hat{P}_{m,e,d_P}^{in}+K_3\hat{C}_{m,e,d_C}^{in}+K_4\hat{F}_{m,e,d_F}^{in}+K_5\hat{P}_{m,e,d_P}^{in}\hat{C}_{m,e,d_C}^{in} \\ +K_6\hat{P}_{m,e,d_P}^{in}\hat{F}_{m,e,d_F}^{in}+K_7\hat{C}_{m,e,d_C}^{in}\hat{F}_{m,e,d_F}^{in}+K_8\hat{P}_{m,e,d_P}^{in}\hat{C}_{m,e,d_C}^{in}\hat{F}_{m,e,d_F}^{in} \end{bmatrix} W_{m,e,d_P,d_C,d_F} \le F_{m,e}^{Pe}$$

$$F_{m,e}^{Pe} \le \sum_{d_P}\sum_{d_C}\sum_{d_F}\begin{bmatrix} K_1+K_2\hat{P}_{m,e,d_P+1}^{in}+K_3\hat{C}_{m,e,d_C+1}^{in}+K_4\hat{F}_{m,e,d_F+1}^{in}+K_5\hat{P}_{m,e,d_P+1}^{in}\hat{C}_{m,e,d_C+1}^{in} \\ +K_6\hat{P}_{m,e,d_P+1}^{in}\hat{F}_{m,e,d_F+1}^{in}+K_7\hat{C}_{m,e,d_C+1}^{in}\hat{F}_{m,e,d_F+1}^{in}+K_8\hat{P}_{m,e,d_P+1}^{in}\hat{C}_{m,e,d_{C+1}}^{in}\hat{F}_{m,e,d_F}^{in} \end{bmatrix} W_{m,e,d_P,d_C,d_F} \tag{140}$$

Where variable W_{m,e,d_P,d_C,d_F}, substitutes the product of the binary variables $y_{m,e,d_P}^{\hat{P}in} y_{m,e,d_C}^{\hat{C}in} y_{m,e,d_F}^{\hat{F}in}$, with the next constrains:

$$W_{m,e,d_P,d_C,d_F} \le y_{m,e,d_P}^{\hat{P}in} \tag{141}$$

$$W_{m,e,d_P,d_C,d_F} \le y_{m,e,d_C}^{\hat{C}in} \tag{142}$$

$$W_{m,e,d_P,d_C,d_F} \le y_{m,e,d_F}^{\hat{F}in} \tag{143}$$

$$W_{m,e,d_P,d_C,d_F} \ge y_{m,e,d_P}^{\hat{P}in} + y_{m,e,d_C}^{\hat{C}in} + y_{m,e,d_F}^{\hat{F}in} - 2 \tag{144}$$

$$\sum_{d_P}\sum_{d_C}\sum_{d_F}\begin{bmatrix} K_1+K_2\left(\hat{P}_{m,e,d_P}^{in}\right)^2+K_3\left(\hat{C}_{m,e,d_C}^{in}\right)^2+K_4\left(\hat{F}_{m,e,d_F}^{in}\right)^2+K_5\hat{P}_{m,e,d_P}^{in}+K_6\hat{C}_{m,e,d_C}^{in}+K_7\hat{F}_{m,e,d_F}^{in} \\ +K_8\left(\hat{P}_{m,e,d_P}^{in}\right)^2\left(\hat{C}_{m,e,d_C}^{in}\right)^2+K_9\left(\hat{P}_{m,e,d_P}^{in}\right)^2\left(\hat{F}_{m,e,d_F}^{in}\right)^2+K_{10}\left(\hat{C}_{m,e,d_C}^{in}\right)^2\left(\hat{F}_{m,e,d_F}^{in}\right)^2 \\ +K_{11}\left(\hat{P}_{m,e,d_P}^{in}\right)^2\left(\hat{C}_{m,e,d_C}^{in}\right)^2\left(\hat{F}_{m,e,d_F}^{in}\right)^2+K_{12}\hat{P}_{m,e,d_P}^{in}\hat{C}_{m,e,d_C}^{in}+K_{13}\hat{P}_{m,e,d_P}^{in}\hat{F}_{m,e,d_F}^{in} \\ +K_{14}\hat{C}_{m,e,d_C}^{in}\hat{F}_{m,e,d_F}^{in}+K_{15}\hat{P}_{m,e,d_P}^{in}\hat{C}_{m,e,d_C}^{in}\hat{F}_{m,e,d_F}^{in} \end{bmatrix} W_{m,e,d_P,d_C,d_F} \le C_{m,e}^{Pe}$$

$$C_{m,e}^{Pe} \le \sum_{d_P}\sum_{d_C}\sum_{d_F}\begin{bmatrix} K_1+K_2\left(\hat{P}_{m,e,d_P+1}^{in}\right)^2+K_3\left(\hat{C}_{m,e,d_C+1}^{in}\right)^2+K_4\left(\hat{F}_{m,e,d_F+1}^{in}\right)^2+K_5\hat{P}_{m,e,d_P+1}^{in}+K_6\hat{C}_{m,e,d_C+1}^{in}+K_7\hat{F}_{m,e,d_F+1}^{in} \\ +K_8\left(\hat{P}_{m,e,d_P+1}^{in}\right)^2\left(\hat{C}_{m,e,d_C+1}^{in}\right)^2+K_9\left(\hat{P}_{m,e,d_P+1}^{in}\right)^2\left(\hat{F}_{m,e,d_F+1}^{in}\right)^2+K_{10}\left(\hat{C}_{m,e,d_C+1}^{in}\right)^2\left(\hat{F}_{m,e,d_F+1}^{in}\right)^2 \\ +K_{11}\left(\hat{P}_{m,e,d_P+1}^{in}\right)^2\left(\hat{C}_{m,e,d_C+1}^{in}\right)^2\left(\hat{F}_{m,e,d_F+1}^{in}\right)^2+K_{12}\hat{P}_{m,e,d_P+1}^{in}\hat{C}_{m,e,d_C+1}^{in}+K_{13}\hat{P}_{m,e,d_P+1}^{in}\hat{F}_{m,e,d_F+1}^{in} \\ +K_{14}\hat{C}_{m,e,d_C+1}^{in}\hat{F}_{m,e,d_F+1}^{in}+K_{15}\hat{P}_{m,e,d_P+1}^{in}\hat{C}_{m,e,d_C+1}^{in}\hat{F}_{m,e,d_F+1}^{in} \end{bmatrix} W_{m,e,d_P,d_C,d_F} \tag{145}$$

Equation 145 corresponds to the quadratic metamodel, for the linear metamodel equation will look like equation 144 with the corresponding coefficients. (Details of the fitted coefficients and metamodel construction are presented in section 6.1).

When running the quadratic metamodel MILP with 6,7,8 and 10 intervals to partition the decision variables, a sequence of slowly increasing lower bound values ($1,554,772, $1,590,182, $1,619,466, $1,632,549) at an elevated computational cost of 1.1, 2.0, 4.2, and 8 hours, respectively, are obtained. In all cases, the upper bound rendered an optimum with an objective of $1,869,372 (which is 4.9% larger than the optimum identified with the extended interval elimination using the rigorous MINLP). The gap with the MINLP at the best feasible solution attained was 12.7%. Once again when bound contraction procedure was applied using two intervals, none of the bounds for the partitioned variables could be contracted.

When running the linear metamodel MILP with 6,8,10 and 16 intervals to partition the decision variables, a sequence of slowly increasing lower bound values ($1,358,000, $1,482,000, $1,500,000, $1,536,000) at computational times of 0.1, 0.5, 1.17, and 2.5 hours, respectively, are obtained. This time the computational costs are lower than in previous cases (Images of monotonic functions, and quadratic metamodel), rendering in all cases an optimum upper bound of $1,728,753 which underestimate significantly the upper bound value, because of the simplifications of the linear expressions used. When bound contraction was implemented using two intervals, despite it allowed to contract C_1^{HPP}, C_2^{B}, C_1^{RO}, Fs, Npv_1 and Δp_1^{HPP} variables, allowing three iterations, the final gap was 30.2% ($1,205,246 vs. $1,728,753 lower and upper bounds, respectively). With such results, the linear metamodel MILP approach could not be recommended to solve this problem.

Rysia using the monotone partitioned functions (rigorous approach) was also used to solve the same optimization problem (35,000 ppm seawater concentration and 100 kg/s permeate flow target), but this time for a single stage reverse osmosis network, to see if the same convergences difficulties are presented in a simpler problem (less optimization and binary variables). Results are presented in Table 5, the best gap obtained was 13.5% ($1.628.467 vs. $1.881.776) with a computational time of 8.3 hours. This time the MINLP objective value was 3.7% larger than the MINLP value for two stages ($1,881,776 vs. $1,814,528), results consistent with the literature, and mathematically validated in section 6.2.

Table 5. Results using RYSIA for one stage RON

	4 intervals	5 intervals	6 intervals	7 intervals	10 intervals
Lower Bound	1,239,876.	1,379,018	1,523,356	1,535,628	1,628,467
Upper Bound	1,881,776	1,881,776	1,881,776	1,881,776	1,881,776
Time	00:00:30	00:01:13	00:04:40	00:58:50	08:20:50

When bound contraction procedure using extended interval elimination was implemented for a single stage using 5 intervals, despite the variables Fs and F^{inem} could be contracted, allowing three iterations the final gap at the end of the procedure was 26.2% ($1,389,058 vs. $1,881,776), results are presented in Table 6.

Table 6. Bound contraction using extended interval elimination (5 intervals) single stage RON.

Variables to contract	Original Bounds		1 iteration		2 iteration		3 iteration	
	Lower	upper	Lower	upper	Lower	upper	Lower	upper
FS	150	200	160	200	160	176	166.4	172.8
Finem	1.5	3.5	1.5	2.7	1.5	2.7	1.5	2.7
Pnro	60	80	60	80	60	80	60	80
LB	1,379,018		1,379,405		1,389,058		1,389,058	
UB	1,881,776		1,881,776		1,881,776		1,881,776	

6 STOCHASTIC-DETERMINISTIC METHODOLOGY RESULTS FOR REVERSE OSMOSIS NETWORKS.

6.1 Reverse osmosis metamodel adjustment

The nonlinear mathematical model needs to solve a non-linear system equation with 17 variables to establish the relationship between the feed flow rate and composition with the permeate composition and flow rate. The largest computational time-consuming part of the algorithm is the calculation of the permeate conditions.

To address the above issue, it was built a mesh with the rigorous model solutions and regressed them using a linear and non-linear metamodel. Table 7 presents the limits for each variable of the mesh and the total number of data points used to fitting the metamodel.

Table 7. Limits and points of solution mesh for RO metamodel.

Variable	lower Bound	Upper Bound	Interval	Points
Inlet salt concentration	20000	85000	2500	28
Feed flow rate	1	3.6	0.1	28
Inlet pressure	30	80	2.5	22
			Total Points	**8624**

Figure 20 shows the influence of feed pressure and concentration on the permeate concentration using the rigorous method. The reduction in feed pressure and the increase in the feed concentration increases the permeate concentration. This is explained by the salt transport through the membrane being mainly diffusive; thus, an increase in the feed concentration increases the salt concentration difference through the membrane increases the salt transport. On the other hand, a reduction in pressure increases the permeate concentration because at low pressure the water transport is low. For high pressure and low concentration, the permeate concentration has a linear behavior, while a pressure reduction and an increase in the concentration renders a non-linear behavior. Figure 20 shows a boundary in the permeate concentration behavior from linear to non-linear.

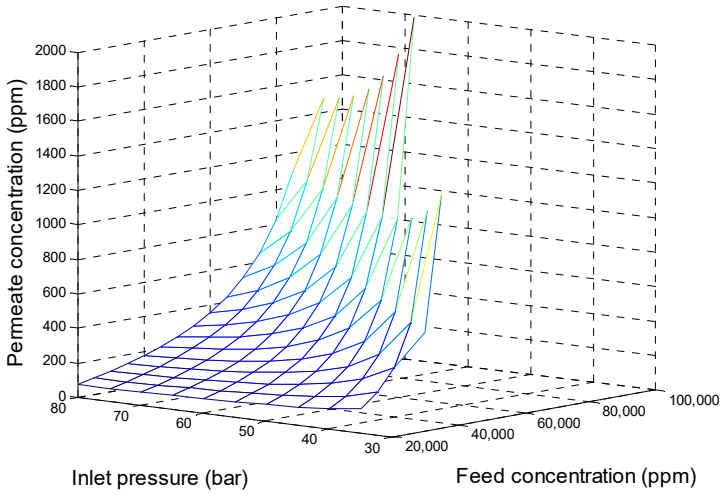

(a)

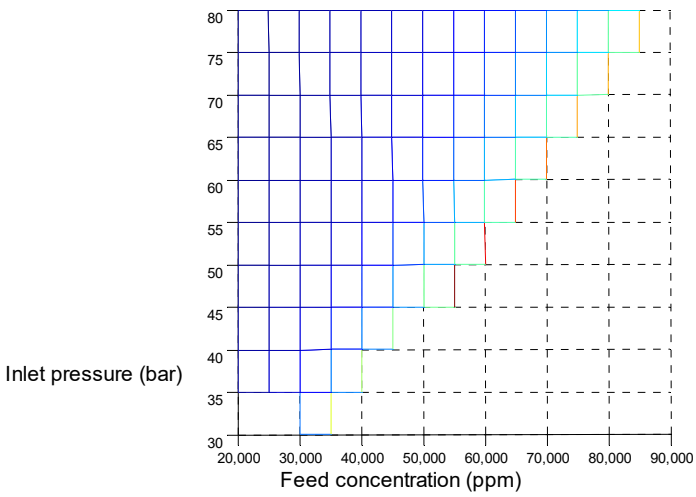

(b)

Figure 20. Influence of feed pressure and concentration on the permeate concentration. a) Lateral view. b) Top View.

Figure 21 shows the influence of feed pressure and concentration on the permeate flow rate, brine concentration, and brine flow rate using the rigorous method. It shows a linear behavior for all the studied region. The permeate flow increases with the pressure and decreases with the salt concentration (Figure 21-a), explained by the increase in pressure, which augments the water that crosses through the membrane, thus increasing the permeate flow. Next, the permeate flow decreases with the increase in salt concentration because it increases the osmotic pressure in the brine, which reduces the driving force for the transport of water, thus reducing the permeate flow. In turn, the brine concentration (Figure 21-b) increases with the feed

pressure and concentration because the increase in the pressure increases the amount of water that crosses through the membrane, thus increasing the salt concentration in the brine. Finally, the brine flow reduces with pressure and increases with salt concentration (Figure 21-c); this behavior is explained by the reasons previously outlined.

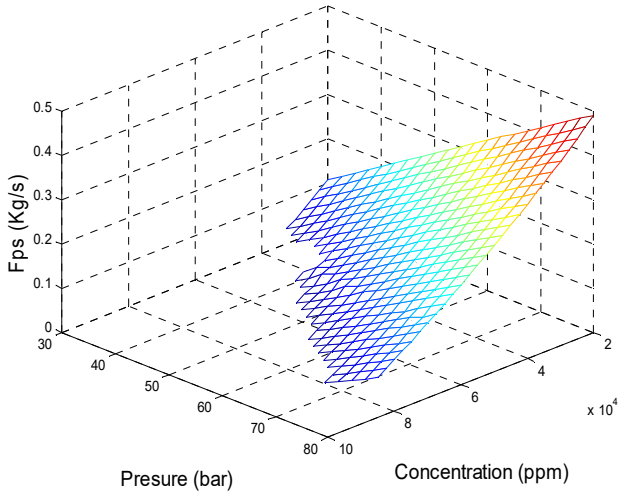

(a)

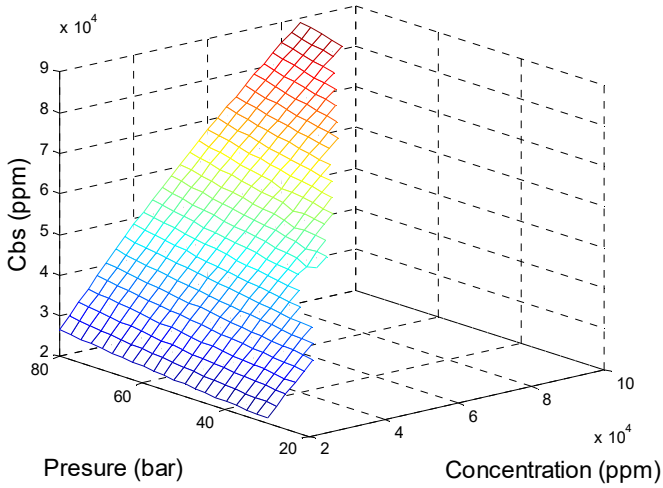

(b)

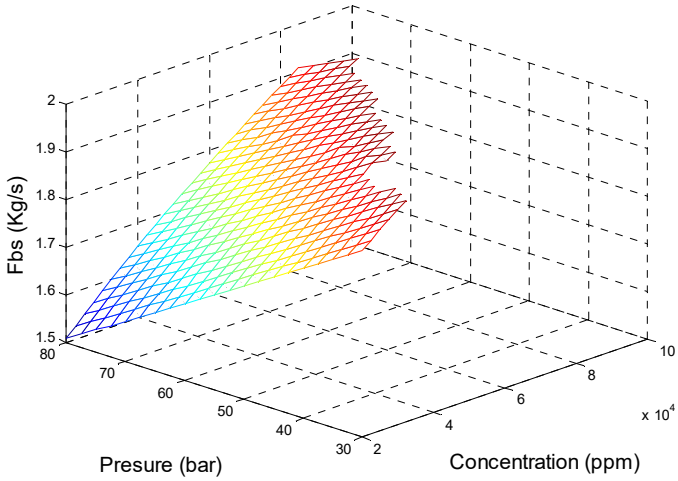

(c)

Figure 21. Influence of feed pressure and concentration on a) permeate flow rate, b) brine concentration and c) brine flow rate.

For the linear metamodel correlation, was chosen feed concentrations between 20,000 and 45,000 ppm, the pressure between 40 and 80 psi and feed flow rate between 1.5 and 3.5 kg/s. As stated, a genetic algorithm was used for the parameters' estimation. Figure 22 compares the rigorous mesh and linear metamodel for a feed flow of 2.5 kg/s. The highest deviation was for the permeate concentration because this variable has the largest non-linear behavior.

Table 8 shows the adjusted parameters for the linear metamodel. It could be noted that several parameters are very small and thus do not contribute much to the correlation.

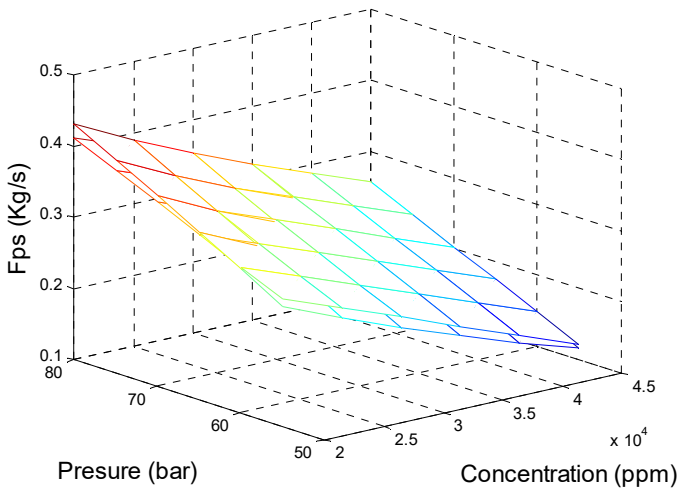

(a)

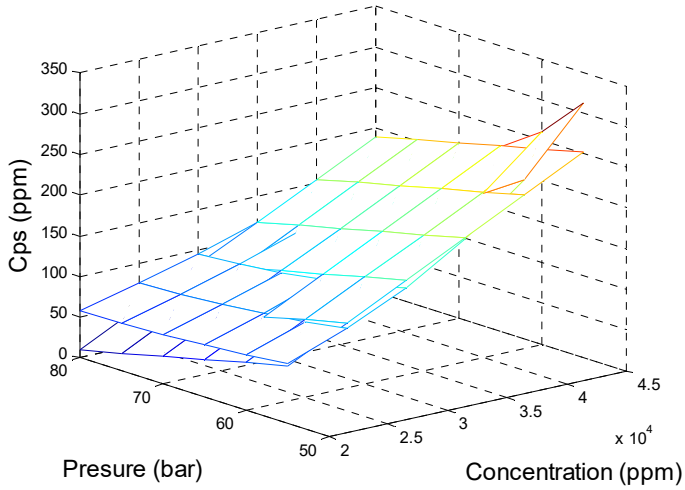

(b)

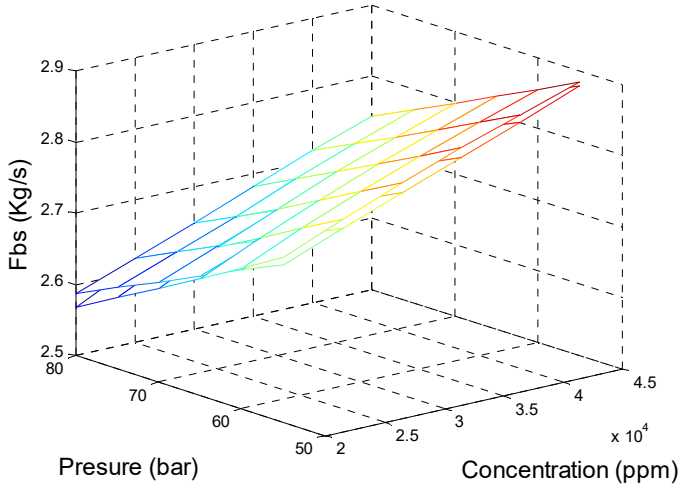

(c)

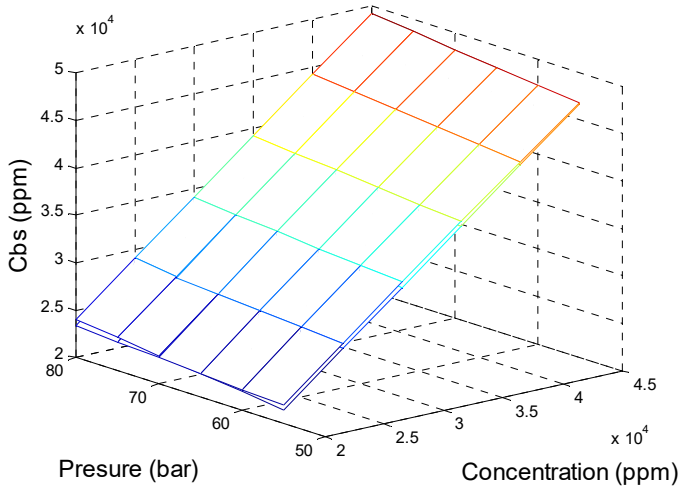

(d)

Figure 22. Linear metamodel correlation and rigorous solutions. a) Permeate Flow; b) Permeate Concentration; c) Brine Flow; d) Brine concentration.

Table 8. Linear metamodel constants

	K1	K2	K3	K4
Fps	0.0139	0.0054	-6.24 e-06	0.0311
Cps	156.9561	-2.7875	9.1532e-3	-35.532
Fbs	-0.0139	-0.0054	6.24 e-06	0.9689
Cbs	150.63	102.24	1.009	-1,490.22

For the non-linear metamodel correlation, were chosen feed concentrations between 20,000 and 80,000 ppm, the pressure between 40 and 80 psi and feed flow rate between 1.5 and 3.5 kg/s. As stated, a genetic algorithm was used for the parameters' estimation. Figure 23 shows the comparison between the rigorous mesh and non-linear metamodel for a feed flow of 2.5 kg/s. The highest deviation was for the behavior of the permeate concentration because this variable has the most non-linear behavior. Table 9 shows the adjusted parameters for the non-linear metamodel. The non-linear fit increases with the number of parameters used in the correlation process. Finally, it could be noted that several parameters are very small and thus do not contribute much to the correlation.

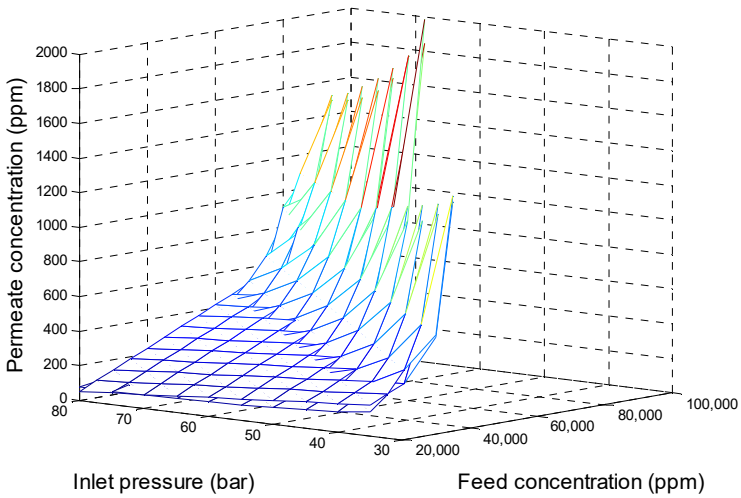

(a)

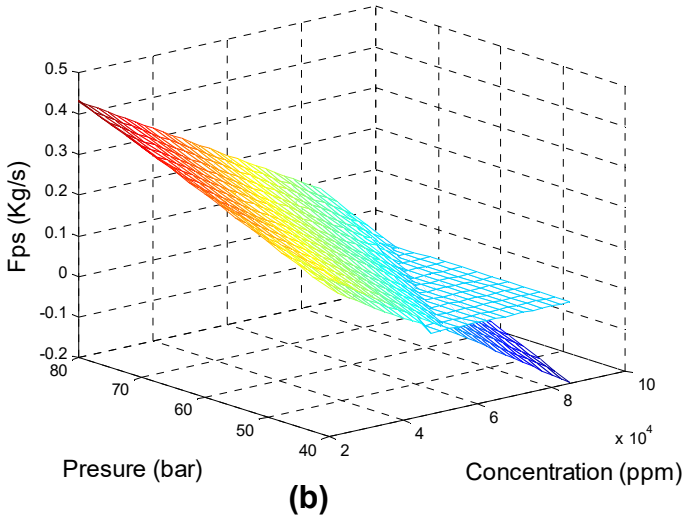

Figure 23. Non-Linear metamodel correlation and validation.

Table 9. Non-Linear metamodel constants and objective function.

	Cps	**Fps**
K1	446.1412	-0.2192
K2	10.0193	5.62130e-4
K3	7.2968 e-06	2.7489 e-06
K4	37.7918	0.1020
K5	-202.9078	-8.7533 e-08
K6	0.2196	5.1089 e-06
K7	-143.1272	-3.1395 e-06
K8	1.3714 e-11	3.4639 e-08
K9	3.4176e-3	
K10	4.3866 e-09	
K11	1.9653 e-13	
K12	1.7407e-2	
K13	6.6979	
K14	-8.8748e-3	
K15	-4.6595 e-05	

6.2 Reverse osmosis network results

The data for the modules are presented in Table 1 and the economic parameters are presented in Table 2. Table 10 shows the optimization results for the RO system for a targeted permeate concentration of 500 ppm and a flow rate of 100kg/s, with an inlet water concentration of 35,000 ppm. A maximum of 87,000 ppm for the brine concentration was set, a reasonable value before scaling onset. The necessary parameters to describe the diploid GA (FONTEIX et al., 1995) used, were: 1000 individuals, 10 generations, 100 survivors, 100 mutants and a mutation rate equal to 0.01 In Table 10 is reported the final number of vessels obtained considering it as a continuous value and in the case of the MINLP, both are reported, the continuous value obtained as well as the fixed value used for the final MINLP run (in between parenthesis). The TAC reported for the MINLP is based on the integer value of the number of vessels. The optimization renders the flow of the brine and the inlet flow needed.

Table 10. Optimization results.

	Genetic Algorithm using the Metamodel		*Genetic Algorithm using the Rigorous Model*		*Rigorous MINLP*	
TAC	$1,796,169		$1,806,500		$ 1,781,499	
Stage	*S1*	*S2*	*S1*	*S1*	*S1*	*S2*
Inlet Pressure (bar)	73	80	67.6	79.9	63	79.4
Salted water flow (kg/s)	167.65		167.65		166.57	
Each Pressure vessel Inlet Flow (kg/s)	3.5	3.5	2.14	3.47	2.6	2.59
Number of modules	8	8	8	8	8	8
Number of pressure vessels As continuous variable- (As integer)	47.9	25.4	78.3	24.5	63.6 (64)	37.2 (37)
Flow Recycle 1 (kg/s)	0		0		0	
Flow Recycle 2 (kg/s)	0		0		0	
Computing time	~20 min		280 hours		5.5 sec	

(Permeate concentration: 500 ppm; permeate flow rate: 100kg/s;
Inlet water concentration: 35000 ppm)

The rigorous MINLP models using the results from the GA's as a starting point, give the same result with slightly different solution times (5.7 seconds for using the initial values from the GA run using metamodel vs 6.8 seconds using the initial values from the GA run with the rigorous model). It should be noted that the genetic algorithm using the rigorous model was

disproportionally time consuming (280 hours vs. 20 minutes). The time-consuming step is the iterative solution of the nonlinear set of equations.

The fitness (TAC) of each individual of the population at each GA iteration is evaluated by solving the membrane module equations (Eqs 31-54). This is done as follows: The total inlet flow and the inlet concentration are known from the problem specification then Eqs 31-54 are solved to obtain permeate flow and concentration, the brine flow and concentration are calculated from the mass balance. It needs to be reminded that the Matlab "solve" feature is used in this step, of which there is little detailed information. These values are then used as the inlet conditions for the next module. Once the last module is solved, the concentration of the recycle is known and one can start at the first module again upon convergence.

Each solution of Eqs 31-54 takes for a single membrane module 5 to 60 seconds to be solved, and a single stage takes about 10 iterations to converge. Thus, this explains the large computing time when realizing it that 1000 individuals and 10 generations are used. Conversely, the metamodel does not need to iterate to solve the same module equations.

Table 10 presented the *TAC* for the rigorous MINLP fixing the number of pressure vessels *Npv* to the nearest integers values obtained from the rigorous MINLP (considering *Npv* as continuous), the TAC values differ only in a 0.00033% indicating that the approximation does not introduce a significant error.

Because several runs were made using the GA with the metamodel followed by the rigorous MINLP (as detailed below), finding similar times (less than 30 minutes), one could be confident that the pattern will repeat for other cases and/or with other parameter data.

Thus, for the rest of this chapter, it will be used a genetic algorithm using metamodels to initialize a rigorous MINLP model.

The results for different inlet water concentrations and different targets permeate flows and a permeate concentration of 500 ppm are shown, for two stages, in Table 11.

It could be noted that in this case, the permeate flow is no longer fixed, instead, the inlet flow is fixed maintaining a maximum brine concentration of 87,000 ppm.

Results presented in Table 11 do not show a brine recycle flow, despite that recycling helps reducing concentration polarization (increasing the velocity through the membrane module). Optimal solutions avoid it because the recycle pumps (HPPR) needed to compensate for the pressure drop of the membrane module, thus increasing the total capital cost and power consumption since they are high-pressure pumps. Incidentally, brine recycles also increases the

system salt passage leading to unacceptable salt permeate concentrations in some cases (DOW WATER & PROCESS SOLUTIONS, 2011).

Table 11. Optimal solutions for different scenarios

Feed seawater concentration (ppm)	*30000*				*40000*				*50000*			
	GA with metamodel		*Rigorous MINLP*		*GA with metamodel*		*Rigorous MINLP*		*GA with metamodel*		*Rigorous MINLP*	
TAC	$4,723,835		$4,700,784		$2,582,401		$2,629,873		$532,703		$551,140	
Stage	*S1*	*S2*	*S1*	*S2*	*S1*	*S2*	*S1*	*S2*	*S1*	*S2*	*S1*	*S2*
Inlet Pressure (bar)	78.4	80	55.8	73.5	73.4	78.8	65.9	75.3	75.4	77.6	78.1	76.8
Salted water flow (kg/s)	450		450		250		250		50		50	
Permeate flow (kg/s)	296.5		296.5		135.8		135.8		21.38		21.38	
Pressure vessel Inlet Flow (kg/s)	4.0	4.0	1.8	1.5	4.0	4.0	2.4	2.1	4.0	4.0	2.5	2.7
Number of modules	8	8	8	8	7	8	7	8	5	7	5	7
Number of pressure vessels- As continuous variable (As integer)	112.5	52.9	245.6 (246)	155.6 (156)	62.6	38.2	103.6 (104)	73.9 (74)	12.5	9.0	19.6 (20)	12.8 (13)
Flow Recycle 1 (kg/s)	0		0		0		0		0		0	
Flow Recycle 2 (kg/s)	0		0		0		0		0		0	
Computing time	~20 min		4.2 sec		~22 min		5.1 sec		~24 min		4.7 sec	

(Permeate maximum concentration: 500 ppm)

The main differences in the operation conditions (decision variables) between the genetic algorithm using the metamodel and the rigorous MINLP (Table 11) are associated to the precision of the metamodel, which underestimates some values of the operating variables in the region closer to the bounds. Thus, although the genetic metamodel is not completely suitable to determine operating conditions, it produces good initial estimates as starting points for the rigorous MINLP.

Now is presented an analysis of the effect of the feed flow and the salt concentration in the feed on the total annualized cost. Figure 24 presents the rigorous solution obtained for a feed flow between 50 and 450 kg/s and a feed salt concentration between 20,000 and 50,000 ppm and running the GA with the metamodel, followed by the rigorous MINLP solved using Dicopt with initial values obtained from the GA.

The results show that the TAC presents two regions with an apparent maximum at 30,000 ppm of feed concentration. It cannot be said for sure that the maximum is exactly at 30,000 ppm, given the discrete nature of the number of points investigated. For a fixed flow the differences in the extremes are -3,6% (cost for 20,000 ppm vs cost of 30,000 ppm) and -2.6% (cost for 50,000 ppm vs cost of 30,000 ppm).

For a feed concentration of 30,000 ppm and larger the TAC does not change significantly because the requirements for a larger pump power are compensated by less membrane area due to higher concentrations. On the other side, for feed concentrations of 20,000 and 25,000 ppm, the reduction is due to the use of membrane module with high retention parameters for seawater, while these concentrations are more related to brackish water concentrations.

The reduction in TAC here is due to smaller pumping needs driven by lower concentrations.

With such small differences in TAC for a large range of feed, concentrations lead to conclude that an average TAC for each flow is a good representation of all.

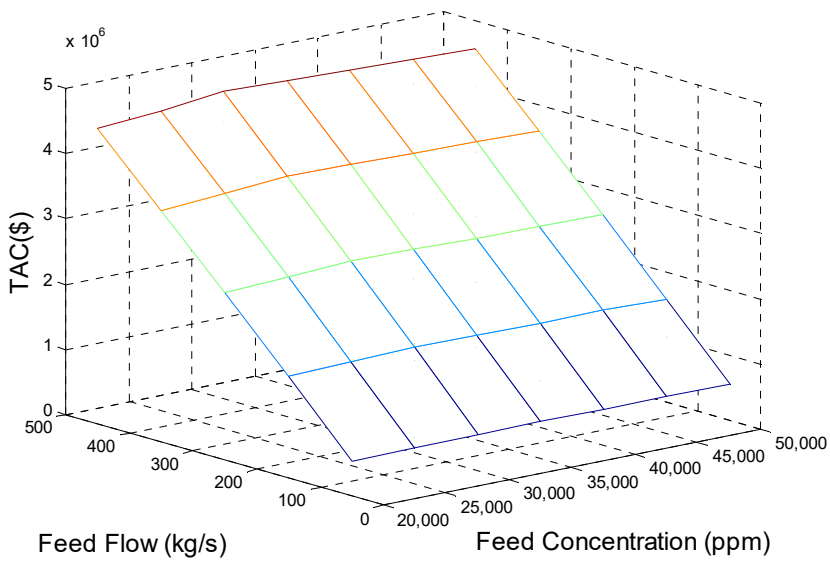

Figure 24. TAC for different inlet flows and seawater concentrations (two stages)

Now is explored the influence of the number of RO stages. The results are presented in Figure 25: the maximum TAC difference between 3 stages and 2 stages is about 1.6% (Figure 25a); although it is not noticeable in the figure the surfaces have a transition point from constant TAC to monotone TAC at 30,000 ppm, as explained above.

The TAC values for two stages are lower than for three stages for feed concentrations of 40,000 ppm and larger. For feed concentrations of 35,000 ppm and lower the design for three stages is lower in cost than for two stages, again barely noticeable in the figure.

This behavior is obtained using linear cost for pumps as a function of power (Equations 69-71). It could be argued that the use of a power law for cost, with other exponents, might change the results. Indeed, Lu et al. (2013) and Kim et al. (2009) used a power law with an exponent of 0.96 and the general literature on costs suggests values as low as 0.5.

The model was tested for various points using 0.96, 0.7 and 0.5. The results are always the same: for every flowrate, the region where 3 stages are of lower cost than 2 stages are for every flow below 35,000 ppm. For 40,000 ppm and above two stages are cheaper than three. This is consistent with the fact that at higher concentrations the power is constant because the pressure has reached its maximum.

Thus, two pumps make more sense than three pumps in that region. Below 40,000 ppm, more pumps are compensated by a smaller number of membrane modules (lower membrane area). The extreme differences (cost of 3 stages vs cost of two stages) are -1.59% and +5.97 % for n=0.96, -3.38% and +18.30 % for n=0.7, and -3.51% and +19.25 % for n=0.5. These are big differences and are a warning about the cost functions that need to be used.

In turn, the optimal TAC results for one stage are larger than those for two stages with a maximum difference close to 7% (Figure 25b).

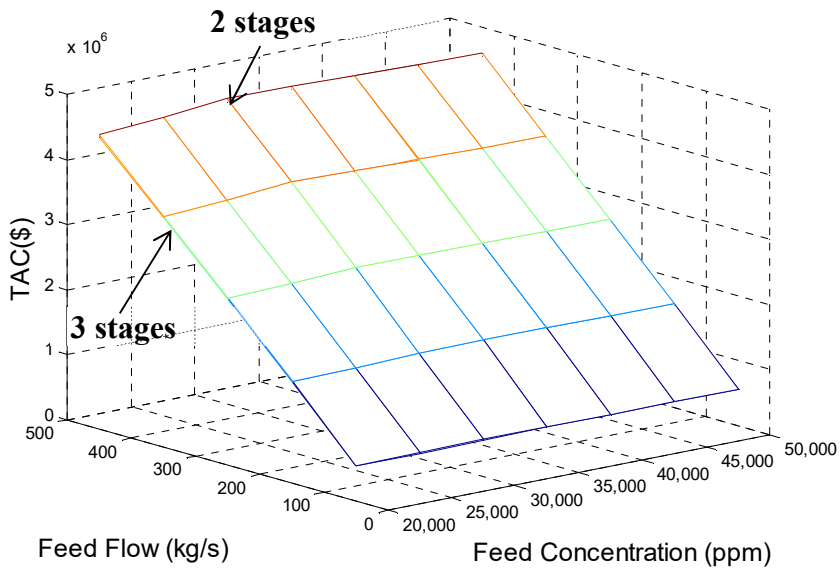

(a)

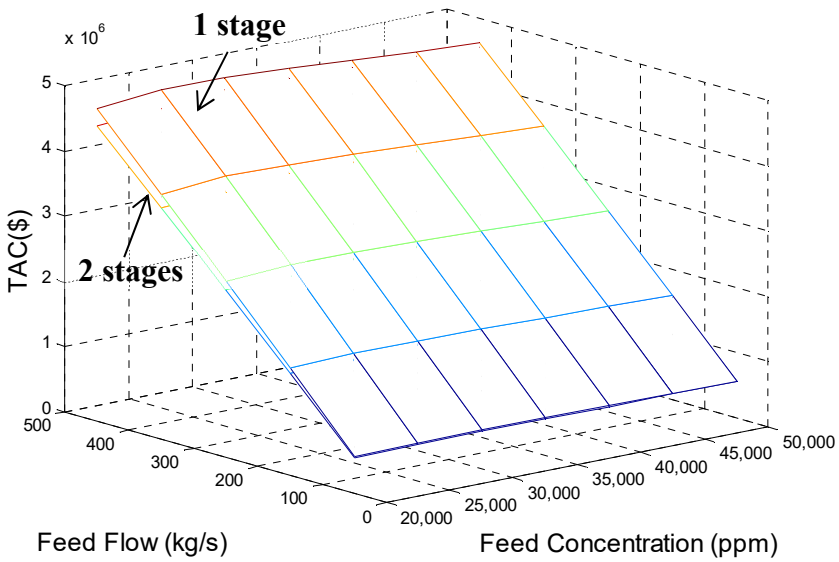

(b)

Figure 25. Effect of the number of stages. (a) 2 vs 3 stages, (b) 1 vs 2 stages

When analyzing the results, there were solutions that used the maximum membrane modules allowed in a pressure vessel according to the fabricant, especially those corresponding to 35,000 ppm or lower. So, a new set of solutions was obtained allowing the variable to use up 16 membrane modules. In this case, solutions using up to 14 membrane modules were found. These results are presented in Figure 26. The maximum difference between the use of a maximum of 8 modules and 16 modules was lower than 0.7% (indistinguishable in the figure), so there is no improvement in using a larger number of membrane modules per vessel. This behavior is explained because an increase in the maximum membrane modules is compensated with variations on the inlet stage conditions (Pressure and pressure vessel inlet flow F_m^{inem}), but these variations have not significant effect on the TAC. It could be concluded that the model is rather insensitive to the number of modules and that also perhaps explains the convergence difficulties.

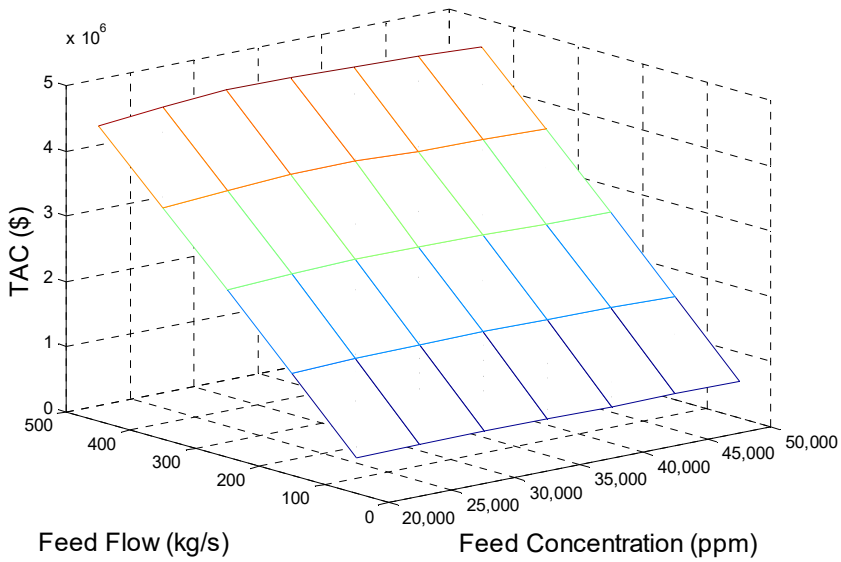

Figure 26. TAC for different inlet flows and seawater concentrations max number of membrane modules (N^{max}_e) equal to 16

All the above results represent optimal values obtained minimizing the TAC for a fixed concentration and flowrate of the permeate (Table 10), or flowrate of the feed (rest of results). Now is investigated the minimization of the cost per unit of freshwater produced with a fixed targeted concentration. Results are shown in Figure 27. It could be observed a sensitivity to the feed concentration and the feed flow, different from the observed in Figure 24. In the case of Figure 24, for a fixed permeate concentration of 500 ppm, the TAC is not significantly affected by the change in the feed concentration when the feed is maintained constant. However, when the inlet concentration varies, the amount of permeate flow decreases with feed concentration (shown in Figure 28). Since the TAC values for both figures (Figure 24 and Figure 27) are the same, but the amount of obtained freshwater varies with the inlet concentration the cost per unit of produce fresh waters increases with the feed concentration.

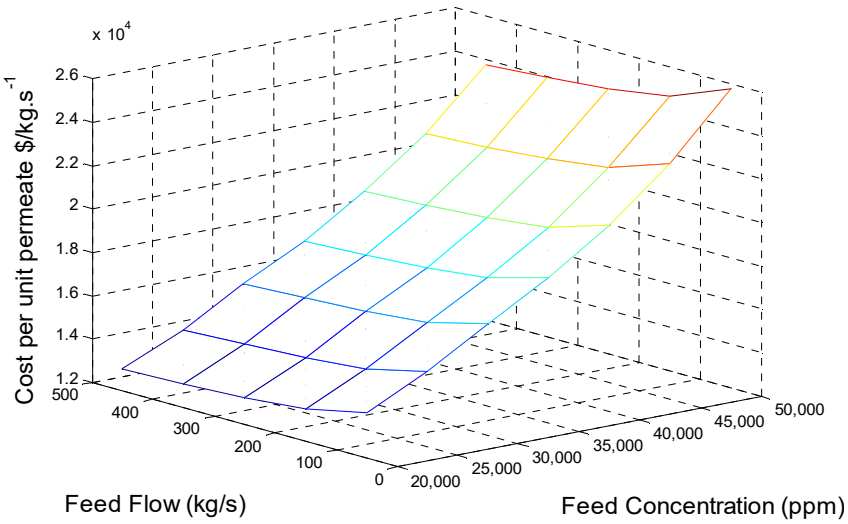

Figure 27. Optimal TAC per unit permeate flow. Concentration of permeate: 500 ppm.

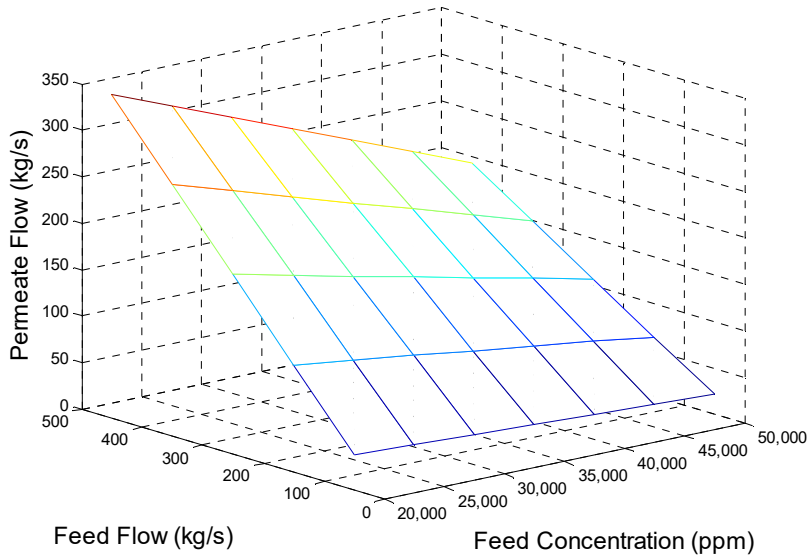

Figure 28. Permeate flow (2 stages, 500 ppm permeate).

6.3 Water production costs comparison with existing facilities:

Table 12 presents water production costs in US $/m^3 for operating plants around the world, for two installed capacities range. Basically, the water production costs reduce as the installed plant capacity increases because of a scale economy.

According to Ghaffour et al. (2013) the water cost was US$ 2.10/m^3 in 1975 and the price has been reduced to US$ 0.5/m3 for SWRO in 2004.

Table 12. Water production costs for existing plants.

Source	Plant size (m^3/day)	Water production cost (US $/m^3)	References
Seawater	1,000 – 4,800	0.70 – 1.72	Avlonitis (2002) Rayan (2003) Zejli et al. (2004) Atikol; Aybar (2005) Hafez; El-Manharawy (2003)
	15,000 – 60,000	0.48 – 1.62	Avlonitis (2002) Leitner (1991) Poullikkas (2001) Wade (2001) Wu; Zhang (2003) Agashichev (2004) Agashichev; El-Nashar (2005)

In Table 13 are presented the minimum water production costs calculated with the rigorous MINLP, using the proposed stochastic-deterministic optimization methodology, are also presented the total capital investment and the energy consumption. All the values for the water production cost are close to 0.5 US $/m^3, the value reported by Ghaffour et al. (2013). These values are in the range of the reported production costs of existing facilities in Table 13, allowing to validate what actually is been obtained with the rigorous MINLP. Ghaffour et al. (2013) also reported that the capital investment for each m^3/day of water produced should be between 900 and 2,500 US $, which is consistent with the reported values in Table 13.

In terms of energy consumption Ghaffour et al. (2013) reported between 3 and 4 kWh/m^3 for existing facilities, and according to Shrivastava et al. (2015) the minimum specific energy, defined as the energy required to produce unit volume of freshwater from the thermodynamically point of view for 50% of recovery, and 32,000 ppm of NaCl at 25°C is 2.12

kWh/m^3, which is a consistent value with 2.86 kWh/m^3 obtained with the MINLP. The difference between both energy consumption values is because of the main energy consuming equipment efficiencies (0.75 for both pumps and turbines), and the entropy creation.

Table 13. Water production costs calculated with the model (Feed concentration 30,000 ppm).

Plant size (m^3/day)	**Water production cost (US \$/m^3)**	**Total Capital investment (US\$)**	**Capital investment (US \$/m^3/day)**	**Energy consumption (kwh/m^3)**
2,846	0.54	2,805,200	986	2.86
19,927	0.51	17,020,000	854	2.86
25,620	0.51	21,536,000	841	2.86
31,314	0.49	26,000,000	830	2.86
59,781	0.49	47,805,000	800	2.86

7 STOCHASTIC-DETERMINISTIC METHODOLOGY RESULTS FOR RO+PRO HYBRID SUPERSTRUCTURES.

7.1 Pressure retarded osmosis metamodel adjustment

The nonlinear mathematical model needs to solve a non-linear system equation with 15 variables to establish the relationship between flow and concentration of the draw and feed solutions (input parameters) with the salt and water fluxes (with these two variables output flows and concentrations can be calculated).

So, there are five input parameters $F^{D,in}, C^{D,in}, F^{F,in}, C^{F,in}$, feed and draw solutions conditions basically, and the fifth parameter is the feed input pressure $P^{D,in}$, but as mentioned in the PRO description the optimal pressure difference that maximizes the power generation ($\Delta p = \frac{\Delta \pi}{2}$) is used, so, the inlet pressure is not an input parameter in this work.

Finally, since the PRO is incorporated in the RON structure as an energy recovery system, using the brine from the second stage of the RO as draw solution, and the brine concentration is fixed at 87,000 ppm, the metamodel is constructed with a mesh for the flow and concentration of the feed solution (pre-treated seawater) and the draw solution (brine) flow. Table 14 presents the limits for each variable of the mesh and the total number of data points used to fitting the metamodel. The feed concentration studied range is for seawater typical values, and the draw and feed solutions flow are selected according to recommendations of the membrane fabricant.

Table 14. Limits and points of solution mesh for PRO metamodel.

Variable	lower Bound	Upper Bound	Interval	Points
Feed concentration	20000	40000	5000	5
Feed Flow	2	3	0.25	5
Draw Flow	2	4	0.25	9
			Total Points	**225**

Figure 29 presents the rigorous and metamodel meshes for water flux, Figure 29 a) presents the fitting for a fixed feed concentration of 35.000 ppm, Figure 29 b) presents the fitting for a fixed draw flow of 2.5 kg/s. In both cases, the rigorous solution mesh is below the metamodel mesh predicted. The behavior is well represented by a plane since the permitted feed and draw flows intervals are tight. As it could be seen an increase in the draw flow produces

greater water fluxes for a given feed flow. Increasing the feed concentration reduces water fluxes since it reduces the osmotic gradient.

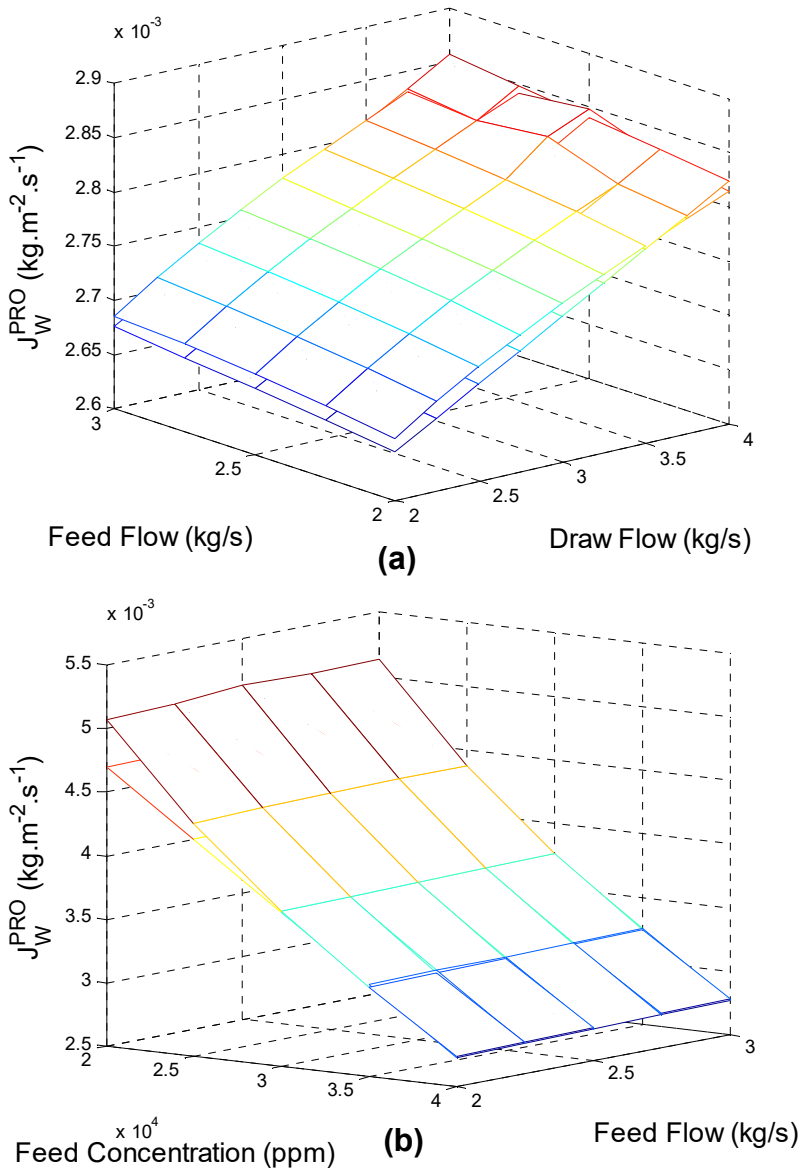

Figure 29. Water flux rigorous and metamodel meshes. (a) Fixed feed concentration: 35.000 ppm, (b) Fixed feed flow: 2.5 kg/s.

Figure 30 presents the solute flux rigorous and metamodel meshes, Figure 30 a) is plotted for a fixed feed concentration of 35.000 ppm, Figure 30 b) is plotted for a fixed draw flow of 2.5 kg/s. This time the behavior is not as linear as the water flux, and in both figures, the predicted metamodel mesh values are below the rigorous mesh. As the draw flow increases the solute flux decreases since greater velocities reduce the effect of the external concentration polarization.

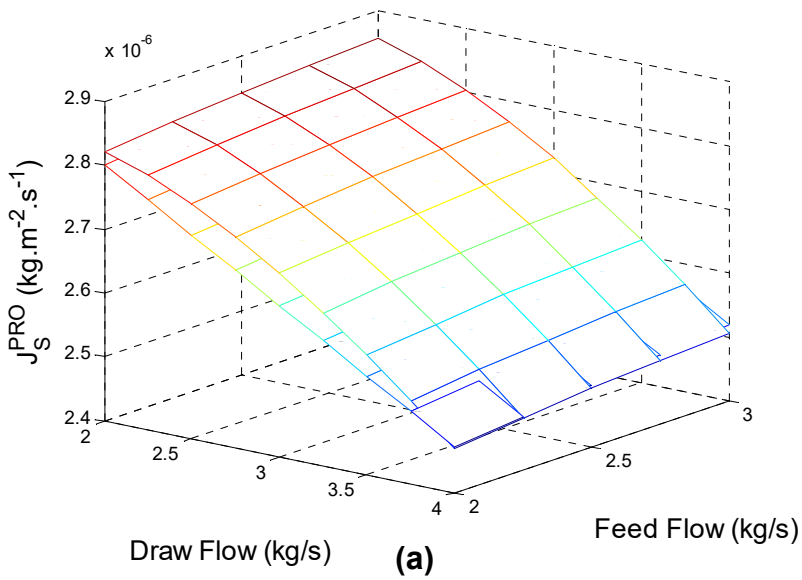

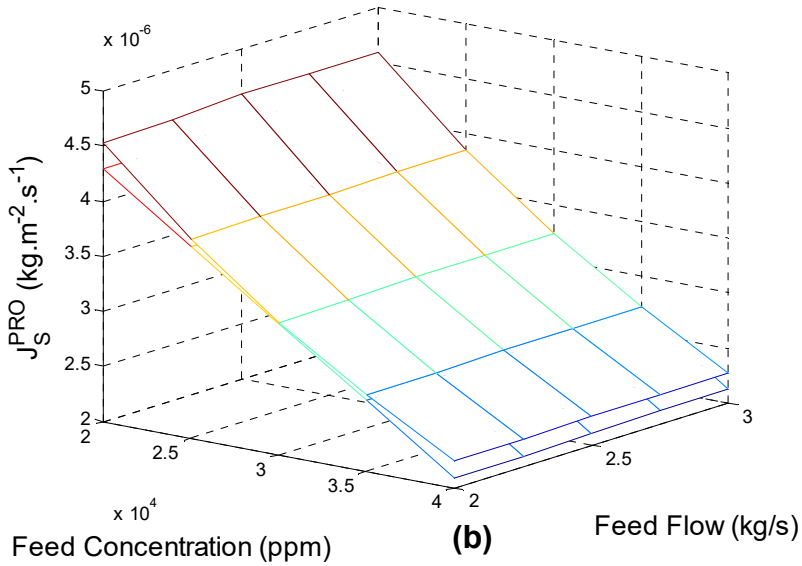

Figure 30. Solute flux rigorous and metamodel meshes. (a) Fixed feed concentration: 35.000 ppm, (b) Fixed feed flow: 2.5 kg/s.

In Table 15 are presented the fitted coefficients for the linear PRO metamodel.

Table 15. Linear metamodel constants for PRO model

	K1	K2	K3	K4
J_W^{PRO}	6.3275 x 10^{-03}	8.9959 x 10^{-05}	3.2968 x 10^{-05}	-9,8237 x 10^{-08}
J_S^{PRO}	6.9048 x 10^{-06}	-1.6486 x 10^{-07}	4.8152 x 10^{-08}	-1.1057 x 10^{-10}

7.2 Reverse osmosis – pressure retarded osmosis (RO+PRO) results:

The data for the RO and PRO modules are presented in Tables 1 and 2 respectively, the economic parameters are presented in Table 3. Table 16 shows the optimization results for the RO system and both RO+PRO configurations for a targeted permeate concentration of 500 ppm and a flow rate of 90 kg/s, with an inlet water concentration of 35,000 ppm. It was set a maximum of 87,000 ppm for the RO second stage brine concentration, a reasonable value before scaling onset.

Table 16. Optimization results for hybrid RO+PRO.

	RO single Network		*RO+PRO Configuration 1*		*RO+PRO Configuration 2*	
TAC	$1,615,783		$1,708,970		$ 1,631,059	
Total Salted water flow (kg/s)	150.00		178.62		152.97	
RO Stage	***S1***	***S2***	***S1***	***S1***	***S1***	***S2***
Inlet Pressure (bar)	59.7	74.9	63.6	76.5	63.9	76.5
Each Pressure Vessel Inlet Flow (kg/s)	2.2	1.8	2.6	2.1	2.6	2.2
Number of modules	8	8	8	8	8	8
Number of pressure vessels	70	47	58	40	58	40
Flow Recycle 1 (kg/s)	0		0		0	
Flow Recycle 2 (kg/s)	0		0		0	
PRO Unit						
High Salinity Solution Inlet Flow to each Pressure Vessel (kg/s)	-		3.8		4.0	
Low Salinity Solution Inlet Flow to each Pressure Vessel (kg/s)	-		1.8		1.8	
Number of pressure vessels	-		16		16	
High Salinity Solution Inlet Pressure (bar)	-		2.9		3.2	

(Permeate concentration: 500 ppm; permeate flow rate: 90kg/s; Inlet water concentration: 35000 ppm)

The TAC value for the RO+PRO configuration 1 is greater 5.8 % than the single RO network, this is because of the pre-treatment and pumping costs associated to the additional seawater used as feed solution for the PRO unit (178.62 kg/s of total seawater pre-treated water instead of 150 kg/s for the single RON). Those additional costs are necessary since the PRO is

a membrane unit, so it needs low salinity pre-treated supply water. The TAC value for the RO+PRO configuration 2 is slightly greater than the single RO network (0.94%), and the total pre-treated seawater consume for both cases are similar (152.97 kg/s vs. 150kg/s respectively).

Besides both configurations used the same brine stream as draw solution (the one leaving the second RO stage), the RO+PRO configuration 2 results in an efficient way to integrate the PRO unit as an energy recovery system (ERS) since a fraction of the seawater intake necessary for the single RO network is used as a low salinity (feed solution) for the PRO unit, sharing the pretreatment and pumping systems and just increasing a bit the salt concentration of the RO first stage feed flow without affecting the overall performance.

Since RO+PRO configuration 1 will always produce a higher TAC value than a single RO network, from now it will be explored only the RO+PRO configuration 2.

Table 17 presents optimal solutions for different seawater concentrations and a feed flow of 250 kg/s, the differences in TAC values are lower than 1%, indicating an almost constant behavior for different inlet concentrations. For three cases the feed ratio for high salinity solution (brine of RO second stage) to low salinity feed (seawater) was 2.22 and could be observed how the inlet optimal pressure decreases with an increase in the seawater salinity, this is related with a greater osmotic pressure for the low salinity solution (seawater) reducing the osmotic exploitable gradient.

Table 17. Optimal solutions for different scenarios

	30000 ppm		*40000 ppm*		*50000 ppm*	
TAC	$ 2,658,199		$ 2,672,257		$ 2,684,237	
Total Salted water flow (kg/s)	250		250		250	
RO Stage	***S1***	***S2***	***S1***	***S1***	***S1***	***S2***
Inlet Pressure (bar)	59.8	77.2	68.3	75.4	77.1	76.8
Each Pressure Vessel Inlet Flow (kg/s)	2.5	2.0	2.7	2.4	2.9	2.8
Number of modules	8	8	8	8	8	8
Number of pressure vessels	100	68	95	64	87	61
Flow Recycle 1 (kg/s)	0		0		0	
Flow Recycle 2 (kg/s)	0		0		0	
PRO Unit						
High Salinity Solution Inlet Flow to each Pressure Vessel (kg/s)	4.0		4.0		4.0	
Low Salinity Solution Inlet Flow to each Pressure Vessel (kg/s)	1.8		1.8		1.8	
Number of pressure vessels	22		30		37	
High Salinity Solution Inlet Pressure (bar)	3.6		2.8		2.2	

(Permeate maximum concentration: 500 ppm)

Now an analysis of the effect of the feed flow and the inlet salt on the total annualized cost for the RO integrated with PRO is presented. Figure 31 presents the rigorous solution obtained for a feed flow between 50 and 450 kg/s and a feed salt concentration between 20,000 and 50,000 ppm, running the GA with the metamodel, followed by the rigorous MINLP solved using Dicopt with initial values obtained from the GA. The results show that the TAC of the RO integrated with PRO increase linearly with the feed flow increase and remain almost constant with changes in the salt feed concentration.

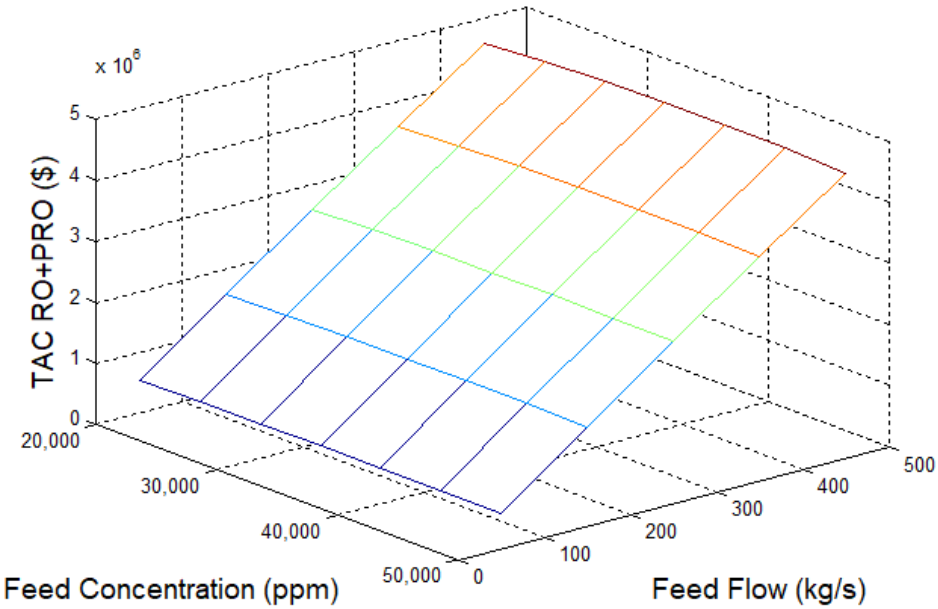

Figure 31. TAC RO+PRO configuration 2 for different inlet flows and seawater concentrations.

Figure 32 shows the comparison between the TAC for the RO with the TAC for the RO integrated with PRO for different feed concentration and feed flow, The RO integrated with PRO shows the highest TAC for all the evaluated coordinates.

Nevertheless, the highest difference between both configurations was 2%. The RO shows lower TAC because is a mature technology researched for a long time. An improvement in PRO technology through research could reduce the TAC of integrated technology.

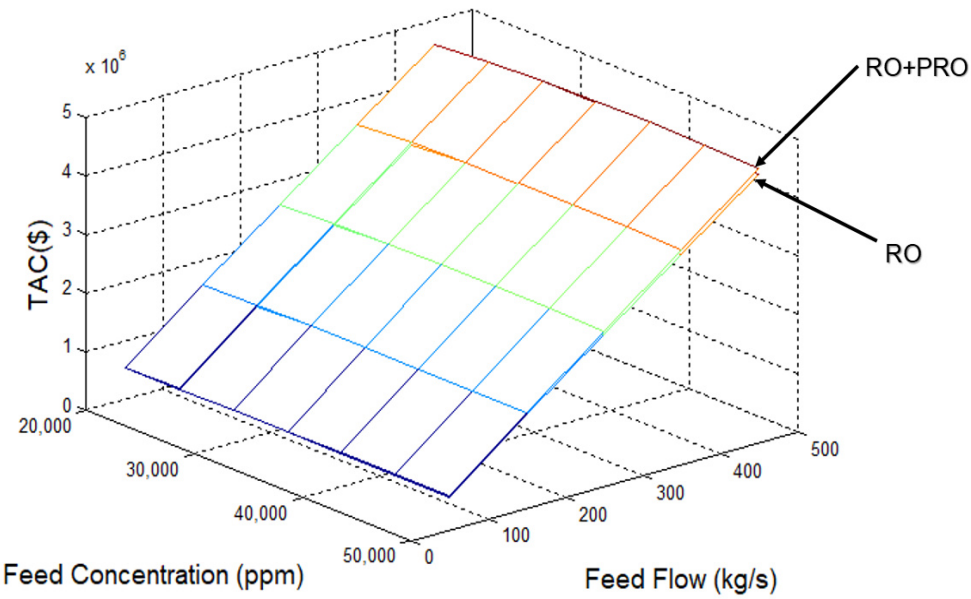

Figure 32. Comparison between TAC for RO and RO+PRO (configuration 2) for different feed concentration and flow.

8 CONCLUSIONS AND RECOMMENDATIONS

8.1 Conclusions

A new methodology to solve a nonlinear mathematical model for the optimal design of RO is proposed. Metamodels were used to reduce the mathematical complexity and get accurate solutions using a genetic algorithm. Then, the results were used as initial values to solve the full nonlinear model using GAMS/DICOPT. This allows getting optimal solutions for a complex MINLP problem with less computational effort. One of the major advances of this approach is that initial values are not needed (always a problem for practitioners using MINLP codes), as the GA provides them.

When the new bound contraction methodology was used, the upper bound is the rigorous MINLP and is run using the results from the lower bound (constructed by images of monotone functions in each domain variable's partition) as initial values. Before trying bound contraction, it was attempted to increase the number of partitions in the lower bound to see if the gap at the root node can be reduced. The result is that a region where there is no improvement in the objective value when the number of intervals for the partitioned variables was increased, was reached. When bound contraction was attempted using two intervals, none of the bounds for the partitioned variables could be contracted.

The new stochastic – deterministic proposed methodology allows exploring the effect of the feed flow, seawater concentration, number of reverse osmosis stages, and the maximum number of membrane modules in each pressure vessel on the total annualized cost of the plant.

The total annualized cost increases with an increase in the feed flow and presents little variations for different feed salt concentrations at a fixed inlet flow, indicating that a reverse osmosis plant could have adaptation capability for variations in the inlet concentration without major effects on the TAC.

The effect of the number of stages was studied for different feed flows and seawater concentrations, finding that one stage has the largest TAC and the differences between two and three stages are small, but dependent on the costing of pumps used.

The effect of the number of membrane modules in a pressure vessel was also investigated, finding that increasing the maximum number of membranes allowed in a commercial pressure vessel does not have any advantage over the TAC values obtained.

Two-hybrid RO+PRO superstructures were the PRO unit uses the chemical potential of the brine stream of the RO to generate electrical power, acting as an energy recovery unit, were proposed, and optimized with the new stochastic-deterministic methodology.

The second proposed configuration for the system RO+PRO showed a lower TAC than the first one. Besides both configurations used the same brine stream as draw solution, the second one results in an efficient way to integrate the PRO unit as an energy recovery system, since a fraction of the seawater intake necessary for the single RO network is used as a low salinity (feed solution) for the PRO unit, sharing the pretreatment and pumping systems and just increasing a bit the salt concentration of the RO first stage feed flow without affecting the overall performance. So, the second configuration is recommended for the industrial implementation of the integrated technology.

The hybrid RO+PRO configuration presents the same behavior to variations in feed flow and concentration as the single RON, this is an increase in TAC values with an increase in the feed flow and little variations for different feed salt concentrations at a fixed inlet flow.

The comparison between the TAC for the RO with the TAC for the RO integrated with PRO for different feed concentration and feed flow was developed. The RO integrated with PRO shows the highest TAC for all the evaluated coordinates. Nevertheless, the highest difference between both configurations was 2%. The RO shows lower TAC because is a mature technology researched for a long time. An improvement in the PRO energy recovery efficiency could reduce the TAC of the integrated technology since the energy cost of the RO network represents its major operational costs.

8.2 Recommendations to future works

As identified in this work, it will be helpful to obtain actualized cost functions for high-pressure pumps and turbines that capture the nonlinear behavior of costs, for example, a power law for cost, with other exponents might change the results.

A sensitivity analysis using different energy cost values will be interesting, the effect of the feed temperature also could be included in this analysis.

Construction of metamodels for different commercial membrane modules, and the use of binary variables for the choice of one or another might help to obtain efficient reverse osmosis networks with lower TAC values.

For the RO+PRO hybrid system, it will be interesting to validate the use of a fraction of permeate as low salinity feed solution since it will increase the osmotic potential.

The use of the proposed optimization methodology could allow constructing technological roadmap of other hybrid technologies as forward osmosis, membrane distillation, or thermal technologies coupled with reverse osmosis.

The proposed stochastic-deterministic methodology with the use of metamodels will be an interesting optimization tool to apply to other engineering problems.

9 REFERENCES

ABDULRAHIM, H. K.; ALASFOUR, F. N. **Multi-Objective Optimisation of hybrid MSF RO desalination system using Genetic Algorithm**. *International Journal of Exergy*, [s.l.], v. 7, nº 3, p. 387, 2010. ISSN: 1742-8297, DOI: 10.1504/IJEX.2010.031991.

ABOU RAYAN, M.; KHALED, I. **Seawater desalination by reverse osmosis (case study)**. *Desalination*, [s.l.], v. 153, nº 1–3, p. 245–251, 2003. ISSN: 0011-9164, DOI: 10.1016/S0011-9164(02)01143-8.

ACHILLI, A.; CATH, T. Y.; CHILDRESS, A. E. **Power generation with pressure retarded osmosis : An experimental and theoretical investigation**. [s.l.], v. 343, p. 42–52, 2009. DOI: 10.1016/j.memsci.2009.07.006.

AGASHICHEV, S. P. **Analysis of integrated co-generative schemes including MSF, RO and power generating systems (present value of expenses and "levelised" cost of water)**. *Desalination*, [s.l.], v. 164, nº 3, p. 281–302, 2004. ISSN: 0011-9164, DOI: 10.1016/S0011-9164(04)00196-1.

AGASHICHEV, S. P.; EL-NASHAR, A. M. **Systemic approach for techno-economic evaluation of triple hybrid (RO, MSF and power generation) scheme including accounting of CO2 emission**. *Energy*, [s.l.], v. 30, nº 8, p. 1283–1303, 2005. ISSN: 0360-5442, DOI: 10.1016/J.ENERGY.2004.02.002.

AL-BASTAKI, N. M.; ABBAS, A. **Predicting the performance of RO membranes**. *Desalination*, [s.l.], v. 132, nº 1–3, p. 181–187, 2000. ISSN: 00119164, DOI: 10.1016/S0011-9164(00)00147-8.

ALBASTAKI, N.; ABBAS, A. **Modeling an industrial reverse osmosis unit1**. *Desalination*, [s.l.], v. 126, nº 1–3, p. 33–39, 1999. ISSN: 00119164, DOI: 10.1016/S0011-9164(99)00152-6.

ALMANSOORI, A.; SAIF, Y. **Structural optimization of osmosis processes for water and power production in desalination applications**. *Desalination*, [s.l.], v. 344, p. 12–27, 2014. ISSN: 00119164, DOI: 10.1016/j.desal.2014.03.002.

ALNOURI, S. Y.; LINKE, P. **A systematic approach to optimal membrane network synthesis for seawater desalination**. *Journal of Membrane Science*, [s.l.], v. 417–418, p. 96–112, 2012. ISSN: 03767388, DOI: 10.1016/j.memsci.2012.06.017.

ALTAEE, A.; SHARIF, A. **Pressure retarded osmosis: advancement in the process applications for power generation and desalination**. *Desalination*, [s.l.], 2014. ISBN: 4479865179, ISSN: 00119164, DOI: 10.1016/j.desal.2014.09.028.

ANSARI, K.; SAYYAADI, H.; AMIDPOUR, M. **Thermoeconomic optimization of a hybrid pressurized water reactor (PWR) power plant coupled to a multi effect distillation desalination system with thermo-vapor compressor (MED-TVC)**. *Energy*, [s.l.], v. 35, nº 5, p. 1981–1996, 2010. ISSN: 03605442, DOI: 10.1016/j.energy.2010.01.013.

ATIKOL, U.; AYBAR, H. S. **Estimation of water production cost in the feasibility analysis of RO systems**. *Desalination*, [s.l.], v. 184, nº 1–3, p. 253–258, 2005. ISSN: 0011-9164, DOI: 10.1016/J.DESAL.2005.02.065.

AVLONITIS, S. A. **Operational water cost and productivity improvements for small-size RO desalination plants**. *Desalination*, [s.l.], v. 142, nº 3, p. 295–304, 2002. ISSN: 0011-9164, DOI: 10.1016/S0011-9164(02)00210-2.

BAKER, R. W. **Membrane Technology and Applications**. 2 ed. [s.l.]: John Wiley & Sons, Inc., 2004. ISBN: 0470854456.

BEH, E. H. Y. et al. **Environmental Modelling & Software Robust optimization of water infrastructure planning under deep uncertainty using metamodels**. *Environmental Modelling and Software*, [s.l.], v. 93, p. 92–105, 2017. ISSN: 1364-8152, DOI: 10.1016/j.envsoft.2017.03.013.

BROAD, D. R.; DANDY, G. C.; MAIER, H. R. **Environmental Modelling & Software A systematic approach to determining metamodel scope for risk- based optimization and its application to water distribution system**. *Environmental Modelling and Software*, [s.l.], v. 69, p. 382–395, 2015. ISSN: 1364-8152, DOI: 10.1016/j.envsoft.2014.11.015.

BUCHER, C. **Metamodels of optimal quality for stochastic structural optimization**. *Probabilistic Engineering Mechanics*, [s.l.], 2017. ISSN: 0266-8920, DOI: 10.1016/j.probengmech.2017.09.003.

CARVALHO, M.; SECCHI, A. R.; BAGAJEWICZ, M. **Model Reformulation and Global Optimization of Oil Production Using Gas Lift**. *Industrial and Engineering Chemistry Research*, [s.l.], v. 55, nº 38, 2016. ISSN: 15205045, DOI: 10.1021/acs.iecr.6b00223.

CHOI, J. S.; KIM, J. T. **Modeling of full-scale reverse osmosis desalination system: Influence of operational parameters**. *Journal of Industrial and Engineering Chemistry*, [s.l.], v. 21, p. 261–268, 2015. ISSN: 22345957, DOI: 10.1016/j.jiec.2014.02.033.

DAHDAH, H.; MITSOS, A. **Structural optimization of seawater desalination : I . A flexible superstructure and novel MED – MSF configurations**. *Desalination*, [s.l.], v. 344, nº 2014, p. 252–265, 2014. DOI: 10.1016/j.desal.2014.03.030.

DOW WATER & PROCESS SOLUTIONS. **FILMTEC ™ Reverse Osmosis Membranes Technical Manual, Formno.609-00071-1009.** [s.l.]: [s.n.], 2011. 181 p. ISBN: 6090007110.

DRUETTA, P.; AGUIRRE, P.; MUSSATI, S. **Optimization of Multi-Effect Evaporation desalination plants**. *Desalination*, [s.l.], v. 311, p. 1–15, 2013. ISSN: 00119164, DOI: 10.1016/j.desal.2012.10.033.

DU, Y. et al. **Optimization of Reverse Osmosis Networks with Spiral-Wound Modules**. *Industrial & Engineering Chemistry Research*, [s.l.], v. 51, p. 11764–11777, 2012.

DU, Y. et al.**Optimization of reverse osmosis networks with split partial second pass design**. *Desalination*, [s.l.], v. 365, p. 365–380, 2015. ISSN: 00119164, DOI: 10.1016/j.desal.2015.03.019.

EDGAR, T. F.; HIMMELBLAU, D. M.; LASDON, L. S. **Optimization of Chemical Processes**. 2 ed. [s.l.]: McGraw-Hill, 2001. 651 p. ISBN: 9780070393592, ISSN: 00092509, DOI: 10.1016/0009-2509(89)85111-5.

EL-HALWAGI, M. M. **Synthesis of Reverse-Osmosis Networks for Waste Reduction.** *AIChE Journal,* [s.l.], v. 38, no 8, p. 1185–1198, 1992.

EL-HALWAGI, M.; AL-AHMAD, M.; ZHU, M. **Optimal design and scheduling of flexible reverse osmosis networks**. *Journal of Membrane Science*, [s.l.], v. 129, p. 161–174, 1997.

EVANGELISTA, F. **A Short Cut Method for the Design of Reverse Osmosis Desalination Plants**. *Industrial & Engineering Chemistry Process Design and Development*, [s.l.], v. 24, p. 211–223, 1985.

FARIA, C.; BAGAJEWICZ, M. J. **A New Approach for Global Optimization of a Class of MINLP Problems with Applications to Water Management and Pooling Problems**. *AICHE Journal*, [s.l.], v. 58, nº 8, 2012. DOI: 10.1002/aic.

FLOUDAS, C. A.; GOUNARIS, C. E. **A review of recent advances in global optimization**. *Journal of Global Optimization*, [s.l.], v. 45, nº 1, p. 3–38, 2009. ISBN: 0925-5001, ISSN: 09255001, DOI: 10.1007/s10898-008-9332-8.

FLOUDAS, C. a. **Nonlinear and Mixed-Integer Optimization: Fundamentals and Applications**. *Handbook of Applied Optimization*. [s.l.]: Oxford University Press, 1995. 462 p. ISBN: 0-19-510056-5, ISSN: 09255001, DOI: 10.1023/A:1008256302713.

FONTEIX, C. et al. **Haploid and diploid algorithms, a new approach for global optimization: Compared performances**. *International Journal of Systems Science*, [s.l.], v. 26, nº 10, p. 1919–1933, 1995. ISBN: 0020-7721, ISSN: 14645319, DOI: 10.1080/00207729508929145.

GERALDES, V.; PEREIRA, N. E.; NORBERTA DE PINHO, M. **Simulation and Optimization of Medium-Sized Seawater Reverse Osmosis Processes with Spiral-Wound Modules**. *Industrial & Engineering Chemistry Research*, [s.l.], v. 44, p. 1897–1905, 2005. ISBN: 0035121841751, ISSN: 0888-5885, DOI: 10.1021/ie049357s.

GHAFFOUR, N. et al. **Renewable energy-driven desalination technologies: A comprehensive review on challenges and potential applications of integrated systems**. *Desalination*, [s.l.], v. 356, p. 94–114, 2015. ISBN: 00119164, ISSN: 00119164, DOI: 10.1016/j.desal.2014.10.024.

GHAFFOUR, N.; MISSIMER, T. M.; AMY, G. L. **Technical review and evaluation of the economics of water desalination: Current and future challenges for better water supply sustainability**. *Desalination*, [s.l.], v. 309, nº 2013, p. 197–207, 2013. ISBN: 0011-9164, ISSN: 00119164, DOI: 10.1016/j.desal.2012.10.015.

GHOBEITY, A.; MITSOS, A. **Optimal design and operation of desalination systems : new challenges and recent advances**. *Current Opinion in Chemical Engineering*, [s.l.], v. 6, p. 61–68, 2014. ISSN: 2211-3398, DOI: 10.1016/j.coche.2014.09.008.
GROSSMANN, I. et al. **DICOPT**. *GAMS Development Corporation*. 2016. Disponível em: <https://www.gams.com/>.

GUTHRIE, K. M. **Data and Techniques for Preilinary Capital Cost Estimation**. *Chemical Engineering*, [s.l.], nº March 24, p. 114–142, 1969.

HABERT, A. C.; BORGES, C. P.; NOBREGA, R. **Processos de Separação por Membranas**. [s.l.]: e-papers, 2006. 180 p. ISBN: 857650085X.

HAFEZ, A.; EL-MANHARAWY, S. **Economics of seawater RO desalination in the Red Sea region, Egypt. Part 1. A case study**. *Desalination*, [s.l.], v. 153, nº 1–3, p. 335–347, 2003. ISSN: 0011-9164, DOI: 10.1016/S0011-9164(02)01122-0.

HELFER, F.; LEMCKERT, C.; ANISSIMOV, Y. G. **Osmotic power with Pressure Retarded Osmosis: Theory, performance and trends - A review**. *Journal of Membrane Science*, [s.l.], v. 453, p. 337–358, 2014. ISBN: 0376-7388, ISSN: 03767388, DOI: 10.1016/j.memsci.2013.10.053.

JAFFAL, I.; INARD, C. **A metamodel for building energy performance**. *Energy & Buildings*, [s.l.], v. 151, p. 501–510, 2017. ISSN: 0378-7788, DOI: 10.1016/j.enbuild.2017.06.072.

JIANG, A. et al. **Mathematical Modeling and Simulation of SWRO Process Based on Simultaneous Method**. *Journal of Applied Mathematics*, [s.l.], v. 2014, 2014.

JIANG, A. et al. **Operational cost optimization of a full-scale SWRO system under multi-parameter variable conditions**. *Desalination*, [s.l.], v. 355, p. 124–140, 2015. ISSN: 0011-9164, DOI: 10.1016/j.desal.2014.10.016.

KAMALI, R. K.; MOHEBINIA, S. **Experience of design and optimization of multi-effects desalination systems in Iran**. *Desalination*, [s.l.], v. 222, nº 1–3, p. 639–645, 2008. ISSN: 00119164, DOI: 10.1016/j.desal.2007.01.182.

KHAWAJI, A. D.; KUTUBKHANAH, I. K.; WIE, J. M. **Advances in seawater desalination technologies**. *Desalination*, [s.l.], v. 221, nº 1–3, p. 47–69, 2008. ISBN: 0011-9164, ISSN: 00119164, DOI: 10.1016/j.desal.2007.01.067.

KIM, S Y; BAGAJEWICZ, M. **Global Optimization of Heat Exchanger Networks. Part 2: Stages/Substages Superstructure with Variable Cp**. *Industrial and Engineering Chemistry Research*, [s.l.], v. 56, nº 20, p. 5958–5969, 2017. DOI: 10.1021/acs.iecr.6b04687.

KIM, Sung Young et al. **Global Optimization of Heat Exchanger Networks. Part 1: Stages/Substages Superstructure**. *Industrial & Engineering Chemistry Research*, [s.l.], v. 56, nº 20, p. 5944–5957, 2017. ISSN: 0888-5885, DOI: 10.1021/acs.iecr.6b04686.

KIM, Sung Young; BAGAJEWICZ, M. **Global optimization of heat exchanger networks using a new generalized superstructure**. *Chemical Engineering Science*, [s.l.], v. 147, p. 30–46, 2016. ISSN: 00092509, DOI: 10.1016/j.ces.2016.02.002.

KIM, Y. S. Y. M. et al. **Overview of systems engineering approaches for a large-scale seawater desalination plant with a reverse osmosis network**. *Desalination*, [s.l.], v. 238, nº 1–3, p. 312–332, 2009. ISBN: 0011-9164, ISSN: 00119164, DOI: 10.1016/j.desal.2008.10.004.

KLEIJNEN, J. P. C. **Regression and Kriging metamodels with their experimental designs in simulation : A review**. [s.l.], v. 256, p. 1–16, 2017.

KUCERA, J. **Desalination: Water from Water**. 1 ed. [s.l.]: John Wiley and Sons, 2014. 664 p. ISBN: 9781118208526.

LEE, J. G. et al. **Numerical study of a hybrid multi-stage vacuum membrane distillation and pressure-retarded osmosis system**. *Desalination*, [s.l.], v. 363, p. 82–91, 2015. ISSN: 00119164, DOI: 10.1016/j.desal.2015.01.043.

LEITNER, G. F. **Total water costs on a standard basis for three large, operating , S.W.R.O. plants**. *Desalination*, [s.l.], v. 81, nº 1–3, p. 39–48, 1991. ISSN: 0011-9164, DOI: 10.1016/0011-9164(91)85043-T.

LU, Y.; LIAO, A.; HU, Y. **Design of reverse osmosis networks for multiple freshwater production**. *Korean Journal of Chemical Engineering*, [s.l.], v. 30, nº 5, p. 988–996, 2013. ISBN: 0256-1115, ISSN: 02561115, DOI: 10.1007/s11814-013-0009-8.

LU, Y. Y. et al. **Optimum design of reverse osmosis system under different feed concentration and product specification**. *Journal of Membrane Science*, [s.l.], v. 287, nº 2, p. 219–229, 2007. ISBN: 5326678187, ISSN: 03767388, DOI: 10.1016/j.memsci.2006.10.037.

MAHMOUDI, S.; TRIVAUDEY, F.; BOUHADDI, N. **Bene fi ts of metamodel-reduction for nonlinear dynamic response analysis of damaged composite structures**. *Finite Elements in Analysis and Design*, [s.l.], v. 119, p. 1–14, 2016. ISSN: 0168-874X, DOI: 10.1016/j.finel.2016.05.001.

MALEK, A.; HAWLADER, M. N. A.; HO, J. C. **Design and economics of RO seawater desalination**. *Desalination*, [s.l.], v. 105, nº 3, p. 245–261, 1996. ISBN: 0011-9164, ISSN: 00119164, DOI: 10.1016/0011-9164(96)00081-1.

MALIK, S. N.; BAHRI, P. A.; VU, L. T. T. **Superstructure Development, Simulation and Optimization of Desalination Systems using Aspen Custom Modeler**. In: *12th International Symposium on Process Systems Engineering and 25th European Symposium on Computer Aided Process Engineering*. [s.l.]: Elsevier, 2015. Disponível em: <http://linkinghub.elsevier.com/retrieve/pii/B9780444635785500591>. ISSN: 1570-7946, DOI: 10.1016/B978-0-444-63578-5.50059-1.

MARCOVECCHIO, M. G. et al. **Optimization of hybrid desalination processes including multi stage flash and reverse osmosis systems**. *Desalination*, [s.l.], v. 182, nº 1–3, p. 111–122, 2005. ISSN: 00119164, DOI: 10.1016/j.desal.2005.03.011.

MARCOVECCHIO, M. G.; AGUIRRE, P. a.; SCENNA, N. J. **Global optimal design of reverse osmosis networks for seawater desalination: modeling and algorithm**. *Desalination*, [s.l.], v. 184, nº 1–3, p. 259–271, 2005. ISSN: 00119164, DOI: 10.1016/j.desal.2005.03.056.

MASKAN, F. et al. **Optimal Design of Reverse Osmosis Module Networks**. *AICHE Journal*, [s.l.], v. 46, nº 5, 2000.

MISENER, R.; FLOUDAS, C. A. **ANTIGONE: Algorithms for continuous / Integer Global Optimization of Nonlinear Equations**. *Journal of Global Optimization*, [s.l.], v. 59, nº 2–3, p. 503–526, 2014. ISBN: 1573-2916, ISSN: 15732916, DOI: 10.1007/s10898-014-0166-2.

NAGHILOO, A. et al. **Modeling and design of a 25MW osmotic power plant (PRO) on Bahmanshir River of Iran**. *Renewable Energy*, [s.l.], v. 78, nº November 2009, p. 51–59, 2015. ISSN: 18790682, DOI: 10.1016/j.renene.2014.12.067.

OH, H. J.; HWANG, T. M.; LEE, S. **A simplified simulation model of RO systems for seawater desalination**. *Desalination*, [s.l.], v. 238, nº 1–3, p. 128–139, 2009. ISBN: 0011-9164, ISSN: 00119164, DOI: 10.1016/j.desal.2008.01.043.

PARK, S.-M. et al. **Optimization of hybrid system consisting of forward osmosis and reverse osmosis: a Monte Carlo simulation approach**. *Desalination and Water Treatment*, [s.l.], v. 43, nº 1–3, p. 274–280, 2012. ISSN: 1944-3994, DOI: 10.1080/19443994.2012.672196.

POULLIKKAS, A. **Optimization algorithm for reverse osmosis desalination economics**. *Desalination*, [s.l.], v. 133, nº 1, p. 75–81, 2001. ISSN: 0011-9164, DOI: 10.1016/S0011-9164(01)00084-4.

PRACTICE, S. M. **Simulation Modelling Practice and Theory Interval metamodels for the analysis of simulation Input – Output relations**. [s.l.], v. 54, p. 86–100, 2015. DOI: 10.1016/j.simpat.2015.03.008.

PRANTE, J. L. et al. **RO-PRO desalination: An integrated low-energy approach to seawater desalination**. *Applied Energy*, [s.l.], v. 120, p. 104–114, 2014. ISBN: 0306-2619, ISSN: 03062619, DOI: 10.1016/j.apenergy.2014.01.013.

PSALTIS, A.; SINOQUET, D.; PAGOT, A. **Systematic optimization methodology for heat exchanger network and simultaneous process design**. *Computers and Chemical Engineering*, [s.l.], v. 95, p. 146–160, 2016. ISSN: 0098-1354, DOI: 10.1016/j.compchemeng.2016.09.013.

ROSENTHAL, R. E. **GAMS — A User ' s Guide**. [s.l.], nº October, 2015.

SAHINIDIS, N. V. **BARON: A general purpose global optimization software package**. *Journal of Global Optimization*, [s.l.], v. 8, nº 2, p. 201–205, 1996. ISBN: 0925-5001, ISSN: 0925-5001, DOI: 10.1007/BF00138693.

SAIF, Y.; ALMANSOORI, A.; ELKAMEL, A. **Optimal Design of Split Partial Second Pass Reverse Osmosis Network for Desalination Applications**. [s.l.], v. 60, nº 2, 2014. DOI: 10.1002/aic.

SAITO, K. et al. **Power generation with salinity gradient by pressure retarded osmosis using concentrated brine from SWRO system and treated sewage as pure water**. *Desalination and Water Treatment*, [s.l.], v. 41, nº 1–3, p. 114–121, 2012. ISBN: 1944-3994, ISSN: 19443986, DOI: 10.1080/19443994.2012.664696.

SASSI, K. M.; MUJTABA, I. M. **Effective design of reverse osmosis based desalination process considering wide range of salinity and seawater temperature**. *Desalination*, [s.l.], v. 306, p. 8–16, 2012. ISBN: 0011-9164, ISSN: 00119164, DOI: 10.1016/j.desal.2012.08.007.

SASSI, K. M.; MUJTABA, I. M. **MINLP based superstructure optimization for boron removal during desalination by reverse osmosis**. *Journal of Membrane Science*, [s.l.], v. 440, p. 29–39, 2013. ISSN: 03767388, DOI: 10.1016/j.memsci.2013.03.012.

SCHOCK, G.; MIQUEL, A. **Mass transfer and pressure loss in spiral wound modules**. *Desalination*, [s.l.], v. 64, nº C, p. 339–352, 1987. ISBN: 0011-9164, ISSN: 00119164, DOI: 10.1016/0011-9164(87)90107-X.

SHAKIB, S. E.; AMIDPOUR, M.; AGHANAJAFI, C. **Simulation and optimization of multi effect desalination coupled to a gas turbine plant with HRSG consideration**. *Desalination*, [s.l.], v. 285, p. 366–376, 2012. ISSN: 00119164, DOI: 10.1016/j.desal.2011.10.028.

SHATAT, M.; RIFFAT, S. B. **Water desalination technologies utilizing conventional and renewable energy sources**. *International Journal of Low-Carbon Technologies*, [s.l.], v. 9, nº 1, p. 1–19, 2014. ISBN: 1748-1317, ISSN: 17481317, DOI: 10.1093/ijlct/cts025.

SHRIVASTAVA, A.; ROSENBERG, S.; PEERY, M. **Energy efficiency breakdown of reverse osmosis and its implications on future innovation roadmap for desalination**. *Desalination*, [s.l.], v. 368, p. 181–192, 2015. ISSN: 0011-9164, DOI: 10.1016/J.DESAL.2015.01.005.

SKIBOROWSKI, M. et al. **Model-based structural optimization of seawater desalination plants**. *Desalination*, [s.l.], v. 292, p. 30–44, 2012. ISSN: 0011-9164, DOI: 10.1016/j.desal.2012.02.007.

THE MATHWORKS INC. **MATLAB - MathWorks**. *www.mathworks.com/products/matlab*. 2016. Disponível em: <http://www.mathworks.com/products/matlab/>. DOI: 2016-11-26.

VINCE, F. et al. **Multi-objective optimization of RO desalination plants**. *Desalination*, [s.l.], v. 222, nº 1–3, p. 96–118, 2008. ISBN: 0011-9164, ISSN: 00119164, DOI: 10.1016/j.desal.2007.02.064.

VOROS, N. G.; MAROULIS, Z. B. **Short-cut structural design of reverse osmosis desalination plants**. [s.l.], v. 127, p. 47–68, 1997.

VOROS, N.; MAROULIS, Z. B. **Pergamon FOR SEAWATER DESALINATION**. *Science*, [s.l.], v. 20, nº 96, 1996.

VOROS, N.; MAROULIS, Z. B.; MARINOS-KOURIS, D. **Optimization of reverse osmosis networks for seawater desalination**. *Computers & Chemical Engineering*, [s.l.], v. 20, p. S345–S350, 1996. ISSN: 00981354, DOI: 10.1016/0098-1354(96)00068-3.

VOUTCHKOV, N. **Desalination Engineering: Planning and Design**. 1 ed. [s.l.]: McGraw-Hill, 2012. 688 p. ISBN: 0071777156 / 9780071777155, ISSN: 1098-6596, DOI: 10.1007/s13398-014-0173-7.2.

WADE, N. M. **Distillation plant development and cost update**. *Desalination*, [s.l.], v. 136, nº 1–3, p. 3–12, 2001. ISSN: 0011-9164, DOI: 10.1016/S0011-9164(01)00159-X.

WAN, C. F.; CHUNG, T. S. **Osmotic power generation by pressure retarded osmosis using seawater brine as the draw solution and wastewater retentate as the feed**. *Journal of Membrane Science*, [s.l.], v. 479, p. 148–158, 2015. ISBN: 0014-4827, ISSN: 18733123, DOI: 10.1016/j.memsci.2014.12.036.

FENG, C.; CHUNG, T. **Energy recovery by pressure retarded osmosis (PRO) in SWRO-PRO integrated processes**. *Applied Energy*, [s.l.], v. 162, p. 687–698, 2016. ISSN: 03062619, DOI: 10.1016/j.apenergy.2015.10.067.

WANG, Jian et al. **Operational Optimization of Large-Scale Parallel-Unit SWRO Desalination Plant Using Differential Evolution Algorithm**. *Scientific World Journal*, [s.l.], v. 2014, 2014. ISSN: 1537-744X, DOI: 10.1155/2014/584068.

WANG, Jinwen et al. **A critical review of transport through osmotic membranes**. *Journal of Membrane Science*, [s.l.], v. 454, p. 516–537, 2014. ISSN: 0376-7388, DOI: 10.1016/j.memsci.2013.12.034.

WEN, J. et al. **International Journal of Heat and Mass Transfer Energy and cost optimization of shell and tube heat exchanger with helical baffles using Kriging metamodel based on MOGA**. [s.l.], v. 98, p. 29–39, 2016. DOI: 10.1016/j.ijheatmasstransfer.2016.02.084.

WU, S.; ZHANG, Z. **An approach to improve the economy of desalination plants with a nuclear heating reactor by coupling with hybrid technologies**. *Desalination*, [s.l.], v. 155, nº 2, p. 179–185, 2003. ISSN: 0011-9164, DOI: 10.1016/S0011-9164(03)00295-9.

ZAK, G.; MITSOS, A. **Hybrid thermal-thermal desalination structures**. *Desalination and Water Treatment*, [s.l.], v. 52, p. 2905–2919, 2014.

ZEJLI, D. et al. **Economic analysis of wind-powered desalination in the south of Morocco**. *Desalination*, [s.l.], v. 165, p. 219–230, 2004. ISSN: 0011-9164, DOI: 10.1016/J.DESAL.2004.06.025.

APPENDIX

Appendix 1.

Reverse osmosis network general mathematical model

The State Space version of a generalized superstructure with all the possible connections between units is shown in Figure A1. In this representation, the inputs of the distribution box are considered splitting nodes and all the outputs are considered mixing nodes.

Distribution box:

The distribution box is a network, describing the connection between the units and the feed and product streams, and consists of a series of splitting nodes (inputs) and mixing nodes (outputs), all the streams are characterized by a flow rate (*F*), a salt concentration (*C*) and a pressure (*P*), the superscripts *HPP, T, RO, P,* and *B* represents high-pressure pump, turbine, reverse osmosis stage, permeate and brine respectively, therefore *B-HPP* indicates the distribution from *B* to *HPP*, and so. The subscripts *p*, *t* and *m* are indexes that indicate the number of pumps, turbines and reverse osmosis stages respectively. The subscripts *S, P* and *B* means seawater, permeate and brine.

In addition, each stream that is distributed from a unit to another has a binary decision variable associated with it, that will take the value of one (1) if the stream exists or zero (0) if not. For example, if a distribution from a (p) pump to a reverse osmosis stage (m) $F_{p,m}^{HPP-RO} > 0$, the corresponding binary variable $y_{p,m}^{HPP-RO}$ takes a value of one.

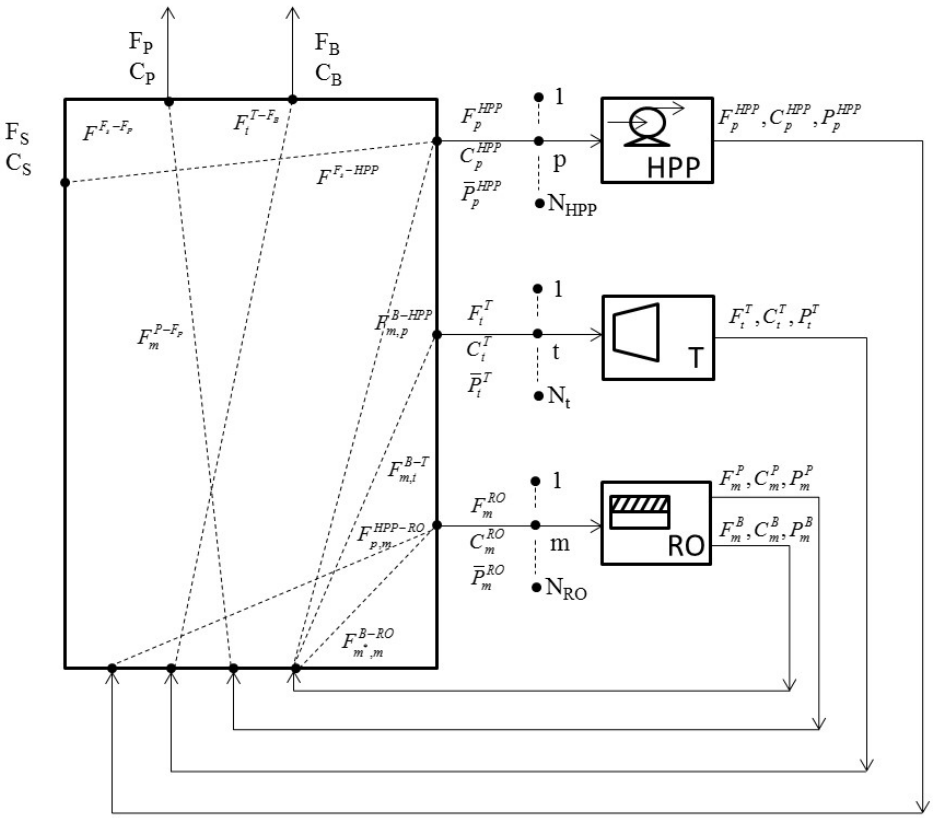

Figure A1. State Space Representation of the Superstructure of a reverse osmosis network.

Mixing Models:

Where mixing takes place one or more streams may be arriving at the node and are grouped into an output stream of the node, since in this type of node can occur mixture of different stream, the global mass balance is accompanied by the salt balance.

Pumps Mixing:

$$F_p^{HPP} = F_p^{F_s-HPP} + \sum_{m=1}^{N_{RO}} F_{m,p}^{B-HPP} \qquad \text{A1.(1)}$$

$$F_p^{HPP} C_p^{HPP} = F_p^{F_s-HPP} \hat{C}_S + \sum_{m=1}^{N_{RO}} F_{m,p}^{B-HPP} C_m^B \qquad \text{A1.(2)}$$

Turbines Mixing: (No flow from pumps is considered):

$$F_t^T = \sum_{m=1}^{N_{RO}} F_{m,t}^{B-T} \qquad \text{A1.(3)}$$

$$F_t^T C_t^T = \sum_{m=1}^{N_{RO}} F_{m,t}^{B-T} C_m^B \qquad \text{A1.(4)}$$

Reverse Osmosis units Inlet balances:

$$F_m^{RO} = \sum_{m^*=1}^{N_{RO}} F_{m^*,m}^{B-RO} + \sum_{p=1}^{N_{HPP}} F_{p,m}^{HPP-RO} \qquad \text{A1.(5)}$$

$$F_m^{RO} C_m^{RO} = \sum_{m^*=1}^{N_{RO}} F_{m^*,m}^{B-RO} C_{m^*}^{B} + \sum_{p=1}^{N_{HPP}} F_{p,m}^{HPP-RO} C_p^{HPP} \qquad \text{A1.(6)}$$

Balances for the Outlet Permeate stream:

$$\hat{F}_{PO} = \sum_{m=1}^{N_{RO}} F_m^{P-F_{PO}} \qquad \text{A1.(7)}$$

$$\hat{F}_{PO} C_{PO} = \sum_{m=1}^{N_{RO}} F_m^{P-F_{PO}} C_m^{P} \qquad \text{A1.(8)}$$

$$C_{PO} \le C_P^{Max} \qquad \text{A1.(9)}$$

Balances for the Outlet Brine stream:

$$F_{BO} = \sum_{t=1}^{N_T} F_t^{T-F_{BO}} \qquad \text{A1.(10)}$$

$$F_{BO} C_{BO} = \sum_{t=1}^{N_T} F_t^{T-F_{BO}} C_t^{T} \qquad \text{A1.(11)}$$

Additionally, to ensure that only the mixt of streams with pressures larger than or equal to the pressure of the destination unit:

$$Ps \ge Pn_p^{HPP} \quad \text{only if} \quad F_p^{Fs-HPP} > 0 \qquad \text{A1.(12)}$$

$$P_m^{P} \ge Pn_p^{HPP} \quad \text{only if} \quad F_{m,p}^{P-HPP} > 0 \qquad \text{A1.(13)}$$

$$P_{p*}^{HPP} \ge Pn_p^{HPP} \quad \text{only if} \quad F_{p*,p}^{HPP-HPP} > 0 \qquad \text{A1.(14)}$$

$$P_m^{B} \ge Pn_p^{HPP} \quad \text{only if} \quad F_{m,p}^{B-HPP} > 0 \qquad \text{A1.(15)}$$

$$P_m^{B} \ge Pn_t^{T} \quad \text{only if} \quad F_{m,t}^{B-T} > 0 \qquad \text{A1.(16)}$$

$$P_m^{B} \ge Pn_m^{RO} \quad \text{only if} \quad F_{m*,m}^{B-RO} > 0 \qquad \text{A1.(17)}$$

$$P_p^{HPP} \ge Pn_m^{RO} \quad \text{only if} \quad F_{p,m}^{HPP-RO} > 0 \qquad \text{A1.(18)}$$

$$P_m^{P} \ge P^{PPO} \quad \text{only if} \quad F_m^{P-F_P} > 0 \qquad \text{A1.(19)}$$

$$P_t^{T} \ge P^{B} \quad \text{only if} \quad F_t^{T-F_B} > 0 \qquad \text{A1.(20)}$$

These conditions can be rewritten in a form amenable to a MINLP model as follows:

$$F_p^{Fs-HPP} - y_p^{Fs-HPP}\Gamma_F^{Fs-HPP} \leq 0 \qquad \text{A1.(21)}$$

$$Ps \geq Pn_p^{HPP} - (1 - y_p^{Fs-HPP})\Gamma_P^{Fs-HPP} \qquad \text{A1.(22)}$$

where Γ_F^{Fs-HPP} and Γ_P^{Fs-HPP} are larger than the maximum flow expected, and maximum pressure expected/allowed. Indeed, when $F_p^{Fs-HPP} > 0$, then y_p^{Fs-HPP} is forced to be one for A1.(21) to hold. Then, if $y_p^{Fs-HPP} = 1$, equation A1.(22) reduces to $Ps \geq Pn_p^{HPP}$. Otherwise, when $F_p^{Fs-HPP} = 0$, then y_p^{Fs-HPP} can take any value, including $y_p^{Fs-HPP} = 0$, which is compatible with $Ps < Pn_p^{HPP}$, if that is necessary.

The rest of the equations for node to node connections are the following:

$$F_{m,p}^{P-HPP} - y_{m,p}^{P-HPP}\Gamma_F^{P-HPP} \leq 0 \qquad \text{A1.(23)}$$

$$P_m^P \geq Pn_p^{HPP} - \left(1 - y_{m,p}^{P-HPP}\right)\Gamma_P^{P-HPP} \qquad \text{A1.(24)}$$

$$F_{m,p}^{B-HPP} - y_{m,p}^{B-HPP}\Gamma_F^{B-HPP} \leq 0 \qquad \text{A1.(25)}$$

$$P_m^B \geq Pn_p^{HPP} - (1 - y_{m,p}^{B-HPP})\Gamma_P^{B-HPP} \qquad \text{A1.(26)}$$

$$F_{m,t}^{B-T} - y_{m,t}^{B-T}\Gamma_F^{B-T} \leq 0 \qquad \text{A1.(27)}$$

$$P_m^B \geq Pn_t^T - \left(1 - y_{m,t}^{B-T}\right)\Gamma_P^{B-T} \qquad \text{A1.(28)}$$

$$F_{m*,m}^{B-RO} - y_{m*,m}^{B-RO}\Gamma_F^{B-RO} \leq 0 \qquad \text{A1.(29)}$$

$$P_{m*}^B \geq Pn_m^{RO} - (1 - y_{m*,m}^{B-RO})\Gamma_P^{B-RO} \qquad \text{A1.(30)}$$

$$F_{p,m}^{HPP-RO} - y_{p,m}^{HPP-RO}\Gamma_F^{HPP-RO} \leq 0 \qquad \text{A1.(31)}$$

$$P_p^{HPP} \geq Pn_m^{RO} - (1 - y_{p,m}^{HPP-RO})\Gamma_P^{HPP-RO} \qquad \text{A1.(32)}$$

$$F_m^{P-F_P} - y_m^{P-F_P}\Gamma_F^{P-F_P} \leq 0 \qquad \text{A1.(33)}$$

$$P_m^P \geq P_P - (1 - y_m^{P-F_P})\Gamma_P^{P-F_P} \qquad \text{A1.(34)}$$

$$F_t^{T-F_B} - y_t^{T-F_B}\Gamma_F^{T-F_B} \leq 0 \qquad \text{A1.(35)}$$

$$P_t^T \geq P_B - (1 - y_t^{T-F_B})\Gamma_P^{T-F_B} \qquad \text{A1.(36)}$$

Splitting:

In splitting nodes an inlet stream can be divided into multiple output streams since in this type of node only streams division takes place, the concentration and pressure of the output streams are equal to the concentration and pressure of the incoming stream.

$$F_S = \sum_{p=1}^{N_{HPP}} F_{s,p}^{F_s-HPP} \qquad \text{A1.(37)}$$

The inlet stream F_S is usually available at atmospheric pressure so it cannot be used in turbines or in reverse osmosis units. Therefore, those streams have not been added. In addition, there is a connection to the Permeate because there is the possibility that the final permeate concentration reaches values lower than the maximum concentration allowed so this way the final permeate flow could be completed. Finally, a feed to brine connection was not added as it would always be uneconomical.

$$F_m^B = \sum_{p=1}^{N_{HPP}} F_{m,p}^{B-HPP} + \sum_{t=1}^{N_T} F_{m,t}^{B-T} + \sum_{m^*=1}^{N_{RO}} F_{m,m^*}^{B-RO} + F_m^R \qquad \text{A1.(38)}$$

$$F_m^P = F_m^{P-F_P} \qquad \text{A1.(39)}$$

$$F_t^T = F_t^{T-F_B} \qquad \text{A1.(40)}$$

$$F_p^{HPP} = F_{p,m}^{HPP-RO} \qquad \text{A1.(41)}$$

Appendix 2.

To deal with the presence of bi-linearities and construct a linear lower bound model a reformulation is necessary.

For example, equation (2) could be rewritten as follows:

$$Z_p^{HPP} = F_p^{F_s-HPP}\hat{C}_S + \sum_{m=1}^{N_{RO}} Z_{m,p}^{B-HPP} \qquad \text{A2.(1)}$$

Where the product of the two variables was substituted by:

$$Z_p^{HPP} = F_p^{HPP} C_p^{HPP} \qquad \text{A2.(2)}$$

$$Z_{m,p}^{B-HPP} = F_{m,p}^{B-HPP} C_m^{B} \qquad \text{A2.(3)}$$

Now it is necessary to choose which one of the two variables is going to be discretized in D-1 intervals, in this case, it was picked the concentration variables, so they became:

$$DC_{p,d}^{HPP} = C_p^{HPP.L} + (d-1)\frac{(C_p^{HPP.UP} - C_p^{HPP.L})}{D-1} \quad \forall d = 1..D-1 \quad C_p^{HPP.L} \le C_p^{HPP} \le C_p^{HPP.UP} \qquad \text{A2.(4)}$$

$$DC_{m,d}^{B} = C_m^{B.L} + (d-1)\frac{(C_m^{B.UP} - C_m^{B.L})}{D-1} \quad \forall d = 1..D-1 \quad C_m^{B.L} \le C_m^{B} \le C_m^{B.UP} \qquad \text{A2.(5)}$$

Where the super index (L) and (UP) indicate the lower and upper bounds of the variable.

Now the variable is substituted by its discrete bounds, thus allowing Z to be inside of one of the intervals, that is, between two successive discrete values. Binary variables (*vd*) are used to guaranty that only one interval is picked.

$$Z_p^{HPP} \le \sum_{d=1}^{D-1} DC_{p,d+1}^{HPP} w_{p,d}^{HPP} \qquad \text{A2.(6)}$$

$$Z_{m,p}^{B-HPP} \le \sum_{d=1}^{D-1} DC_{m,d+1}^{B} w_{m,p,d}^{B-HPP} \qquad \text{A2.(7)}$$

And:

$$Z_p^{HPP} \ge \sum_{d=1}^{D-1} DC_{p,d}^{HPP} w_{p,d}^{HPP} \qquad \text{A2.(8)}$$

$$Z_{m,p}^{B-HPP} \ge \sum_{d=1}^{D-1} DC_{m,d}^{B} w_{d}^{B-HPP} \qquad \text{A2.(9)}$$

The discretized variables need to satisfy:

$$C_p^{HPP} \leq \sum_{d=1}^{D-1} DC_{p,d+1}^{HPP} v_{p,d}^{HPP} \qquad \text{A2.(10)}$$

$$C_p^{HPP} \geq \sum_{d=1}^{D-1} DC_{p,d}^{HPP} v_{p,d}^{HPP} \qquad \text{A2.(11)}$$

$$C_m^{B} \leq \sum_{d=1}^{D-1} DC_{m,d+1}^{B} v_{m,d}^{B} \qquad \text{A2.(12)}$$

$$C_m^{B} \geq \sum_{d=1}^{D-1} DC_{m,d}^{B} v_{m,d}^{B} \qquad \text{A2.(13)}$$

And Finally to guaranty that only one interval is picked:

$$\sum_{d=1}^{D-1} v_{p,d}^{HPP} = 1 \qquad \text{A2.(14)}$$

$$\sum_{d=1}^{D-1} v_{m,d}^{B} = 1 \qquad \text{A2.(15)}$$

Now the *wd* expressions are defined as follows (those are to linearize the product of a continuous and a binary variable:

$$w_{p,d}^{HPP} - F_p^{HPP.UP} v_{p,d}^{HPP} \leq 0 \qquad \text{A2.(16)}$$

$$(F_p^{HPP} - w_{p,d}^{HPP}) - F_p^{HPP.UP}(1 - v_{p,d}^{HPP}) \qquad \text{A2.(17)}$$

$$F_p^{HPP} - w_{p,d}^{HPP} \geq 0 \qquad \text{A2.(18)}$$

$$w_{m,p,d}^{B-HPP} - F_{m,p}^{B-HPP.UP} v_{m,d}^{B} \leq 0 \qquad \text{A2.(19)}$$

$$(F_{m,p}^{B-HPP} - w_{m,p,d}^{B-HPP}) - F_{m,p}^{B-HPP.UP}(1 - v_{m,d}^{B}) \leq 0 \qquad \text{A2.(20)}$$

$$F_{m,p}^{B-HPP} - w_{m,p,d}^{B-HPP} \geq 0 \qquad \text{A2.(21)}$$

The same procedure is applied to each one of the bi-linear terms.

Appendix 3.

After an algebraic manipulation of equations 65 – 88, the following expressions are obtained:

$$W1_{m,e} = W2_{m,e} - \hat{P}^{Pe}_{m,e} W3 - \hat{a}_{\pi} \hat{T} W4_{m,e} + \hat{a}_{\pi} \hat{T} W5_{m,e} * \hat{S}_{mem} 1000 \hat{\rho}_P + \hat{a}_{\pi} \hat{T} W6_{m,e} * 1000 \hat{\rho}_P \quad \text{A3.(1)}$$

$$W7_{m,e} = \hat{b}\left(W8_{m,e} - W9_{m,e} \hat{S}_{mem} 1000 \hat{\rho}_P - W10_{m,e} (1000 \hat{\rho}_P) \right) \quad \text{A3.(2)}$$

Where $W1_{m,e}$ to $W10_{m,e}$ are functions to be discretized according to the next equations:

$$\sum_{d_{\Delta P}} \sum_{d_F} \sum_{d_{\hat{J}}} \begin{bmatrix} \Delta \hat{P}^{nd}_{m,e,d_{\Delta P}} \hat{F}^{in}_{m,e,d_F} (\hat{a} \Delta \hat{P}^{nd}_{m,e,d_{\Delta P}} + \hat{J}^{S}_{m,e,d_{\hat{J}}}) \\ -\Delta \hat{P}^{nd}_{m,e,d_{\Delta P}} (\hat{a} \Delta \hat{P}^{nd}_{m,e,d_{\Delta P}} + \hat{J}^{S}_{m,e,d_{\hat{J}}})^2 \hat{S}_{mem} \end{bmatrix} W^{\Delta \hat{P}, \hat{F}in, \hat{J}s}_{m,e,d_{\Delta P}, d_F, d_{\hat{J}}} \le W1_{m,e}$$

$$W1_{m,e} \le \sum_{d_{\Delta P}} \sum_{d_F} \sum_{d_{\hat{J}}} \begin{bmatrix} \Delta \hat{P}^{nd}_{m,e,(d_{\Delta P}+1)} \hat{F}^{in}_{m,e,(d_F+1)} (\hat{a} \Delta \hat{P}^{nd}_{m,e,(d_{\Delta P}+1)} + \hat{J}^{S}_{m,e,(d_{\hat{J}}+1)}) \\ -\Delta \hat{P}^{nd}_{m,e,(d_{\Delta P}+1)} (\hat{a} \Delta \hat{P}^{nd}_{m,e,(d_{\Delta P}+1)} + \hat{J}^{S}_{m,e,(d_{\hat{J}}+1)})^2 \hat{S}_{mem} \end{bmatrix} W^{\Delta \hat{P}, \hat{F}in, \hat{J}s}_{m,e,d_{\Delta P}, d_F, d_{\hat{J}}} \quad \text{A3.(3)}$$

Where the product of binary variables is substituted by the following variable and its corresponding set of equations:

$$W^{\Delta \hat{P}, \hat{F}in, \hat{J}s}_{m,e,d_{\Delta P}, d_F, d_{\hat{J}}} \le y^{\Delta \hat{P}}_{m,e,d_{\Delta P}} \quad \text{A3.(4)}$$

$$W^{\Delta \hat{P}, \hat{F}in, \hat{J}s}_{m,e,d_{\Delta P}, d_F, d_{\hat{J}}} \le y^{\hat{F}in}_{m,e,d_F} \quad \text{A3.(5)}$$

$$W^{\Delta \hat{P}, \hat{F}in, \hat{J}s}_{m,e,d_{\Delta P}, d_F, d_{\hat{J}}} \le y^{\hat{J}s}_{m,e,d_{\hat{J}}} \quad \text{A3.(6)}$$

$$W^{\Delta \hat{P}, \hat{F}in, \hat{J}s}_{m,e,d_{\Delta P}, d_F, d_{\hat{J}}} \ge y^{\Delta \hat{P}}_{m,e,d_{\Delta P}} + y^{\hat{F}in}_{m,e,d_F} + y^{\hat{J}s}_{m,e,d_{\hat{J}}} - 2 \quad \text{A3.(7)}$$

$$\sum_{d_P} \sum_{d_{\Delta P}} \sum_{d_F} \sum_{d_{\hat{J}}} \left[P^{in}_{m,e,d_P} - \frac{9532.4}{2} \left(\frac{2F^{in}_{m,e,d_F} - (\hat{a} \Delta P^{nd}_{m,e,d_{\Delta P}} + J^{S}_{m,e,d_{\hat{J}}}) \hat{S}_{mem}}{2 \hat{\rho}_{av}} \right)^{1.7} \right]$$
$$\left[F^{in}_{m,e,d_F} - (\hat{a} \Delta P^{nd}_{m,e,d_{\Delta P}} + J^{S}_{m,e,d_{\hat{J}}}) \hat{S}_{mem} \right] \left[\hat{a} \Delta P^{nd}_{m,e,d_{\Delta P}} + J^{S}_{m,e,d_{\hat{J}}} \right] W^{\hat{P}in, \Delta \hat{P}, \hat{F}in, \hat{J}s}_{m,e,d_P, d_{\Delta P}, d_F, d_{\hat{J}}} \le W2_{m,e}$$

$$W2 \le \sum_{d_P} \sum_{d_{\Delta P}} \sum_{d_F} \sum_{d_{\hat{J}}} \left[P^{in}_{m,e,(d_P+1)} - \frac{9532.4}{2} \left(\frac{2F^{in}_{m,e,(d_F+1)} - (\hat{a} \Delta P^{nd}_{m,e,(d_{\Delta P}+1)} + J^{S}_{m,e,(d_{\hat{J}}+1)}) \hat{S}_{mem}}{2 \hat{\rho}_{av}} \right)^{1.7} \right]$$
$$\left[F^{in}_{m,e,(d_F+1)} - (\hat{a} \Delta P^{nd}_{m,e,(d_{\Delta P}+1)} + J^{S}_{m,e,(d_{\hat{J}}+1)}) \hat{S}_{mem} \right] \left[\hat{a} \Delta P^{nd}_{m,e,(d_{\Delta P}+1)} + J^{S}_{m,e,(d_{\hat{J}}+1)} \right] W^{\hat{P}in, \Delta \hat{P}, \hat{F}in, \hat{J}s}_{m,e,d_P, d_{\Delta P}, d_F, d_{\hat{J}}}$$

A3.(8)

$$W^{\hat{P}in, \Delta \hat{P}, \hat{F}in, \hat{J}s}_{m,e,d_P, d_F, d_{\Delta P}, d_{\hat{J}}} \le W^{\Delta \hat{P}, \hat{F}in, \hat{J}s}_{m,e,d_{\Delta P}, d_F, d_{\hat{J}}} \quad \text{A3.(9)}$$

$$W^{\hat{P}in, \Delta \hat{P}, \hat{F}in, \hat{J}s}_{m,e,d_P, d_F, d_{\Delta P}, d_{\hat{J}}} \le y^{\hat{P}in}_{m,e,d_P} \quad \text{A3.(10)}$$

$$W^{\hat{P}in, \Delta \hat{P}, \hat{F}in, \hat{J}s}_{m,e,d_P, d_F, d_{\Delta P}, d_{\hat{J}}} \ge W^{\Delta \hat{P}, \hat{F}in, \hat{J}s}_{m,e,d_{\Delta P}, d_F, d_{\hat{J}}} + y^{\hat{P}in}_{m,e,d_P} - 1 \quad \text{A3.(11)}$$

$$\sum_{d_{\Delta P}} \sum_{d_F} \sum_{d_{\hat{J}}} \left[\hat{F}^{in}_{m,e,d_F} (\hat{a}\Delta\hat{P}^{nd}_{m,e,d_{\Delta P}} + \hat{J}^{S}_{m,e,d_{\hat{J}}}) - (\hat{a}\Delta\hat{P}^{nd}_{m,e,d_{\Delta P}} + \hat{J}^{S}_{m,e,d_{\hat{J}}})^2 \hat{S}_{mem} \right] W^{\Delta\hat{P},\hat{F}in,\hat{J}s}_{m,e,d_F,d_{\Delta P},d_{\hat{J}}} \le W3_{m,e}$$

$$W3_{m,e} \le \sum_{d_{\Delta P}} \sum_{d_F} \sum_{d_{\hat{J}}} \left[\hat{F}^{in}_{m,e,(d_F+1)} (\hat{a}\Delta\hat{P}^{nd}_{m,e,(d_{\Delta P}+1)} + \hat{J}^{S}_{m,e,(d_{\hat{J}}+1)}) - (\hat{a}\Delta\hat{P}^{nd}_{m,e,(d_{\Delta P}+1)} + \hat{J}^{S}_{m,e,(d_{\hat{J}}+1)})^2 \hat{S}_{mem} \right] W^{\Delta\hat{P},\hat{F}in,\hat{J}s}_{m,e,d_F,d_{\Delta P},d_{\hat{J}}}$$

A3.(12)

$$\sum_{d_{\Delta P}} \sum_{d_F} \sum_{d_C} \sum_{d_{\hat{J}}} \left[\hat{F}^{in}_{m,e,d_F} \hat{C}^{in}_{m,e,d_C} (\hat{a}\Delta\hat{P}^{nd}_{m,e,d_{\Delta P}} + \hat{J}^{S}_{m,e,d_{\hat{J}}}) \right] W^{\Delta\hat{P},\hat{F}in,\hat{C}in\hat{J}s}_{m,e,d_{\Delta P},d_F,d_C,d_{\hat{J}}} \le W4_{m,e}$$

$$W4_{m,e} \ge \sum_{d_{\Delta P}} \sum_{d_F} \sum_{d_C} \sum_{d_{\hat{J}}} \left[\hat{F}^{in}_{m,e,(d_F+1)} \hat{C}^{in}_{m,e,(d_C+1)} (\hat{a}\Delta\hat{P}^{nd}_{m,e,(d_{\Delta P}+1)} + \hat{J}^{S}_{m,e,(d_{\hat{J}}+1)}) \right] W^{\Delta\hat{P},\hat{F}in,\hat{C}in\hat{J}s}_{m,e,d_{\Delta P},d_F,d_C,d_{\hat{J}}}$$

A3.(13)

$$W^{\Delta\hat{P},\hat{F}in,\hat{C}in\hat{J}s}_{m,e,d_{\Delta P},d_F,d_C,d_{\hat{J}}} \le W^{\Delta\hat{P},\hat{F}in,\hat{J}s}_{m,e,d_{\Delta P},d_F,d_{\hat{J}}}$$

A3.(14)

$$W^{\Delta\hat{P},\hat{F}in,\hat{C}in\hat{J}s}_{m,e,d_{\Delta P},d_F,d_C,d_{\hat{J}}} \le y^{\hat{C}in}_{m,e,d_C}$$

A3.(15)

$$W^{\Delta\hat{P},\hat{F}in,\hat{C}in\hat{J}s}_{m,e,d_{\Delta P},d_F,d_C,d_{\hat{J}}} \ge W^{\Delta\hat{P},\hat{F}in,\hat{J}s}_{m,e,d_{\Delta P},d_F,d_{\hat{J}}} + y^{\hat{C}in}_{m,e,d_C} - 1$$

A3.(16)

$$\left[\hat{J}^{S}_{m,e,d_{\hat{J}}} (\hat{a}\Delta\hat{P}^{nd}_{m,e,d_{\Delta P}} + \hat{J}^{S}_{m,e,d_{\hat{J}}}) \right] W^{\Delta\hat{P},\hat{J}s}_{m,e,d_{\Delta P},d_{\hat{J}}} \le W5_{m,e}$$

$$W5_{m,e} \le \left[\hat{J}^{S}_{m,e,(d_{\hat{J}}+1)} (\hat{a}\Delta\hat{P}^{nd}_{m,e,(d_{\Delta P}+1)} + \hat{J}^{S}_{m,e,(d_{\hat{J}}+1)}) \right] W^{\Delta\hat{P},\hat{J}s}_{m,e,d_{\Delta P},d_{\hat{J}}}$$

A3.(17)

$$W^{\Delta\hat{P},\hat{J}s}_{m,e,d_{\Delta P},d_{\hat{J}}} \le y^{\Delta\hat{P}}_{m,e,d_{\Delta P}}$$

A3.(18)

$$W^{\Delta\hat{P},\hat{J}s}_{m,e,d_{\Delta P},d_{\hat{J}}} \le y^{\hat{J}s}_{m,e,d_{\hat{J}}}$$

A3.(19)

$$W^{\Delta\hat{P},\hat{J}s}_{m,e,d_{\Delta P},d_{\hat{J}}} \ge y^{\Delta\hat{P}}_{m,e,d_{\Delta P}} + y^{\hat{J}s}_{m,e,d_{\hat{J}}} - 1$$

A3.(20)

$$\sum_{d_{\Delta P}} \sum_{d_F} \sum_{d_{\hat{J}}} \left[\hat{F}^{in}_{m,e,d_F} \hat{J}^{S}_{m,e,d_{\hat{J}}} - (\hat{a}\Delta\hat{P}^{nd}_{m,e,(d_{\Delta P}+1)} + \hat{J}^{S}_{m,e,d_{\hat{J}}})^2 \hat{S}_{mem} \right] W^{\Delta\hat{P},\hat{F}in,\hat{J}s}_{m,e,d_{\Delta P},d_F,d_{\hat{J}}} \le W6_{m,e}$$

$$W6_{m,e} \le \sum_{d_{\Delta P}} \sum_{d_F} \sum_{d_{\hat{J}}} \left[\hat{F}^{in}_{m,e,(d_F+1)} \hat{J}^{S}_{m,e,(d_{\hat{J}}+1)} - (\hat{a}\Delta\hat{P}^{nd}_{m,e,d_{\Delta P}} + \hat{J}^{S}_{m,e,(d_{\hat{J}}+1)})^2 \hat{S}_{mem} \right] W^{\Delta\hat{P},\hat{F}in,\hat{J}s}_{m,e,d_{\Delta P},d_F,d_{\hat{J}}}$$

A3.(21)

$$\sum_{d_{\Delta P}} \sum_{d_F} \sum_{d_{\hat{J}}} \begin{bmatrix} \hat{J}^S_{m,e,d_{\hat{J}}} \hat{F}^{in}_{m,e,d_F} (\hat{a}\Delta\hat{P}^{nd}_{m,e,d_{\Delta P}} + \hat{J}^S_{m,e,d_{\hat{J}}}) \\ -\hat{J}^S_{m,e,d_{\hat{J}}} (\hat{a}\Delta\hat{P}^{nd}_{m,e,d_{\Delta P}} + \hat{J}^S_{m,e,d_{\hat{J}}})^2 \hat{S}_{mem} \end{bmatrix} W^{\Delta\hat{P},\hat{F}in,\hat{J}s}_{m,e,d_{\Delta P},d_F,d_{\hat{J}}} \le W7_{m,e}$$

$$W7_{m,e} \le \sum_{d_{\Delta P}} \sum_{d_F} \sum_{d_{\hat{J}}} \begin{bmatrix} \hat{J}^S_{m,e,(d_{\hat{J}}+1)} \hat{F}^{in}_{m,e,(d_F+1)} (\hat{a}\Delta\hat{P}^{nd}_{m,e,(d_{\Delta P}+1)} + \hat{J}^S_{m,e,(d_{\hat{J}}+1)}) \\ -\hat{J}^S_{m,e,(d_{\hat{J}}+1)} (\hat{a}\Delta\hat{P}^{nd}_{m,e,(d_{\Delta P}+1)} + \hat{J}^S_{m,e,(d_{\hat{J}}+1)})^2 \hat{S}_{mem} \end{bmatrix} W^{\Delta\hat{P},\hat{F}in,\hat{J}s}_{m,e,d_{\Delta P},d_F,d_{\hat{J}}} \qquad \text{A3.(22)}$$

$$\sum_{d_{\Delta P}} \sum_{d_F} \sum_{d_C} \sum_{d_{\hat{J}}} \left[\hat{F}^{in}_{m,e,(d_F+1)} \hat{C}^{in}_{m,e,d_C} e^{\frac{\hat{a}\Delta\hat{P}^{nd}_{m,e,d_{\Delta P}} + \hat{J}^S_{m,e,d_{\hat{J}}}}{0.04\hat{S}c^{0.33} \frac{\hat{D}}{\hat{d}} \hat{\rho}_P \left(\frac{\hat{d}_h \hat{\rho}}{\hat{\mu}}\right)^{0.75} \left[\frac{2\hat{F}^{in}_{m,e,(d_F+1)} - (\hat{a}\Delta\hat{P}^{nd}_{m,e,d_{\Delta P}} + \hat{J}^S_{m,e,d_{\hat{J}}})\hat{S}_{mem}}{2\hat{\rho}\hat{S}_{fc}}\right]^{0.75}}} \right] W^{\Delta\hat{P},\hat{F}in,\hat{C}in\,\hat{J}s}_{m,e,d_{\Delta P},d_F,d_C,d_{\hat{J}}} \le W8_{m,e}$$

$$W8_{m,e} \ge \sum_{d_{\Delta P}} \sum_{d_F} \sum_{d_C} \sum_{d_{\hat{J}}} \left[\hat{F}^{in}_{m,e,d_F} \hat{C}^{in}_{m,e,(d_C+1)} e^{\frac{\hat{a}\Delta\hat{P}^{nd}_{m,e,(d_{\Delta P}+1)} + \hat{J}^S_{m,e,(d_{\hat{J}}+1)}}{0.04\hat{S}c^{0.33} \frac{\hat{D}}{\hat{d}} \hat{\rho}_P \left(\frac{\hat{d}_h \hat{\rho}}{\hat{\mu}}\right)^{0.75} \left[\frac{2\hat{F}^{in}_{m,e,d_F} - (\hat{a}\Delta\hat{P}^{nd}_{m,e,(d_{\Delta P}+1)} + \hat{J}^S_{m,e,(d_{\hat{J}}+1)})\hat{S}_{mem}}{2\hat{\rho}\hat{S}_{fc}}\right]^{0.75}}} \right] W^{\Delta\hat{P},\hat{F}in,\hat{C}in\,\hat{J}s}_{m,e,d_{\Delta P},d_F,d_C,d_{\hat{J}}} \qquad \text{A3.(23)}$$

$$\sum_{d_{\Delta P}} \sum_{d_F} \sum_{d_{\hat{J}}} \left[\hat{J}^S_{m,e,d_{\hat{J}}} (\hat{a}\Delta\hat{P}^{nd}_{m,e,d_{\Delta P}} + \hat{J}^S_{m,e,d_{\hat{J}}}) e^{\frac{\hat{a}\Delta\hat{P}^{nd}_{m,e,d_{\Delta P}} + \hat{J}^S_{m,e,d_{\hat{J}}}}{0.04\hat{Sc}^{0.33}\frac{\hat{D}}{\hat{d}}\hat{\rho}_P\left(\frac{\hat{d}_h\hat{\rho}}{\hat{\mu}}\right)^{0.75}\left[\frac{2\hat{F}^{in}_{m,e,(d_F+1)} - (\hat{a}\Delta\hat{P}^{nd}_{m,e,d_{\Delta P}} + \hat{J}^S_{m,e,d_{\hat{J}}})\hat{S}_{mem}}{2\hat{\rho}\hat{S}_{fc}}\right]^{0.75}}} \right] W^{\Delta\hat{P},\hat{F}in,\hat{J}s}_{m,e,d_{\Delta P},d_F,d_{\hat{J}}} \le W9_{m,e}$$

$$W9_{m,e} \le \sum_{d_{\Delta P}} \sum_{d_F} \sum_{d_{\hat{J}}} \left[\hat{J}^S_{m,e,(d_{\hat{J}}+1)} (\hat{a}\Delta\hat{P}^{nd}_{m,e,(d_{\Delta P}+1)} + \hat{J}^S_{m,e,(d_{\hat{J}}+1)}) e^{\frac{\hat{a}\Delta\hat{P}^{nd}_{m,e,(d_{\Delta P}+1)} + \hat{J}^S_{m,e,(d_{\hat{J}}+1)}}{0.04\hat{Sc}^{0.33}\frac{\hat{D}}{\hat{d}}\hat{\rho}_P\left(\frac{\hat{d}_h\hat{\rho}}{\hat{\mu}}\right)^{0.75}\left[\frac{2\hat{F}^{in}_{m,e,d_F} - (\hat{a}\Delta\hat{P}^{nd}_{m,e,(d_{\Delta P}+1)} + \hat{J}^S_{m,e,(d_{\hat{J}}+1)})\hat{S}_{mem}}{2\hat{\rho}\hat{S}_{fc}}\right]^{0.75}}} \right] W^{\Delta\hat{P},\hat{F}in,\hat{J}s}_{m,e,d_{\Delta P},d_F,d_{\hat{J}}} \quad \text{A3.(24)}$$

$$\sum_{d_{\Delta P}} \sum_{d_F} \sum_{d_{\hat{J}}} \left[\left[\hat{F}^{in}_{m,e,(d_F+1)} \hat{J}^S_{m,e,d_{\hat{J}}} - \hat{J}^S_{m,e,d_{\hat{J}}} (\hat{a}\Delta\hat{P}^{nd}_{m,e,d_{\Delta P}} + \hat{J}^S_{m,e,d_{\hat{J}}}) \hat{S}_{mem} \right] e^{\frac{\hat{a}\Delta\hat{P}^{nd}_{m,e,d_{\Delta P}} + \hat{J}^S_{m,e,d_{\hat{J}}}}{0.04\hat{Sc}^{0.33}\frac{\hat{D}}{\hat{d}}\hat{\rho}_P\left(\frac{\hat{d}_h\hat{\rho}}{\hat{\mu}}\right)^{0.75}\left[\frac{2\hat{F}^{in}_{m,e,(d_F+1)} - (\hat{a}\Delta\hat{P}^{nd}_{m,e,d_{\Delta P}} + \hat{J}^S_{m,e,d_{\hat{J}}})\hat{S}_{mem}}{2\hat{\rho}\hat{S}_{fc}}\right]^{0.75}}} \right] W^{\Delta\hat{P},\hat{F}in,\hat{J}s}_{m,e,d_{\Delta P},d_F,d_{\hat{J}}} \le W10_{m,e}$$

$$W10_{m,e} \le \sum_{d_{\Delta P}} \sum_{d_F} \sum_{d_{\hat{J}}} \left[\left[\hat{F}^{in}_{m,e,d_F} \hat{J}^S_{m,e,(d_{\hat{J}}+1)} - \hat{J}^S_{m,e,(d_{\hat{J}}+1)} (\hat{a}\Delta\hat{P}^{nd}_{m,e,(d_{\Delta P}+1)} + \hat{J}^S_{m,e,(d_{\hat{J}}+1)}) \hat{S}_{mem} \right] e^{\frac{\hat{a}\Delta\hat{P}^{nd}_{m,e,(d_{\Delta P}+1)} + \hat{J}^S_{m,e,(d_{\hat{J}}+1)}}{0.04\hat{Sc}^{0.33}\frac{\hat{D}}{\hat{d}}\hat{\rho}_P\left(\frac{\hat{d}_h\hat{\rho}}{\hat{\mu}}\right)^{0.75}\left[\frac{2\hat{F}^{in}_{m,e,d_F} - (\hat{a}\Delta\hat{P}^{nd}_{m,e,(d_{\Delta P}+1)} + \hat{J}^S_{m,e,(d_{\hat{J}}+1)})\hat{S}_{mem}}{2\hat{\rho}\hat{S}_{fc}}\right]^{0.75}}} \right] W^{\Delta\hat{P},\hat{F}in,\hat{J}s}_{m,e,d_{\Delta P},d_F,d_{\hat{J}}}$$

A3.(25)

Thus, the permeate flow and concentration are obtained from the next equations:

$$C_{m,e}^{Pe} = \frac{J_{m,e}^{S}}{\hat{a}\Delta P_{m,e}^{nd} + J_{m,e}^{S}} * 1000\hat{\rho}_P \qquad \text{A3.(26)}$$

$$F_{m,e}^{Pe} = (\hat{a}\Delta P_{m,e}^{nd} + J_{m,e}^{S})\hat{S}_{mem} \qquad \text{A3.(27)}$$

The partitioned variables that appears in equations 113-135 are discretized according to:

$$\sum_{d_{\Delta P}} \Delta\hat{P}_{m,e,d_{\Delta P}}^{nd} y_{m,e,d_{\Delta P}}^{\Delta\hat{P}} \le \Delta P_{m,e}^{nd} \le \sum_{d_{\Delta P}} \Delta\hat{P}_{m,e,(d_{\Delta P}+1)}^{nd} y_{m,e,d_{\Delta P}}^{\Delta\hat{P}} \qquad \text{A3.(28)}$$

$$\sum_{d_{\hat{J}}} \hat{J}_{m,e,d_{\hat{J}}}^{S} y_{m,e,d_{\hat{J}}}^{\hat{J}s} \le J_{m,e}^{S} \le \sum_{d_{\hat{J}}} \hat{J}_{m,e,(d_{\hat{J}}+1)}^{S} y_{m,e,d_{\hat{J}}}^{\hat{J}s} \qquad \text{A3.(29)}$$

$$\sum_{d_F} \hat{F}_{m,e,d_F}^{in} y_{m,e,d_F}^{\hat{F}in} \le F_{m,e}^{in} \le \sum_{d_F} \hat{F}_{m,e,(d_F+1)}^{in} y_{m,e,d_F}^{\hat{F}in} \qquad \text{A3.(30)}$$

$$\sum_{d_C} \hat{C}_{m,e,d_C}^{in} y_{m,e,d_C}^{\hat{C}in} \le C_{m,e}^{in} \le \sum_{d_C} \hat{C}_{m,e,(d_C+1)}^{in} y_{m,e,d_C}^{\hat{C}in} \qquad \text{A3.(31)}$$

$$\sum_{d_P} \hat{P}_{m,e,d_P}^{in} y_{m,e,d_P}^{\hat{P}in} \le P_{m,e}^{in} \le \sum_{d_P} \hat{P}_{m,e,(d_P+1)}^{in} y_{m,e,d_P}^{\hat{P}in} \qquad \text{A3.(32)}$$

With their corresponding binary variables to ensure that only one interval is picked:

$$\sum_{d_{\Delta P}} y_{m,e,d_{\Delta P}}^{\Delta\hat{P}} = 1 \qquad \text{A3.(33)}$$

$$\sum_{d_{\hat{J}}} y_{m,e,d_{\hat{J}}}^{\hat{J}s} = 1 \qquad \text{A3.(34)}$$

$$\sum_{d_F} y_{m,e,d_F}^{\hat{F}in} = 1 \qquad \text{A3.(35)}$$

$$\sum_{d_C} y_{m,e,d_C}^{\hat{C}in} = 1 \qquad \text{A3.(36)}$$

$$\sum_{d_P} y_{m,e,d_P}^{\hat{P}in} = 1 \qquad \text{A3.(37)}$$